

**DEVELOPMENT OF BRIGHT AND DARK PULSED
FIBER LASER BASED ON NONLINEAR
POLARIZATION ROTATION**

TIU ZIAN CHEAK

**THESIS SUBMITTED IN FULFILLMENT OF THE
REQUIREMENT FOR THE DEGREE OF
DOCTOR OF PHILOSOPHY**

**DEPARTMENT OF ELECTRICAL ENGINEERING
FACULTY OF ENGINEERING
UNIVERSITY OF MALAYA
KUALA LUMPUR**

2015

UNIVERSITI MALAYA

ORIGINAL LITERARY WORK DECLARATION

Name of Candidate: Tiu Zian Cheak (I.C/Passport No: 841008015853)

Registration/Matric No: KHA120120

Name of Degree: DOCTOR OF PHILOSOPHY

Title of Project Paper/Research Report/Dissertation/Thesis ("this Work"):

DEVELOPMENT OF BRIGHT AND DARK PULSED FIBER LASER BASED ON
NONLINEAR POLARIZATION ROTATION

Field of Study: Optical Communications

I do solemnly and sincerely declare that:

- (1) I am the sole author/writer of this Work;
- (2) This Work is original;
- (3) Any use of any work in which copyright exists was done by way of fair dealing and for permitted purposes and any excerpt or extract from, or reference to or reproduction of any copyright work has been disclosed expressly and sufficiently and the title of the Work and its authorship have been acknowledged in this Work;
- (4) I do not have any actual knowledge nor do I ought reasonably to know that the making of this work constitutes an infringement of any copyright work;
- (5) I hereby assign all and every rights in the copyright to this Work to the University of Malaya ("UM"), who henceforth shall be owner of the copyright in this Work and that any reproduction or use in any form or by any means whatsoever is prohibited without the written consent of UM having been first had and obtained;
- (6) I am fully aware that if in the course of making this Work I have infringed any copyright whether intentionally or otherwise, I may be subject to legal action or any other action as may be determined by UM.

Candidate's Signature

Date

Subscribed and solemnly declared before,

Witness's Signature

Date

Name:

Designation:

ABSTRACT

Pulsed lasers have many practical applications in both communication and sensing. This thesis describes in detail the generation of bright pulses and dark pulses lasers based on nonlinear polarization rotation (NPR). The passive techniques are explored for pulse generation as they are reliable, compact, producing high beam quality and do not require an external modulator. Various techniques such as film saturable absorber (SAs), fiber SA and NPR techniques are studied to generate pulse. Performance of graphene SA in Erbium-doped fiber laser (EDFL) with three different gain mediums is successfully demonstrated. Q-switched EDFL are also demonstrated using thulium-doped fiber as a SA. NPR technique is adopted in a ring EDFL to generate Q-switched with low pump power. Besides the Q-switching operation, NPR technique is also explored to generate mode-locked, harmonic mode-locked, and multi-wavelength mode-locked. On the other hand, nonlinear Schrödinger equation (NLSE) dark pulse, cubic-quintic nonlinear Schrödinger equation (CQNLSE) dark pulse and domain wall (DW) dark pulse are demonstrated under different EDFL cavities based on NPR technique. Furthermore, multi-wavelength dark pulse is achieved using PCF in figure-of-eight cavity to slice the dark pulse spectrum. Besides, Q-switched dark pulse is achieved in an unstable mode-locking operation, in which the Q-switching operation modulated the dark pulses.

ABSTRAK

Laser berdenyut mempunyai banyak aplikasi praktikal dalam kedua-dua komunikasi dan penderiaan. Tesis ini menerangkan secara terperinci generasi laser denyutan terang dan laser denyutan gelap berasas nonlinear polarization rotation (NPR). Teknik-teknik pasif yang diterokai untuk generasi nadi kerana mereka dipercayai, padat, menghasilkan kualiti rasuk tinggi dan tidak memerlukan peninggirendahan luar. Pelbagai teknik seperti filem saturable absorbers (SAs), serat SA dan teknik NPR dikaji untuk menjana denyut. Prestasi graphene SA di Erbium-doped fiber laser (EDFL) dengan tiga gain medium yang berbeza berjaya ditunjukkan. Q-switched EDFL juga menunjukkan menggunakan gentian thulium-doped fiber sebagai SA. Teknik NPR diguna pakai dalam EDFL untuk menjana Q-switched dengan kuasa pam rendah. Selain operasi Q-switched, teknik NPR juga diteroka untuk menjana mode-locked, harmonik mode-locked, dan laser pelbagai jarak gelombang mode-locked. Sebaliknya, nonlinear Schrödinger equation (NLSE) nadi gelap, Cubic-quintic nonlinear Schrödinger equation (CQNLSE) nadi gelap dan domain wall (DW) nadi gelap yang ditunjukkan di bawah rongga EDFL berbeza berdasarkan teknik NPR. Tambahan pula, pelbagai jarak gelombang nadi gelap dicapai menggunakan PCF dalam rajah-of-lapan rongga untuk keping spektrum denyut gelap. Selain itu, Q-switched nadi gelap dicapai dalam mode-locked operasi yang tidak stabil, di mana operasi Q-menukar termodulat denyutan gelap.

ACKNOWLEDGEMENT

First of all, I would like to express my appreciation to my supervisors, Prof. Dr. Sulaiman Wadi Harun and Prof. Dr. Harith Ahmad for the continuous support, motivation, patience and knowledge throughout my Ph.D study. Their guidance helped me in all times of research and thesis writing.

My sincere gratitude also goes to Dr. Tan Sin Jin, Arman Zarei, Muneswaran Suthaskumar and Dr. Afik for their help and knowledge sharing. You all brought so much ideas to the lab despite the ups and downs that we encountered during our research.

To my wife, parents and sibling, thank you for your encouragement and support. Again, thank you to everyone who had helped me directly or indirectly with my research.

TABLE OF CONTENTS

ABSTRACT	ii
ABSTRAK	iii
ACKNOWLEDGEMENT	iv
TABLE OF CONTENTS	v
LIST OF FIGURES	viii
LIST OF SYMBOLS AND ABBREVIATIONS	xiii
LIST OF PUBLICATION	xv
CHAPTER 1 INTRODUCTION	
1.1 Overview of Pulsed Laser	1
1.2 Thesis Objectives	4
1.3 Thesis Overview	4
1.4 Contribution	6
CHAPTER 2 LITERATURE REVIEW ON PULSE LASER	
2.1 Introduction	8
2.2 Nonlinearity in Optical Fiber	9
2.2.1 Self-Phase Modulation	11
2.2.2 Cross-Phase Modulation	13
2.2.3 Four-wave Mixing	15
2.3 Pulsed Fiber Laser	16
2.3.1 Q-switching operation	16
2.3.2 Mode-locking operation	18
2.3.3 Dark pulse operation	20
2.4 The Nonlinear Schrodinger Equation	21
2.5 Saturable Absorber	22
2.5.1 Artificial Saturable Absorber with Nonlinear Polarization Rotation	22
2.5.2 Artificial Saturable Absorber with Nonlinear Optical Loop Mirror	26

2.5.3	Film Saturable Absorber	28
-------	-------------------------	----

CHAPTER 3 DEVELOPMENT OF PASSIVE Q-SWITCHED ERBIUM -DOPED FIBER LASER

3.1	Introduction	30
3.2	Q-switched EDFL with graphene based SA	31
3.2.1	Fabrication and characterization of Graphene based SA	31
3.2.2	Experimental setup	33
3.2.3	Comparison of Q-switching performance at three different gain media	35
3.3	Q-switched EDFL using a solid state Thulium-doped Fiber SA	42
3.3.1	Configuration of the proposed Q-switched EDFL using a TDF SA	43
3.3.2	Q-switching performance	44
3.4	Q-switching pulse generation using nonlinear polarization rotation technique	49
3.5	Multi-wavelength Q-switched Generation With Graphene Based SA	54
3.6	Summary	61

CHAPTER 4 DEVELOPMENT OF PASSIVE MODE-LOCKED ERBIUM-DOPED FIBER LASERS

4.1	Introduction	63
4.2	NPR based mode-locked EDFL with three switchable operation states	64
4.2.1	Experimental setup	65
4.2.2	Comparison of the three different mode-locked operation states	66
4.3	Mode-locked square pulse emission with ultra-low repetition rate	71
4.3.1	Configuration of the proposed mode-locked square pulse EDFL	72
4.3.2	Mode-locked square pulse performance	73
4.4	Multi-wavelength mode-locked EDFL in figure-of-eight cavity	84
4.4.1	Configuration of the proposed multi-wavelength mode-locked EDFL	85
4.4.2	Multi-wavelength mode-locked performance	86
4.5	Summary	90

CHAPTER 5 GENERATION OF DARK PULSES IN ERBIUM-DOPED FIBER LASER CAVITY USING NONLINEAR POLARIZATION ROTATION APPROACH

5.1	Introduction	92
5.2	Harmonic NLSE dark pulse emission in EDFL	93
5.2.1	Experimental setup	93
5.2.2	NLSE dark pulse performance	95
5.3	Generation of switchable DW and CQNLSE dark pulse	101
5.3.1	Configuration of the switchable DW and CQNLSE dark pulse EDFL	101
5.3.2	DW dark pulse performance	102
5.3.3	CQNLSE dark pulse performance	105
5.4	Multi-wavelength dark pulse EDFL in figure-of-eight cavity	107
5.4.1	Configuration of the proposed multi-wavelength dark pulse EDFL	108
5.4.2	Multi-wavelength dark pulse performance	109
5.5	Generation of Q-switched Mode-locked EDFL operating in dark regime	117
5.5.1	Experimental setup	118
5.5.2	Q-switched dark pulse performance	119
5.6	Summary	124

CHAPTER 6 CONCLUSION AND FUTURE OUTLOOK

6.1	Conclusion	125
6.2	Recommendations for Future Works	128
	REFERENCES	130
	APPENDIX	139

LIST OF FIGURES

Figure 2.1: Gaussian pulse for the temporal variation of SPM induce phase shift and frequency chirp	13
Figure 2.2: Schematic of FWM in frequency domain	15
Figure 2.3: Evolution of non-linear polarization rotation	23
Figure 2.4: Transmittivity of NPR	25
Figure 2.5: Basic configuration of NPR in ring cavity	26
Figure 2.6: Working principle of APM (a) a typical APM coupled cavity laser (b) The pulse of main cavity adds to the pulse of the auxiliary cavity to result in a shortened pulse at the output of beam splitter	27
Figure 2.7: Basic configuration of NOLM	28
Figure 2.8: Basic configuration of film saturable absorber	29
Figure 3.1: Raman spectrum of the fabricated SA	33
Figure 3.2: Schematic configuration of the Q-switched EDFL	35
Figure 3.3: Optical spectrum of the Q-switched EDFLs when the pump is fixed at threshold power	36
Figure 3.4: Pulse repetition rate against pump power for the EDFL configured with three different EDFs	37
Figure 3.5: Pulse width versus pump power for the EDFL configured with three different EDFs	38
Figure 3.6: Pulse train of maximum pulse repetition rate at three different gain medium (a) Silica EDF (400 ppm) (b) Silica EDF (2000 ppm) and (c) Bismuth EDF (3000 ppm)	40
Figure 3.7: Output power against pump power for three different gain medium	41
Figure 3.8: Pulse energy against pump power for three different gain medium	41
Figure 3.9: Schematic configuration of the proposed thulium fiber based Q-switched EDFL	44
Figure 3.10: Q-switched pulse evolution of the proposed Q-switched EDFL against pump power	45

Figure 3.11: Optical spectrum and of the proposed Q-switched EDFL when the pump is fixed at 33.7 mW	46
Figure 3.12: Repetition rate and pulse width of the proposed Q-switched EDFL against the pump power	48
Figure 3.13: Output power and pulse energy of the proposed Q-switched EDFL against the pump power	48
Figure 3.14: Schematic configuration of the proposed Q-switched EDFL	50
Figure 3.15: Pulse evolution of the proposed Q-switched EDFL against pump power	51
Figure 3.16: Optical spectrum for the Q-switched EDFL at threshold pump power	51
Figure 3.17: Output power and pulse energy of the proposed Q-switched EDFL against pump power	53
Figure 3.18: Repetition rate and pulse width of the proposed Q-switched EDFL against pump power	53
Figure 3.19: Schematic configuration of the proposed multi-wavelength Q-switched EDFL	55
Figure 3.20: (a) Optical spectrum and (b) typical pulse train of the proposed multi-wavelength Q-switched EDFL when the pump is fixed at the threshold pump power of 39.6 mW	56
Figure 3.21: Output spectrum evolution of the proposed multi-wavelength Q-switched EDFL against pump power	58
Figure 3.22: Repetition rate and pulse width of the proposed multi-wavelength Q-switched EDFL against pump power	60
Figure 3.23: Output power and pulse energy of the proposed multi-wavelength Q-switched EDFL against pump power	60
Figure 3.24: Output spectrum evolution of the proposed multi-wavelength Q-switched EDFL against time	61
Figure 4.1: Schematic configuration of the mode-locked EDFL	66
Figure 4.2: Typical pulse train of the proposed mode-locked EDFL at two different pump powers of 17.5 mW and 34.3 mW. Inset shows the corresponding cingle pulse envelops	67
Figure 4.3: Typical pulse trains of the mode-locked EDFL at pump powers of 48.2 mW and 116.7 mW, which operate at fundamental mode	69
Figure 4.4: Pulse train obtained from proposed EDFL with pump power of 138.9 mW and 145 mW	69

Figure 4.5: Optical spectrum of the mode-locked laser at various pump powers	71
Figure 4.6: Experimental set-up of the proposed DSR laser	73
Figure 4.7: Optical output spectra of pulse laser at three different pump powers	75
Figure 4.8: Typical pulse train with a fundamental repetition rate at 10.2 kHz	75
Figure 4.9: Oscilloscope trace of the single square pulse envelop at two different pump powers	76
Figure 4.10: Pulse width of the square pulse versus pump power	77
Figure 4.11: RF spectrum of the generated pulses: (a) square pulse and (b) harmonic pulse	78
Figure 4.12: Typical pulse train of the mode-locking pulse at two different pump powers: (a) 100 mW and (b) 108 mW	80
Figure 4.13: Output spectrum of the harmonic mode-locked EDFL	81
Figure 4.14: Measured output power for square and harmonic pulse at various pump powers	82
Figure 4.15: Pulse energy of produced pulse for square and harmonic pulse	83
Figure 4.16: Schematic configuration of the proposed multi-wavelength mode-locked EDFL	86
Figure 4.17: Output of the proposed multi-wavelength mode-locked EDFL at pump power of 146 mW: (a) Optical spectrum and (b) typical mode-locked pulse train	88
Figure 4.18: RF spectrum of the proposed multi-wavelength mode-locked EDFL	90
Figure 5.1: Schematic configuration of the proposed dark pulse EDFL	95
Figure 5.2: Dark pulse emission of the proposed EDFL at different orders of harmonic: (a) fundamental, (b) 2 nd , (c) 3 rd , (d) 4 th , and (e) 5 th	97
Figure 5.3: Threshold pump power and output power at different order harmonic	99
Figure 5.4: Pulse width and pulse energy against different order harmonic	100
Figure 5.5: Output spectra of the dark pulse train at different order harmonics	100
Figure 5.6: Experimental set-up of the proposed mode-locked EDFL, which capable for generating a switchable DW and NLSE dark pulse train	102
Figure 5.7: Typical DW dark pulse train at pump power of 140 mW	103
Figure 5.8: DW dark pulse spectrum of the proposed EDFL at pump power of 140 mW	104

Figure 5.9: DW dark pulse RF spectrum of the proposed EDFL at pump power of 140 mW	105
Figure 5.10: CQNLSE dark pulse train of the proposed EDFL at pump power of 140 mW	106
Figure 5.11: Output optical spectrum of the CQNLSE dark pulse at pump power of 140 mW	107
Figure 5.12: RF spectrum of the CQNLSE dark soliton pulse at pump power of 140 mW	107
Figure 5.13: Schematic configuration of the proposed multi-wavelength mode-locked EDFL	109
Figure 5.14: Multi-wavelength output spectrum evolution against 1480 nm pump power	110
Figure 5.15: Optical spectrum of the proposed multi-wavelength dark pulse EDFL at four different orientation of PC when the pump is fixed at 146 mW (a) fundamental (b) 2 nd order (c) 3 rd order and (d) 4 th order harmonic operation	113
Figure 5.16: Dark pulse train of the proposed multi-wavelength dark pulse EDFL at four different orientation of PC when the pump is fixed at 146 mW (a) fundamental (b) 2 nd order (c) 3 rd order and (d) 4 th order harmonic operation	115
Figure 5.17: Pulse width and pulse energy at different orders of harmonic. Inset shows single dark pulse at 4th order harmonic	117
Figure 5.18: Schematic configuration of the proposed QML EDFL emitting dark pulse	118
Figure 5.19: Emission of Q-switched dark pulse train againsts pump power	119
Figure 5.20: Emission of single Q-switched dark pulse at pump power of 145 mW	120
Figure 5.21: Output spectrum at pump power of 145 mW	120
Figure 5.22: Pulse repetition rate and pulse width of the proposed Q-switched dark pulse EDFL	121
Figure 5.23: Output power and pulse energy of the proposed Q-switched dark pulse EDFL	122
Figure 5.24: Dark square pulse at different pump power, Inset shows single Q-switched dark pulse which consists of first dip and trailing dark pulses	123

LIST OF TABLES

Table 3.1: Summary of laser performance for three different gain media

42

LIST OF SYMBOLS AND ABBREVIATIONS

A_{eff}	Effective area
L_{eff}	Effective length
B_2	Group velocity dispersion parameter
I	Light intensity
α	Nonlinear coefficient
n_2	Nonlinear refractive index
P_{th}	Threshold power
T	Transmittivity of light
λ	Wavelength
AC	Auto-correlator
ASE	Amplified Spontaneous Emission
Bi-EDF	Bismuth-Erbium Doped Fiber
CW	Continuous Wave
DCF	Dispersion Compensation Fiber
DSF	Dispersion Shifted Fiber
DWDM	Dense Wavelength Division Multiplexing
EDF	Erbium Doped Fiber
EDFL	Erbium Doped Fiber Laser
EDFA	Erbium Doped Fiber Amplifier

FWHM	Full Width Half Maximum
FWM	Four-Wave Mixing
GVD	Group Velocity Dispersion
HNLF	Highly Nonlinear Fiber
NRP	Nonlinear Polarization Rotation
NALM	Nonlinear Amplifying Loop Mirror
NOLM	Nonlinear Optical Loop Mirror
OSA	Optical Spectrum Analyzer
OSC	Oscilloscope
OSNR	Optical Signal to Noise Ratio
OTDM	Optical Time Division Multiplexing
PC	Polarization Controller
PCF	Photonic Crystal Fiber
RFSA	Radio Frequency Spectrum Analyzer
SA	Saturable Absorber
SMF	Single Mode Fiber
SNR	Signal to Noise Ratio
SOA	Semiconductor Optical Amplifier
SPM	Self-Phase Modulation
TDM	Time Division Multiplexing
WDM	Wavelength Division Multiplexing
XPM	Cross Phase Modulation

LIST OF PUBLICATION

Journal Publications

- Tiu, Z. C., Ahmad, F., Tan, S. J., Ahmad, H., & Harun, S. W. (2014). Passive Q-switched Erbium-doped fiber laser with graphene–polyethylene oxide saturable absorber in three different gain media. *Indian Journal of Physics*, 88(7), 727-731.
- Tiu, Z. C., Tan, S. J., Zarei, A., Ahmad, H., & Harun, S. W. (2014). Nonlinear Polarization Rotation-Based Mode-Locked Erbium-Doped Fiber Laser with Three Switchable Operation States. *Chinese Physics Letters*, 31(9), 094206.
- Tiu, Z. C., Ahmad, F., Tan, S. J., Zarei, A., Ahmad, H., & Harun, S. W. (2014). Multi-wavelength Q-switched Erbium-doped fiber laser with photonic crystal fiber and multi-walled carbon nanotubes. *Journal of Modern Optics*, 61(14), 1133-1139.
- Tan, S. J., Tiu, Z. C., Harun, S. W., & Ahmad, H. (2014). Square pulse emission with ultra-low repetition rate utilising non-linear polarisation rotation technique. *The Journal of Engineering*, 1(1).
- Tiu, Z. C., Tan, S. J., Ahmad, H., & Harun, S. W. (2014). Dark pulse emission in nonlinear polarization rotation-based multiwavelength mode-locked erbium-doped fiber laser. *Chinese Optics Letters*, 12(11), 113202.
- Tiu, Z. C., Zarei, A., Tan, S. J., Ahmad, H., & Harun, S. W. (2014). Q-Switching Pulse Generation with Thulium-Doped Fiber Saturable Absorber. *Chinese Physics Letters*, 31(12), 124203.
- Zarei, A., Tiu, Z. C., Ahmad, F., Ahmad, H., & Harun, S. W. (2015). Q-switched Brillouin fibre laser with multi-wall carbon nanotube saturable absorber. *IET Optoelectronics*, 9(2), 96-100.
- Zian, C. T., Arman, Z., Sin, J. T., Harith, A., & Sulaiman, W. H. (2015). Harmonic Dark Pulse Emission in Erbium-Doped Fiber Laser. *Chinese Physics Letters*, 32(3), 034203.
- Tiu, Z. C., Ahmad, F., Tan, S. J., Ahmad, H., & Harun, S. W. (2014). Multi-wavelength Q-switched Erbium-doped fiber laser with photonic crystal fiber and graphene-polyethylene oxide saturable absorber. *Optik*, DOI: 10.1016/j.ijleo.2015.04.036.

CHAPTER 1

INTRODUCTION

1.1 Overview of Pulsed Laser

Pulsed lasers have been of great interest as they have many applications in telecommunication, remote sensing, signal processing and medicine. Various laser setups are widely studied to generate pulses with different and distinctive pulse characteristics. Therefore, each of the laser setup can be customized to suit for different applications. For instance, pulsed laser designed with high peak intensity and high pulse energy is widely used for micromachining, cutting and drilling which benefits the electronic and automotive industries (Nikumb et al., 2005). In the medical field, pulsed laser is used in surgeries (Plamann et al., 2010; Serbin et al., 2002). One of the applications of pulsed laser is in eye surgery, where the system is known as the laser-assisted in situ keratomileusis (LASIK) (Kezirian & Stonecipher, 2004; Montés-Micó, Rodríguez-Galietero & Alió, 2007). In LASIK surgery, ultra-violet (UV) laser source is used to photo-ablate the corneal tissue rather than mechanical cutting which will somehow damage the surface layer or cornea and the surrounding cells. On the other hand, pulsed laser is used to mark information such as batch number, manufactured date and logo (Noor et al., 1994) in the electronic semiconductor manufacturing industry. Furthermore, in telecommunication field, ultra-short optical pulses have been widely used in optical transmission technology for achieving a high speed and long distance network (Salehi, Weiner, & Heritage, 1990; Mendez et al., 2000). With the exponentially growth of information technology in past decade, billions of computers are linked and information such as voice, data, image, and video are exchanged. For

instance, services such as voice over Internet Protocol (VoIP) are able to allow users to communicate in very low cost compare to traditional public switched telephone network (PSTN). Nonetheless, the demands of higher data rate transmission are still in a tremendously growth as the number and needs of users are increasing. To achieve a high capacity transmission, multiplexing with Wavelength Division Multiplexing (WDM) and Optical Time Division Multiplexing (OTDM) are effective solutions in current technology.

WDM is a technology by which multiple optical channels can be combined together and simultaneously transmitted at different wavelengths through a single optical fiber. The broad bandwidth supercontinuum (SC) light source generated by a pulsed laser can be sliced into many wavelength channels to serve as a source in WDM system (Morioka et al., 1994). The SC light source can be produced by leading the pulsed laser output into a nonlinear fiber such as photonic crystal fiber (PCF), highly nonlinear fiber (HNLF) and dispersion compensated fiber (DCF) (Hossain, Namihira & Razzak, 2012; Mori et al., 1997). Spectrum broadening is formed as a result of nonlinear interaction such as self-phase modulation (SPM), cross-phase modulation (XPM) and four wave mixing (FWM) in the nonlinear fiber. SC source extending from 1200 nm up to region above 1750 nm has been obtained from an amplified mode-locked pulse of 800 fs in conjunction with 100 m PCF (Shahabuddin et al., 2012). In Dense Wavelength Division Multiplexing (DWDM) system, the broad light spectrum can be sliced into hundreds or even thousands of wavelengths and each of the wavelengths can function as individual channel carrier.

In OTDM technology, high bit rate data stream is achieved by multiplexing a number of low bit rate optical channels in the time domain. Several types of pulsed laser sources are widely utilized in OTDM system, which are included mode-locked fiber laser in ring cavity, semiconductor mode-locked laser and distributed feedback laser

(DFB) with modulator. OTDM system shows a promising potential for next generation of telecommunication technology. For instance, ultra-high speed at 1.28 Tb/s in OTDM transmission over 70 km had been demonstrated using ultra-short femto-second soliton with 10 GHz per channel at the transmitter (Mulvad et al., 2010; Nakazawa, 2000). Furthermore, soliton pulses are desirable transmitting sources for ultra-long haul transmission and it was successfully implemented and demonstrated in a propagation distance up to one million km (Nakazawa et al., 1991). Among the different types of pulses, dark pulse can provide better signals for telecommunications. The dark pulses, which consist of intensity dips under a continuous beam of laser light, are effectively the opposite of the bright bursts in a normal pulsed laser. Dark pulse train can be generated with 90 ps pulse width, and just 30% of the normal intensity is needed compared to conventional bright pulse (Feng et al., 2010).

There are various techniques that can be utilized to generate different types of pulsed laser to fit into different applications. Generally, these methods can be classified into two techniques, which are active and passive pulsing techniques. In active techniques, an external modulator is needed to electronically synchronize to the cavity repetition rate. In passive technique, the external synchronization is not required, but rather adopts an all optical nonlinear process in a laser resonator. The structures of active mode-locked lasers are considered complex, complicated and bulky with the employment of external modulator, whereas for passive method, the mechanism used is by generating saturable absorption action. Saturable absorption can be achieved by real saturable absorbers (SAs) or can also exploit the artificial SAs. Real SAs such as semiconductors and the newly discovered carbon nanotubes (CNTs) and graphene, whereas the most prominent artificial SA is called nonlinear polarization rotation (NPR), which is also known as additive pulse mode-locking (APM) (Haus, Ippen & Tamura, 1994). The advantages of passive over active mode-locking are for its simple

and compact construction, cost efficiency, robustness and ultra-short pulse generation (Sotor et al., 2012). This PhD work is intended to explore several passive pulsing approaches as well as the formation of different pulse profiles.

1.2 Thesis Objectives

Pulsed lasers are important and widely used in communication and electronics industries. This work aim to implement and demonstrate practical pulsed laser based on nonlinear effects in optical fibers. To achieve this, several objectives have been outlined to guide the research direction toward the goal:

1. To study various passive techniques to generate pulsed laser.
2. To demonstrate Q-switched fiber laser using real saturable absorber and artificial saturable absorber.
3. To generate mode-locked fiber laser using NPR technique.
4. To generate dark pulse using NPR technique.

1.3 Thesis Overview

This thesis is organized into six chapters which comprehensively demonstrate the generation of pulsed laser based on nonlinear effects. Chapter 1 gives a brief description on the recent developments and applications of pulsed lasers. Besides, the motivations and objectives of this study are also highlighted. Moreover, an overview and the contributions of this thesis to the pool of knowledge are also summarized. Chapter 2 provides a detailed theoretical background and fundamental principles on the relevant nonlinear effects in the optical fiber that are responsible for the generation of

pulsed lasers. Various pulsing operation and pulsing techniques are also reviewed in this chapter.

Chapter 3 demonstrates Q-switched fiber lasers based on real saturable absorber and artificial saturable absorber. Real saturable absorbers are included graphene film saturable absorber and fiber saturable absorber, whereas the artificial saturable absorber is based on NPR techniques. The performances of these lasers are compared in terms of threshold pump power, pulse stability, pulse energy and pulse repetition rate and ease of implementation. Besides, multi-wavelength Q-switched fiber laser can also be implemented via graphene saturable absorber combined with NPR technique. This chapter concludes that NPR technique is the simplest and most practical. Therefore, NPR technique is chosen for further exploration in realizing mode-locked fiber laser in the following chapters.

Chapter 4 focuses on the generation of mode-locked fiber laser using NPR technique. In this chapter, various NPR based fiber lasers are demonstrated using dispersion compensation fiber (DCF), single mode fiber (SMF) and photonic crystal fiber (PCF) as the nonlinear medium. A new three switchable operation state mode-locked fiber laser is demonstrated by using DCF. Besides, square pulse mode-locking operation is achieved based on a spool of long SMF. Finally, a multi wavelength mode-locked fiber laser with figure-of-eight cavity is proposed using PCF to slice the mode-locked spectrum.

Chapter 5 focuses on generating dark pulses based on NPR techniques. Three different types of dark pulses are demonstrated, which are included nonlinear Schrödinger equation (NLSE) dark pulse, cubic-quintic nonlinear Schrödinger equation (CQNLSE) dark pulse and domain wall (DW) dark pulse. Furthermore, multi-wavelength dark pulse is achieved using PCF in figure-of-eight cavity to slice the dark pulse spectrum. Besides, Q-switched dark pulse is achieved in an unstable mode-

locking operation, in which the Q-switching operation modulated the dark pulses. Finally, chapter 6 summarizes the findings for this PhD work.

1.4 Contributions

The major contributions of this research work are summarized below:

1. Demonstration Q-switched Erbium-doped fiber laser (EDFL) incorporated graphene saturable absorber in three different gain media. The performance of three different gain media is compared in term of pulse energy, pulse width, pulse repetition rate and threshold pump power.
2. Development of fiber saturable absorber based Q-switched fiber laser. Thulium-doped fiber laser is used to achieve saturable absorption in a EDFL which operated at 1570 nm wavelength.
3. Demonstration of multi-wavelength Q-switched EDFL in figure-of-eight cavity. Graphene saturable absorber is used to generate Q-switched in main loop, whereas PCF is incorporated in second loop to slice the Q-switched spectrum into multi-wavelength operation.
4. Demonstration various mode-locked operation. Mode-locked in three switchable operation, mode-locked square pulse operation and multi-wavelength mode-locked operation are implemented in different types of birefringent nonlinear medium.
5. Development of dark pulse EDFL based on several techniques, which are included NLSE dark pulse, CQNLSE dark pulse and DW dark pulse: NLSE dark pulse generation is based on Kerr nonlinearities, whereas CQNLSE dark pulse generation is based on non-Kerr nonlinearities. Besides, DW dark pulse generation is relied on dual wavelength oscillation.

6. Demonstration of multi-wavelength dark pulse: Dark pulse spectrum is sliced into multi-wavelength operation by using PCF to generate NPR effect in figure-of-eight cavity.
7. Demonstration of Q-switched mode-locking operation in dark regime: Q-switched and dark pulse co-existed in the laser cavity. Q-switched operation modulates the dark pulse to achieve Q-switched mode-locking operation in dark regime.

CHAPTER 2

LITERATURE REVIEW ON PULSE LASER

2.1 Introduction

The generation of laser in 1960s has intensively enhanced the developments for both telecommunication (Aubin et al., 1995) and sensor technology (Giallorenzi et al., 1982). The invention of low loss silica based optical fibers further initiated a revolution in optical fiber communication, and induced the discovery of fiber material and the associated nonlinear optical effects. Nonlinear optical effects are one of the interesting phenomena in optical fiber transmission system. In recent years, many researches had been carried out to study nonlinear optical effects such as Self Phase Modulation (SPM) (Agrawal & Olsson, 1989), Cross Phase Modulation (XPM) (Agrawal, 1987), and Four Wave Mixing (FWM) (Deng et al., 1999). The broad studies of nonlinear effects has further triggered the advancement of knowledge in pulsed fiber laser. Unlike the conventional laser which operates in continuous wave (CW), pulsed lasers can generate optical pulses based on either Q-switching or mode-locking principles. Basically, pulsed laser can operate in two different regimes, which are bright regime and dark regime (Sylvestre, 2002). Dark pulses are normally referred to a train of intensity dips in a cw background of the laser emission. However, most of the pulsed lasers operate in bright regime.

Up to date, many techniques have been proposed and demonstrated to generate pulsed fiber laser based on both active and passive techniques (Keller, 2003). Passive techniques use saturable absorber such as graphene (Bao et al., 2009; Luo et al., 2010), carbon nanotubes (Set, et al., 2004; Im et al., 2010), solid-state fiber, semiconductor saturable absorber mirror (SESAM) (Sutter et al., 1999; Chen et al., 2011) as well as

artificial saturable absorber based on nonlinear polarization rotation (NPR) (Kim, Kutz, & Muraki, 2000; Liu et al., 2008). Among these passive techniques, NPR has attracted the attention from scientists due to low cost and ease of implementation in generation of pulsed laser. The NPR effect occurs in nonlinear fiber due to Kerr effect where different intensity of light will rotate at different angle. This allows NPR effect to work as an artificial saturable absorber to generate pulsed laser.

The main objective of this research aims to study on various pulsed fiber laser generation based on NPR technique. In this chapter, literature reviews on nonlinear effects, Q-switching and mode-locking principles, saturable absorbers and dark pulses are presented.

2.2 Nonlinearity in Optical Fiber

Lasers nonlinear response is a phenomenon which does not obey the superposition principle (Lehmann & Romanini, 1996), or whose output is not directly proportional to its input. To visualize the basic idea of nonlinear response, we may derive it in mathematics form. Consider in a system, response is given by

$$y = a_1x \quad (2.1)$$

where x is the input signal and a_1 is the linear gain of the system. An applied field is given by

$$x = V\cos(\omega t) \quad (2.2)$$

Output is given by

$$y = a_1V\cos(\omega t) \quad (2.3)$$

The output is a faithful representation of input within the linear region. When the applied field increases and goes beyond the system's linear region, the output become distorted due to the nonlinear response and can be written as

$$y = a_1x + a_3x^3 \quad (2.4)$$

The cubic distortion has been chosen for the assumption since in most of the nonlinear optic works, the focus has normally be given to the third order nonlinear effect. By substituting equations (2.2) and (2.3) into (2.4), the output become

$$y = a_1V\cos(\omega t) + a_3V^3\cos^3(\omega t) \quad (2.5)$$

Trigonometric identity given as

$$\cos^3(\omega t) = \left(\frac{3}{4}\right)\cos(\omega t) + \left(\frac{1}{4}\right)\cos(3\omega t) \quad (2.6)$$

From above equation, it is found that the cubic distortion increases a modified response in frequency ω , and also creates a new signal at frequency 3ω .

In optical fibers, the nonlinear response may occur due to an intense applied field. In other word, the nonlinear response in optical fibers relies upon the harmonic motion of bound electron affected by the applied field. In linear region, the response of total polarization, P due the electric field, E can be described as

$$P = \varepsilon_0 X^{(1)} E \quad (2.7)$$

where ε_0 is permittivity of free space and $X^{(1)}$ is linear susceptibility, and it can be shown that

$$X^{(1)} = n^2 - 1 \quad (2.8)$$

where n is the refractive index of the medium. This describes the linear propagation give rise to i) Real part, speed of propagation through the medium, and ii) Imaginary part, absorption in the medium. By expanding the polarization in power series in E , it gives

$$P = \varepsilon_0 (X^{(1)} E + X^{(2)} E^2 + X^{(3)} E^3 + \dots) \quad (2.9)$$

where $X^{(2)}$, $X^{(3)}$ and etc are second and third order nonlinear susceptibilities, respectively. The second order susceptibility $X^{(2)}$ is related to the nonlinear effect such as second harmonic generation and sum-frequency generation. In most of the situation,

optical fiber will not exhibit the second order nonlinear effect due to the immersion symmetry molecule characteristic. Obviously, the lowest order nonlinear effect in fiber is caused by third order susceptibility $X^{(3)}$. Kerr effect is a change of the refractive index changed due to the applied electric field. For Kerr effect in fiber optic, the third order susceptibility $X^{(3)}$ is significant. In Sellmeier equation

$$n^2(\omega) = 1 + \sum_{j=1}^m \frac{B_j \omega_j^2}{\omega_j^2 - \omega^2} \quad (2.10)$$

where B_j is the j th resonance and ω_j is the resonance frequency. Thus, the intensity dependence of the refractive index can be expressed as

$$\tilde{n}(\omega, |E|^2) = n(\omega) + n_2 |E|^2 \quad (2.11)$$

where $|E|^2$ is the optical intensity inside the fiber, n_2 is the nonlinear index coefficient.

n_2 is related to $X^{(3)}$ by

$$n_2 = \frac{3}{8n} \text{Re}(X_{xxxx}^3) \quad (2.12)$$

In this case, refractive index is only affected by X_{xxxx}^3 by assuming the optical field is linear polarized. Nonlinear refraction is responsible for several nonlinear effect, and two most widely studied are self-phase modulation (SPM), cross-phase modulation (XPM) and four wave mixing (FWM) (Alfano & Ho, 1988).

2.2.1 Self-Phase Modulation

Self-Phase Modulation (SPM) is a light intensity dependent phenomenon. When the light travels in a medium, it will induce a varying of refractive index upon the medium. This can be explaining by optical Kerr effect. The variation of the refractive index will produce a phase shift in the pulse, and hence lead the change of the frequency

spectrum of the pulse (Stolen & Lin, 1987). Normalize amplitude $U(z, T)$ can be defined as

$$\frac{\partial U}{\partial z} = \frac{ie^{-\alpha z}}{L_{NL}} |U|^2 U \quad (2.13)$$

where α refer to the fiber losses, and the nonlinear length, L_{NL} can be expressed as

$$L_{NL} = (\gamma P_0)^{-1} \quad (2.14)$$

where γ refer to the nonlinearity and P_0 stands for the peak power. By substituting $U = V \exp(i\Phi_{NL})$ and V remain unchanged along the fiber, a general solution obtain as

$$U(L, T) = U(0, T) \exp[i\Phi_{NL}(L, T)] \quad (2.15)$$

where $U(0, T)$ is the field amplitude when $z=0$ and the nonlinear phase shift, Φ_{NL} as

$$\Phi_{NL}(L, T) = |U(0, T)|^2 (L_{eff}/L_{NL}) \quad (2.16)$$

where L_{eff} is the effective length and define as

$$L_{eff} = \frac{[1 - \exp(-\alpha L)]}{\alpha} \quad (2.17)$$

From above, it shows that SPM causes the intensity dependent phase shift and unchanged upon the pulse shape. The nonlinear phase shift depends on the fiber length, L . By assuming $\alpha=0$ and $L_{eff}=L$, the maximum phase shift occur at the center of pulse, $T=0$, which can be express as

$$\Phi_{max} = \frac{L_{eff}}{L_{NL}} \quad (2.18)$$

Obviously, the nonlinear length is the effective propagation distance when $\Phi_{max} = 1$. In dispersion case, the pulse broadening is observed in time domain, whereas SPM induces spectrum broadening. Hence, the pulse broadening is affected by SPM frequency chirp. It can be expressed as

$$\delta\omega(T) = \frac{2m L_{eff}}{T_0 L_{NL}} (T/T_0)^{2m-1} \exp[-(T/T_0)^{2m}] \quad (2.19)$$

In Figure 2.1, a pulse (top curve) propagating a nonlinear medium and induce a self frequency shifting due to SPM. It shifts to a lower frequency and back to the higher frequency.

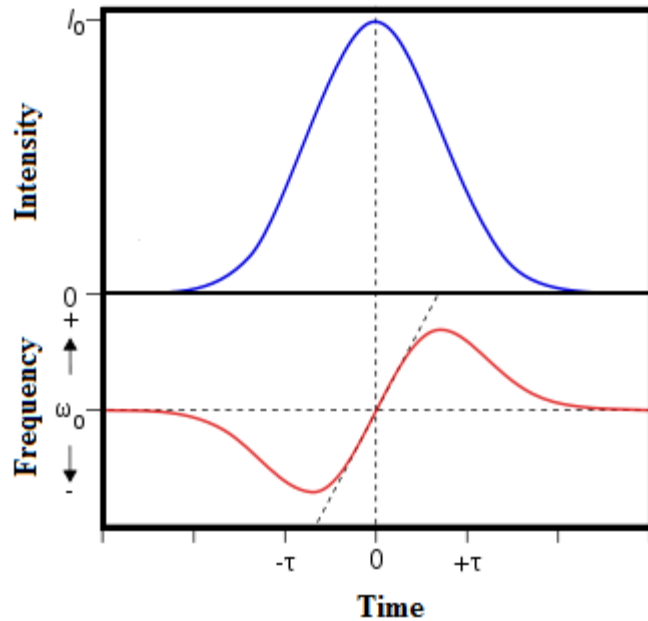


Figure 2.1: Gaussian pulse for the temporal variation of SPM induce phase shift and frequency chirp

2.2.2 Cross-Phase Modulation

Similar with SPM, Cross Phase Modulation (XPM) is another phenomenon due to Kerr effect, which involves the intensity dependent refractive index. In SPM, it only involves single optical field that is propagating inside the fiber, whereas two or more optical field having different wavelengths propagating inside a fiber simultaneously for XPM cases. Hence, in XPM cases, the refractive index not only affected by the optical field itself, but also affected by the co-propagating optical field (Agrawal, Baldeck, & Alfano, 1989). Assume ω_1 and ω_2 are carrier frequencies for two different pulses and E_1 and E_2 are corresponding as the amplitudes for ω_1 and ω_2 . By quasi-monochromatic approximation, different part of electric field can be expressed as

$$E(r, t) = \frac{1}{2} \rightarrow [E_1 \exp(-i\omega_1 t) + E_2 \exp(-i\omega_2 t)] + cc \quad (2.20)$$

Polarization, P_{NL} can be written as

$$\begin{aligned} P_{NL}(r, t) &= \frac{1}{2} \vec{x} P_{NL}(\omega_1) \exp(-i\omega_1 t) + P_{NL}(\omega_2) \exp(-i\omega_2 t) \\ &+ P_{NL}(2\omega_1 - \omega_2) \exp[-i(2\omega_1 - \omega_2)t] \\ &+ P_{NL}(2\omega_2 - \omega_1) \exp[-i(2\omega_2 - \omega_1)t] + cc \end{aligned} \quad (2.21)$$

Notice there's two terms oscillating upon the 2 new frequencies, $2\omega_1 - \omega_2$ and $2\omega_2 - \omega_1$. This is the origin of the four wave mixing (FWM). The main concern in XPM is another 2 terms, which going to affect the refractive index. It can be expressed as $P_{NL}(\omega_k)$, $k=1,2$

$$P_{NL}(\omega_k) = \epsilon_0 \epsilon_k^{NL} E_k \quad (2.22)$$

By combining the linear part, total induce polarization is

$$P(\omega_k) = \epsilon_0 \epsilon_k E_k \quad (2.23)$$

where

$$\epsilon_k = \epsilon_k^L + \epsilon_k^{NL} = (n_k^L + \Delta n_k)^2 \quad (2.24)$$

where n_k^L is the linear part of the refractive index and Δn_k is the different of refractive index due to 3rd order of nonlinear effect. By taking approximation of $\Delta n_k \ll n_k^L$, refractive index for nonlinear part is given as

$$\Delta n_k \approx \frac{\epsilon_k^{NL}}{2n_k} \approx n_2 (|E_k|^2 + 2|E_{3-k}|^2) \quad (2.25)$$

From above, it shows that the refractive index is depending on both of the optical field which co-propagate in the fiber. The intensity dependent nonlinear phase shift as

$$\phi_k^{NL}(z) = \left(\frac{\omega_k}{c}\right) \Delta n_k z = n_2 \left(\frac{\omega_k}{c}\right) (|E_k|^2 + 2|E_{3-k}|^2) z \quad (2.26)$$

The first term from equation above is contributed by SPM, whereas the second term is contributed by XPM. The factor of 2 upon the XPM shows that XPM is twice as effective as SPM in the same intensity.

2.2.3 Four-wave Mixing

Four-wave mixing (FWM) is a type of optical Kerr effect. It can occur when two or more different wavelength optical fields are launched into a fiber. As discussed in XPM, by equation of $P_{NL}(r, t)$, there's two term oscillating in two new frequencies, $2\omega_1 - \omega_2$ and $2\omega_2 - \omega_1$ (Fukuda et al., 2005). This can be visualized in Figure 2.2 in case of two optical fields with different wavelength are launched into a fiber. As shown in Figure 2.2, as two optical fields with different wavelength, ω_1 and ω_2 propagate in a fiber, two sidebands are generated at $2\omega_1 - \omega_2$ and $2\omega_2 - \omega_1$. Generally, the number of sideband generated in the fiber is depended on the number of input optical field wavelengths, N . The number of sideband generated, M is given by

$$M = \frac{N^3 - N^2}{2} \quad (2.27)$$

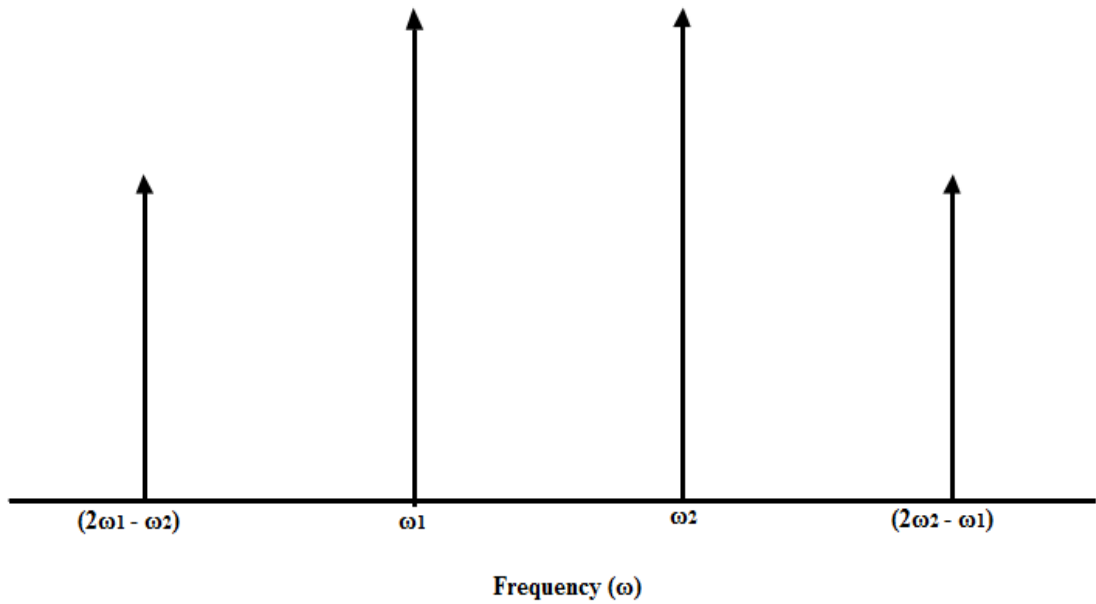


Figure 2.2: Schematic of FWM in frequency domain

2.3 Pulsed Fiber Laser

Pulsed fiber lasers are referring to non CW operation, and optical power appears in pulse train and exhibits certain pulse repetition rate and pulse width. Pulsed fiber laser have been of great interest as they have many applications in telecommunication, remote sensing (Rairoux et al., 2000), signal processing (Stegeman, Hagan, & Torner, 1996) and medicine. Basically, pulsed laser can be categorized based on some important pulse characteristic, such as operation regime, pulse repetition rate, pulsed width and pulse energy. Pulsed laser can operate either in bright regime or dark regime based on intensity direction of the pulse. Furthermore, bright pulses can classify into Q-switching operation and mode-locking operation. The difference between Q-switched and mode-locked can be observed from pulse width, pulse repetition rate and pulse energy.

2.3.1 Q-switching operation

Q-switched is a technique to achieve high energetic short pulses from a laser by modulating the intra-cavity losses (Degnan, 1989). This technique is widely applied for the generation of nanosecond pulses of high energy and peak power. The Q-switched pulse is normally generated when the laser resonator losses are maintained at a high level. Therefore, the lasing cannot be built at that time, and the energy is stored in the gain medium. The amount of stored energy is limited only by spontaneous emission. Moreover, the stored energy can be a multiple of the saturation energy. When the stored energy is saturated, the losses will drop to a low level. Therefore, the power of the laser radiation builds up within a short period of time in the laser resonator. The large intra-cavity power present at that time leads to further depletion of the stored energy after the power decays. The energy of the generated pulse is usually higher than the saturation

energy of the gain medium and can be as high as in mili joule range even for small size lasers. The peak power can be much higher compare to the achievable power in CW operation. Throughout the processes, the Q-switched lasers generate stable pulse trains via repetitive Q-switching operation. The pulse width achieved with Q-switching is typically in the nanosecond range, and usually the pulse repetition rate is higher than the resonator round-trip time. For instance, the pulse repetition rate is typically in the range from 1–100 kHz. Q-switching operation can achieve by active techniques (Zhang et al., 1999) or passive techniques (Zhang et al., 2000).

For active Q-switching, the losses are modulated with an active control element, which are included acousto-optic (Jabczynski, Zendzian, & Kwiatkowski, 2006) and electro-optic modulator (El-Sherif & King, 2003). The pulse is formed based on electronic signal triggered. Commonly, the pulse energy and pulse duration are depending on the energy stored in the gain medium. Therefore, the pulse repetition rate, pulse energy, and pulse width can be controlled by pump power. In the Q-switching operation, the switching time of the modulator is not necessary to be comparable with the pulse duration. This can be explained as the resonator needs to take many round trips time to form a pulse. If the time to form a pulse takes too long, it may lead to multiple pulses or to other instabilities regime. The pulse repetition rate of an actively Q-switched laser can be controlled by the pump power. Higher repetition rates exhibits inversely proportional relationship to pulse energies. If the gain medium cannot recover in time due to very high repetition rates, some pulses may be missing from the pulse train. In the case of low pulse repetition rates, it may obtain short high-energy pulses. The pulse repetition rate is at least of an order of the resonator round-trip time. However, it often substantially longer than round-trip time.

For passive Q-switching, the losses are automatically modulated with a saturable absorber. The pulse is formed when the energy stored in the gain medium has reached

the saturation level. The saturable absorbers have its recovery time. If the recovery time is longer than the pulse duration, it can avoid unnecessary pulse energy lose. However, the recovery time of the absorber should be fast enough to prevent premature lasing when the gain recovers. Recovery time should be between the pulse duration and the upper-state lifetime of the gain medium. Ideally, a saturable absorber should only absorb a minor fraction of the energy of the generated pulses. This can be achieved if the saturation energy of the absorber is below the gain medium. However, significant non-saturable losses are frequently occurred in practical. Thus, practical limitations such as damage thresholds are possible to reduce the saturation energy. Hence, the power efficiency may greatly reduce in most of the practical case. Compared with active Q-switching, passive Q-switching is usually simple and cost-effective. Besides, it is suitable to generate high pulse repetition rates. However, the pulse energies are typically lower. Moreover, passive technique cannot be triggered externally. Furthermore, pulse energy and duration are independent of the pump power.

2.3.2 Mode-locking operation

Mode-locking refers to a process of locking multiple longitudinal modes in a laser cavity (Haus, Namihira, & Razzak, 2012). The pulsed radiation can be achieved when the phases of different modes are forced to be 'locked' to one another. Fixing the phase relationship of multiple longitudinal modes in the laser cavity causes pulsing simply through the periodic constructive interference lined up by the locking of the modes at all other points in time. When the phase relationships are fixed together and achieve a stable condition, it can be interpreted as the Fourier components of a periodic function. The case in which the phases of all the modes oscillating in the laser are locked together produces the narrowest pulse. When a single pulse is propagating a ring

cavity, the period, T , is $T = L/c$ where L is the length of the cavity and c is the speed of light. Similar to Q-switching operation, methods for producing mode-locking in a laser may be classified as either active or passive.

Amplitude modulation and phase modulation are the main techniques to achieve active mode-locking (Jeon et al., 1998). However, active mode-locking is not an ideal solution for generating pulses with pulse width less than 1 ps. This can be explained by the mechanical limitations resulting from using an active modulator (Hudson et al., 2005). These relatively long pulse durations arise from periodically modulating resonator losses or round-trip phase changes at the laser cavity frequency. Various techniques had been used as modulators, which included acousto-optic, electro-optic, Mach-Zehnder integrated-optic and semiconductor electro-absorption modulators. One of the important conditions to achieve the pulse formation is to match between frequency of the modulator and cavity's repetition rate.

Passive mode-locking has been widely used to generate the shortest pulses from fiber lasers. Typically, passive mode-locking relies on semiconductor based saturable absorbers to generate pulse-shaping action. A significant difference between the active and passive mode-locking is whereby passive mode-locking does not need on any physical modulator changing cavity parameters. Passive techniques are faster as they bias the cavity to create pulses as a steady state solution of the laser cavity. The cavity is designed to favor the pulse generation over the continuous wave operation. Passive mode-locking can be achieved with several techniques such as nonlinear polarization rotation (NPR) and by using saturable absorber. The commonly used saturable absorber for the mode-locking are included semiconductor saturable absorber mirror (SESAM), graphene and carbon nanotube (CNT).

2.3.3 Dark pulse operation

Dark pulses are referred to a train of intensity dips in a cw background under a laser emission. A mode-locked laser can produce dark pulses, although dark pulse operating regime is rare. A similar analogy to a dark pulse in a mode-locked laser is a dark soliton. Optical dark solitons are solutions to the nonlinear Schrödinger equation (NLSE) (Serkin & Hasegawa, 2000; Blow & Doran, 1985). The existence of dark solitons can also be identified by a complex Ginzburg-Landau equation (CGLE) (Lega & Fauve, 1997; Triki et al., 2012). The NLSE describes propagation in nonlinear medium such as optical fiber. Dark solitons are revealed to be less affected in the presence of fiber loss and to be more stable in the presence of noise. However, experimental work on dark solitons has been limited due to difficulty of its generation. Several techniques have been proposed and demonstrated to generate a single dark pulse or dark pulse train. Most of the techniques are based on external manipulation of laser light using pulse-shaping techniques. Methods to generate dark pulse are included intensity modulation of a CW laser beam by an electro-optic modulator (Zhao & Bourkoff, 1990), nonlinear conversion of a beat frequency signal in a normal dispersion decreasing fiber (Pitois, Fatome, & Millot, 2002), electro-optic phase modulation in a linear loop mirror (Tang, Shu, & Lee, 2001), and passive filtering of a mode-locked bright pulse train with a spatial mask (Haelterman & Emplit, 1993).

The fundamental of dark pulse generation can be classified into three categories, which are NLSE dark pulse (Tang et al., 2013), Cubic-quintic NLSE (CQNLSE) dark pulse (Crosta, Fratolocchi, & Trillo, 2011; Adib, Heidari, & Tayyari, 2009) and domain wall (DW) dark pulse (Zhang et al., 2011; Zhang et al., 2010). NLSE dark pulse is dependent on the Kerr nonlinearities in the cavity. Different from NLSE dark pulse, CQNLSE dark pulse generation can be generated when the non-Kerr nonlinearities dominated the Kerr nonlinearities in the cavity. On the other hand, DW

dark pulse is based on two or more lases in different wavelengths oscillate and causing the topological defects in temporal domain.

2.4 The Nonlinear Schrodinger Equation

Pulse propagation in a fiber is widely explained by Nonlinear Schrodinger Equation (NLSE). The NLSE can be described in variety of different forms, depending on which approximations are appropriate. The NLSE can be written as

$$\frac{\delta E}{\delta z} - \frac{\beta_2}{2} \frac{\delta^2}{\delta T^2} + \gamma |E|^2 E = 0 \quad (2.27)$$

where E is the complex field envelope, z is the distance, β_2 is the second order dispersion and γ is the nonlinear coefficient. T is the retarded time and expressed as

$$T = \tau - \frac{z}{v_g} \quad (2.28)$$

where τ is the physical time and v_g is the group velocity. Basically, equation above does not provide a complete description for the light propagation in optical fiber. With the incorporation of the effect of fiber loss, third order dispersion (TOD) and dispersion, a more realistic model of light propagation in optical fiber can be visualized as

$$\begin{aligned} \frac{\delta E}{\delta z} + \alpha E + i\beta_2 \omega_0 \frac{\delta^2 E}{\delta T^2} - \left(\frac{\beta_3(\omega_0)}{6} \right) \left(\frac{\delta^3 E}{\delta T^3} \right) = \\ i\gamma \left[|E|^2 E + (i/\omega_0) \frac{\delta(|E^2|E)}{\delta T} - \rho\tau_{R1} \frac{(\delta|E^2|)}{\delta T} E \right] \end{aligned} \quad (2.29)$$

On the left hand side, the first term is the electric field, which varies with the change of fiber length. In the second term, α govern the fiber loss. Third term accounts for first order group velocity dispersion (GVD). Fourth term is referring to the second order group velocity dispersion. On the right high side of the equation, the first term is

referring to SPM. Self-steeping effect is governed by second term. The intra-pulse Raman scattering effect is represented in the last term.

2.5 Saturable Absorber

Saturable absorption is a characteristic of materials to absorb light, in which the absorption of light exhibits an inversely proportional relationship to the light intensity. Most of the materials exhibit certain saturable absorption ability. However, in most of the materials, saturable absorption can be observed only with very high optical intensity. From solid state theory point of view, atoms in the ground state of a saturable absorber material can be excited into an upper energy state with sufficiently high incident light intensity. If under a rate that there is insufficient of time for atoms to decay back to the ground state before the ground state is depleted, subsequently the saturable absorption formed. Saturable absorbers had been widely used to generate pulses in laser cavity. Some important characteristic of a saturable absorber are included absorption wavelength range, recovery time, saturation intensity and fluence.

2.5.1 Artificial Saturable Absorber with Nonlinear Polarization Rotation

In fiber lasers, nonlinear polarization rotation (NPR) is a technique which had been widely used as an artificial saturable absorber (Ippen, 1994 ; Luo et al., 2011). The working principle of this technique is based on the fact that the nonlinear medium rotates the azimuth of the elliptically polarized light in proportion to the light intensity. Different light intensity experience different angles of rotation after propagate through a nonlinear medium. Since there is an intensity dependent polarization in the pulse, a polarizer converts this into an intensity dependent transmission. This method can be

controlled to choose the high intensity parts of the pulse to propagate while suppressing the low intensity parts (Matsas et al, 1992).

The fundamental principle of NPR is rooted upon the principle of the intensity-dependent nonlinear refractive index which causes a rotation of the polarization of the pulses (Salhi, Leblond, & Sanchez, 2003). The amount of rotation is nonlinear in that it relies on the change of refractive index according to the light intensity. Figure 2.3 shows the basic components that are needed to induce NPR. The basic components are included polarization controller (PC), nonlinear medium and polarizer.

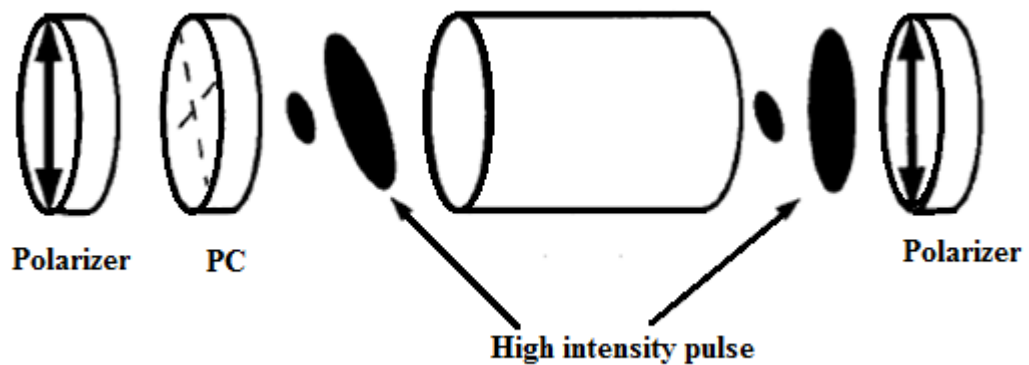


Figure 2.3: Evolution of non-linear polarization rotation

The oscillation light propagates through a polarization beam splitter (PBS) prism or polarizer to become a linearly polarized light. And after the linearly polarized light passed through a polarization controller, it will become an ellipse polarized light. The ellipse polarized light can be further divided into two mutually perpendicular linear polarized lights, which are A_x and A_y . The two beams linear polarized light of A_x and A_y propagate in optical fiber. The two polarization direction accumulated different nonlinear phase shift due to the nonlinear effects such as SPM and XPM phenomenon. In the output the pulse is the synthesis of A_x and A_y which has experienced different

nonlinear phase shift (Song, et al., 2009). By controlling the wave plates at the back end of the fiber, we can obtain the desired condition that the different power of pulse has difference loss when propagate through the PBS. The state-of-polarization of the light experienced a rotation as it propagates in a nonlinear medium due to the Kerr effect (Xu, et al., 2008). The angle of rotation exhibits directly proportional relationship to the light intensity. High intensity light will accumulate different nonlinear phase shift compared to the low intensity light (Nelson, et al., 1997). Therefore, with proper controlled of the polarization in the cavity, high intensity light will propagate through, whereas the low intensity light is blocked. The combination of polarizer and PC acts as a polarization dependent loss element. The transmittivity of this structure can be represented as:

$$T = \cos^2 \alpha_1 \cos^2 \alpha_2 + \sin^2 \alpha_1 \sin^2 \alpha_2 + \frac{1}{2} \sin 2\alpha_1 \sin 2\alpha_2 \times \cos (\Delta_{\phi L} + \Delta_{\phi NL}) \quad (2.30)$$

where

$$\Delta_{\phi} = \frac{2\pi L}{\lambda} (n_y - n_x)$$

$$\Delta_{\phi} = \frac{2\pi L n_2 P}{3A_{eff} \lambda} \cos 2\alpha_1$$

$\Delta_{\phi L}$ is the linear phase shift resulting from modal birefringence, $\Delta_{\phi NL}$ is the nonlinear phase shift in which the magnitude is the summation of SPM and XPM. n_x and n_y are the refractive index of the respective fast and slow axes of the optical fiber. L is the length of the optical fiber between PC 1 and PC 2, which is approximately equal of the laser cavity length. λ is the operating wavelength, n_2 is the nonlinear (Kerr) coefficient and P is the instantaneous peak power of the input signal.

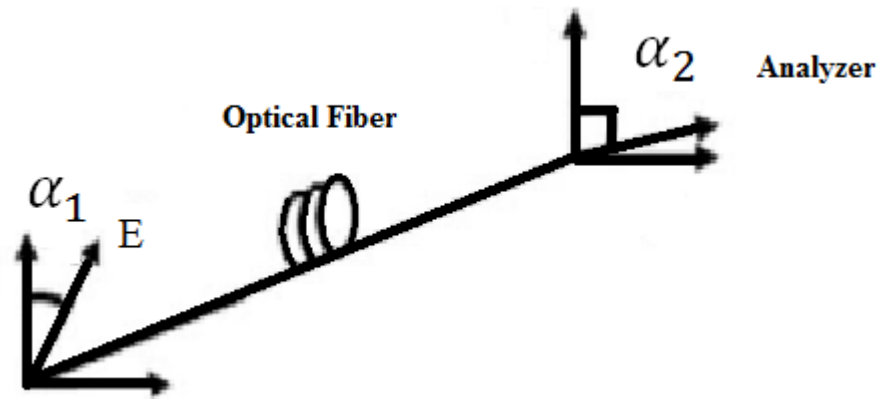


Figure 2.4: Transmittivity of NPR

Fig. 2.5 shows the simplest configuration of a NPR based ring fiber laser, where a polarization dependent isolator (PDI) is incorporated in the cavity to function as an artificial saturable absorber with the help of two PCs. A piece of Erbium-doped fiber, which is pumped by a pump laser via a wavelength division multiplexer (WDM), is used as the gain medium to provide lasing at 1550 nm region. The pump laser functions to create a population inversion by exciting the Erbium ion from ground state to the excited state. The amplified spontaneous emission (ASE) is generated when the Erbium ions drop to the ground state to release energy through a spontaneous emission. The ASE oscillates in the ring cavity to generate laser. An optical isolator also functions to ensure unidirectional operation of the laser. As discussed earlier, PC in combination with a polarizer (in this case PDI), are used for achieving NPR for mode-locking pulse train generation.

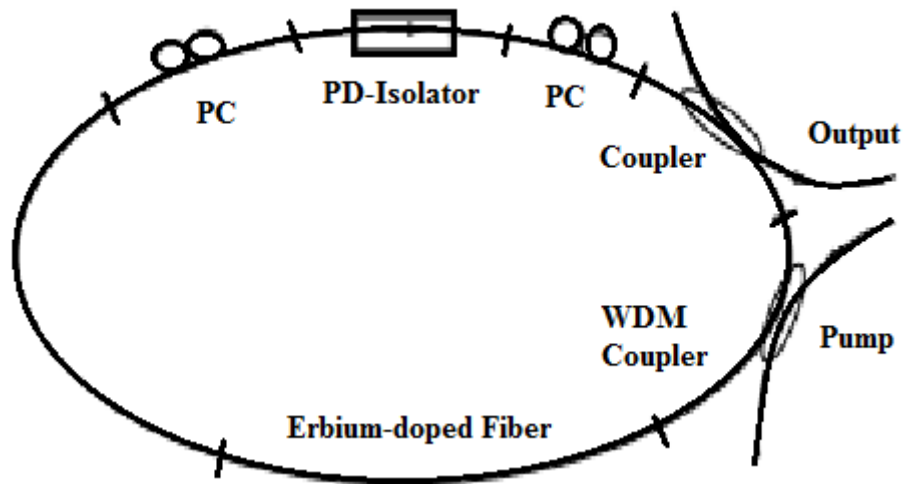


Figure 2.5: Basic configuration of NPR in ring cavity

2.5.2 Artificial Saturable Absorber with Nonlinear Optical Loop Mirror

Additive pulse mode-locking (APM) or coupled cavity mode-locking (CCM) achieves fast saturable absorber action by exploiting the Kerr effect in an interferometric configuration. The principle of APM is pulse shortening by coherent addition of two versions of the same pulse, one of which passed through a Kerr medium. Fig. 2.6 illustrates the working principle of a typical APM coupled cavity laser. The fiber in the feedback cavity acts as the Kerr medium and the coherent addition takes place at the output beam splitter. The pulse returning from the feedback cavity into the main cavity is constructively/destructively interfering with those pulses that are already in the main cavity. By properly adjusting the cavity parameters, it is possible to create a situation such that there is constructive interference near the peak of the pulses but destructive interference in the wings. This is possible because the peak and wings of the pulse acquire a different nonlinear phase shift in the fiber. Thus the peak of the circulating pulse can be enhanced while the wings are attenuated, which

essentially shortens the pulse. This approach can be realized using two coupled resonators such as figure-of-eight lasers.

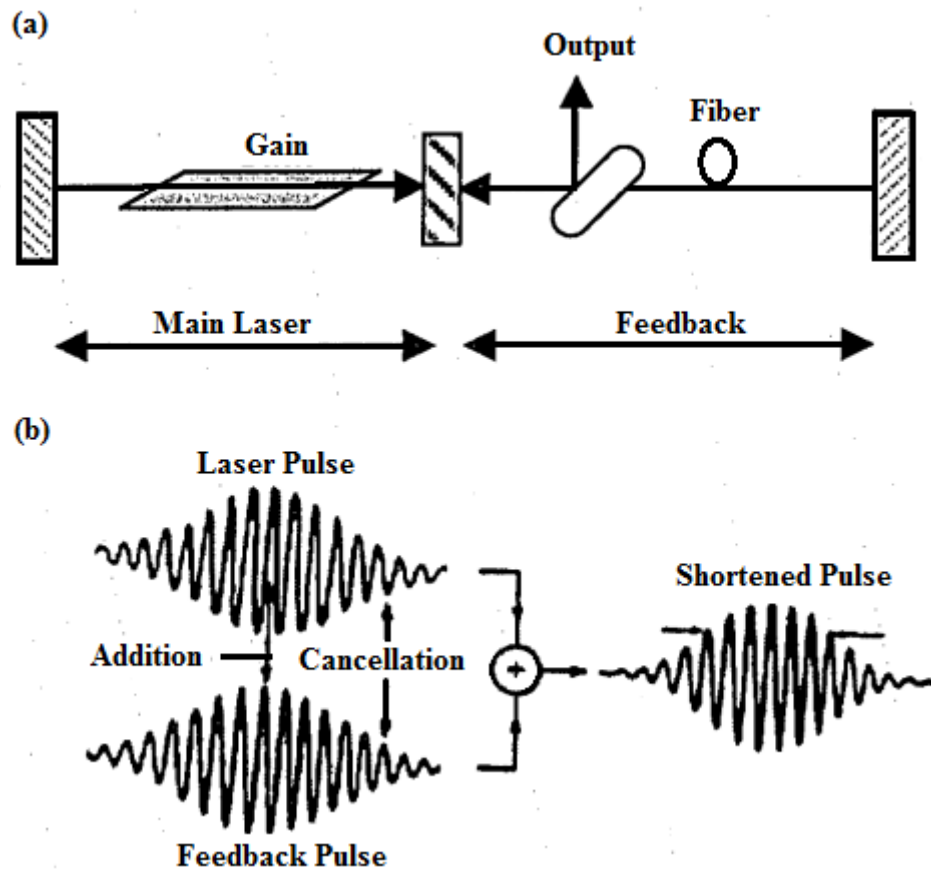


Figure 2.6: Working principle of APM (a) a typical APM coupled cavity laser (b) The pulse of main cavity adds to the pulse of the auxiliary cavity to result in a shortened pulse at the output of beam splitter.

A fiber Sagnac interferometer can be added into a ring cavity to construct a figure-of-eight fiber lasers. There are two main types of Sagnac interferometers; the nonlinear-optical loop mirror (NOLM) (Doran & Wood, 1988; Ilday, Wise & Sosnowski, 2002) and the nonlinear-amplifying loop mirror (NALM) (Fermanm et al., 1990). They are employed in numerous applications such as optical switching and mode-locking of fiber lasers. Fig. 2.7 shows a simple NOLM, which consists of a 2x2 directional fiber coupler with two output ports connected by a length of optical fiber. Two PCs can also be incorporated inside the loop to adjust the polarization of the

oscillating light, which affects the cavity parameters. The counter propagation of light in NOLM is mismatched in intensity by an uneven splitting due to the coupler. With a sufficiently high intensity of light, significant differential phased shift will be generated between both of the counter propagating fields due to the nonlinear index of the fiber. The phase shift in the loop mirror is light intensity dependent. If a certain phase shift is attained, the loop mirror will become totally transmissive. Therefore, the increase of transmission with the intensity of light causes the NOLM acts as a fast saturable absorber.

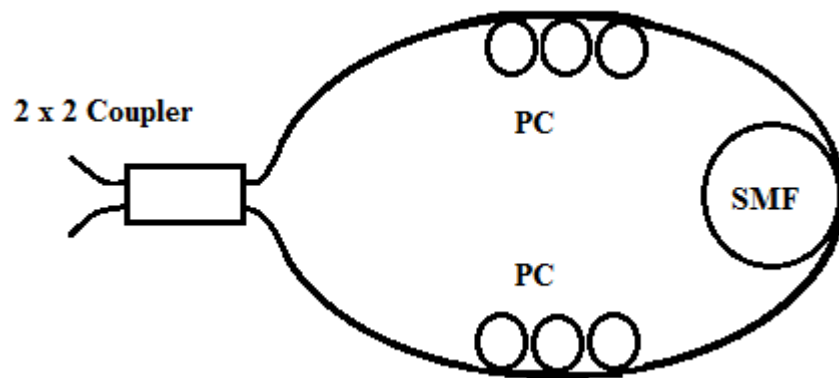


Figure 2.7: Basic configuration of NOLM

2.5.3 Film Saturable Absorber

Q-switched and mode-locked fiber lasers can be realized by using either passive or active techniques. The passive techniques have been intensively investigated in recent years using various types of saturable absorbers (SAs) such as single wall carbon nanotubes (SWCNTs) (Yu et al., 2014 ; Going et al., 2012), graphene (Baek et al., 2012), graphene oxide (GO) (Chen et al., 2014) and reduced graphene oxide (rGO) (Pan et al, 2014). SWCNTs are simple and cost effective. However, the operating wavelength of lasers employing SWCNTs is determined by diameters of the individual nanotubes and this limitation is a constraint on their operation and tenability (Gao et al, 2003). On

the other hand, graphene based SAs have shown outstanding potential for both Q-switching and mode-locking applications due to their high saturable absorption rates and ultrafast recovery times (Martinez & Sun, 2013). Many approaches such as aerosol spraying (Zhu et al, 2009), chemical vapor deposition (Kong, Cassell, & Dai, 1998) and polymer composite methods have been proposed to fabricate SAs using graphene and CNT. Among these techniques, the polymer composite methods are the simplest. It is required to incorporate a host material to make the SA into film form. Typically, polyethylene Oxide (PEO) and polyvinyl alcohol (PVA) polymer are used for the host polymer material. Figure 2.8 shows a basic configuration of pulsed laser using film saturable. Film saturable absorber can be inserted into the ring cavity by sandwiching it between two fiber connectors. In this thesis, various Q-switched fiber lasers are demonstrated using a film based SAs. These Q-switched fiber lasers have been of great interest as they have many applications in telecommunication, remote sensing, signal processing and medicine. Films based saturable absorbers are attractive due to compactness, simplicity and flexibility in construction.

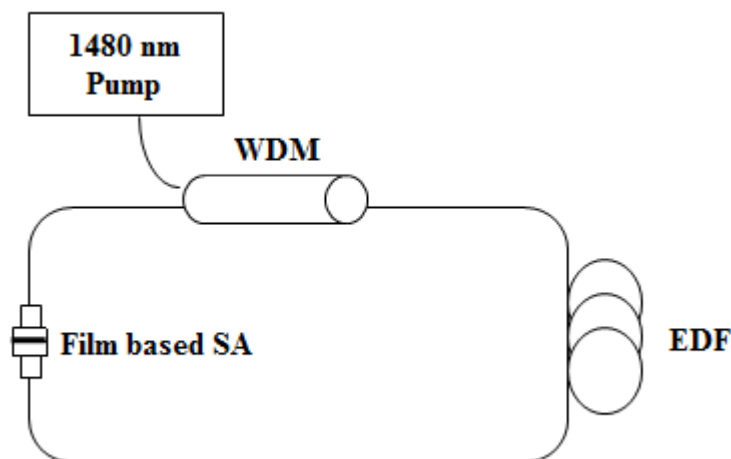


Figure 2.8: Basic configuration of film saturable absorber

CHAPTER 3

DEVELOPMENT OF PASSIVE Q-SWITCHED ERBIUM-DOPED FIBER LASER

3.1 Introduction

Q-switched Erbium-doped fiber lasers (EDFLs) have been of great interest as they have many applications in telecommunication, remote sensing, signal processing and medicine. They are normally realized by active or passive techniques. Actively Q-switched techniques usually involve external mechanical devices such as chopper wheel, shutter and modulator (Cordova-Plaze, Dignonnet, & Shaw, 1987; Eichler et al., 1996). On the other hand, passively Q-switched techniques are commonly realized with saturable absorbers (SAs) (Zhang et al., 1997). In a laser cavity, SA can store energy until it reached a saturation level. When SA goes beyond the saturation level, it will release the stored energy and form a Q-switched pulse. Compared to active techniques, passive Q-switched fiber lasers are more attractive due to compactness, simplicity and flexibility in construction.

In this thesis, passively Q-switched fiber lasers are demonstrated using various SAs. Firstly, the Q-switching operation in EDFL is investigated for three different types of gain medium by using a homemade graphene film as a SA. Next, a new approach for generating Q-switching pulse train is proposed and demonstrated using a solid state Thulium-doped fiber (TDF) as a SA. An artificial SA by nonlinear polarization rotation (NPR) technique is also proposed and demonstrated for Q-switching. Finally a multi-wavelength Q-switched EDFL is demonstrated based on NPR effect using a graphene film SA as a Q-switcher.

3.2 Q-switched EDFL with graphene based SA

Graphene based SAs have shown outstanding potential for both Q-switching and mode-locking applications due to their high saturable absorption rates and ultrafast recovery times (Bonaccorso et al., 2010). Moreover, they are easier to fabricate and less complex to operate. Many approaches such as aerosol spraying, chemical vapor deposition and polymer composite methods have been proposed to fabricate the Graphene based SA (Huang et al., 2012). Among these techniques, the polymer composite methods are the simplest. In this section, we experimentally demonstrate the generation of Q-switching pulse in EDFL using a graphene embedded in polymer composite as SA.

3.2.1 Fabrication and characterization of Graphene based SA

The Polyethylene Oxide (PEO) is used for the host polymer material because it can be dispersed easily in water, making the fabrication process easier. Furthermore, it has the advantage of a lower melting point as compared to the typically used polyvinyl alcohol (PVA) and having no adverse effects. The saturable absorber was made of graphene flakes, which were obtained from electrochemical exfoliation process. In this process, a constant voltage difference of 20 V was applied to two electrodes (graphite rods), which were placed 1 cm apart in an electrolysis cell filled with electrolyte (1% SDS in deionized water). Hydroxyl and oxygen radicals were generated from electrolysis of water at the electrodes during electrochemical process. Then oxygen

radicals started to corrode the graphite anode. This was followed by intercalation of anionic surfactant and finally graphene sheets were created in the solution. In our work, black sediments (graphene) started to peel off from the anode after several minutes. The exfoliation process continued for 2 h until a stable graphene suspension in SDS solution was observed. The stable graphene suspension was centrifuged at 3000 rpm for 30 min to remove large agglomerates. Afterward, supernatant portion of the suspension was decanted. Concentration of centrifuged graphene was estimated from the weight of suspension used. To fabricate the composite, 1 g of polyethylene oxide (PEO) ($M_w = 1000000 \text{ gmol}^{-1}$) was dissolved in 120 ml of deionized water. The graphene solution obtained from electrochemical exfoliation was then mixed with PEO solution at ratios of 1:5 (graphene: PEO) in ml respectively. The solution was dried in petri dish at 56°C to obtain a film with $50 \mu\text{m}$ thickness. Raman spectroscopy was performed to confirm the presence of graphene layer in fabricated thin film using laser excitation at 532 nm (2.33eV) with an exposure time of 10 s. The detector was a charge-coupled device (CCD) camera.

Figure 3.1 shows Raman spectrum of graphene film sandwiched between two fiber ferrules. Three prominent peaks are located at approximately 1351 cm^{-1} , 1617 cm^{-1} and 2911 cm^{-1} , generally known as D, G and 2D band, respectively. The G band contributes to an E_{2g} mode of graphite and is related to the in-plane vibration of sp^2 -bonded carbon atoms, while D band is associated with vibrations of carbon atoms with sp^3 electronic configuration of disordered graphite. The intensity ratio of the D and G bands of graphene sheets is about 1.2, indicating defects in graphene samples. However, the amount of structural defects is not large since the D peak is not very broad. Intensity ratio between G and 2-D peak can be used to determine the number of graphene layer. It was reported that single-layer graphene has a low intensity ratio, usually lower than 0.5 while multi-layer graphene shows higher intensity ratio (≥ 1). As indicated in Figure 3.2,

we obtained a G/2-D peak ratio of 3.2, which indicates that we had multi-layer graphene on the fabricated film. Shape of 2-D peak can also be used to estimate number of graphene layers. As graphene layer increases, full-width half maximum (FWHM) of 2-D peak follows. As also shown in Figure 3.1, FWHM for G and 2D peaks are obtained at 39 and 67 cm^{-1} , respectively. From the intensity ratio of G and 2-D peaks and their FWHM, it can be inferred that number of graphene layers are more than four. Weak 2D peak is due to multi-layered graphene, which significantly decreases the relative intensity.

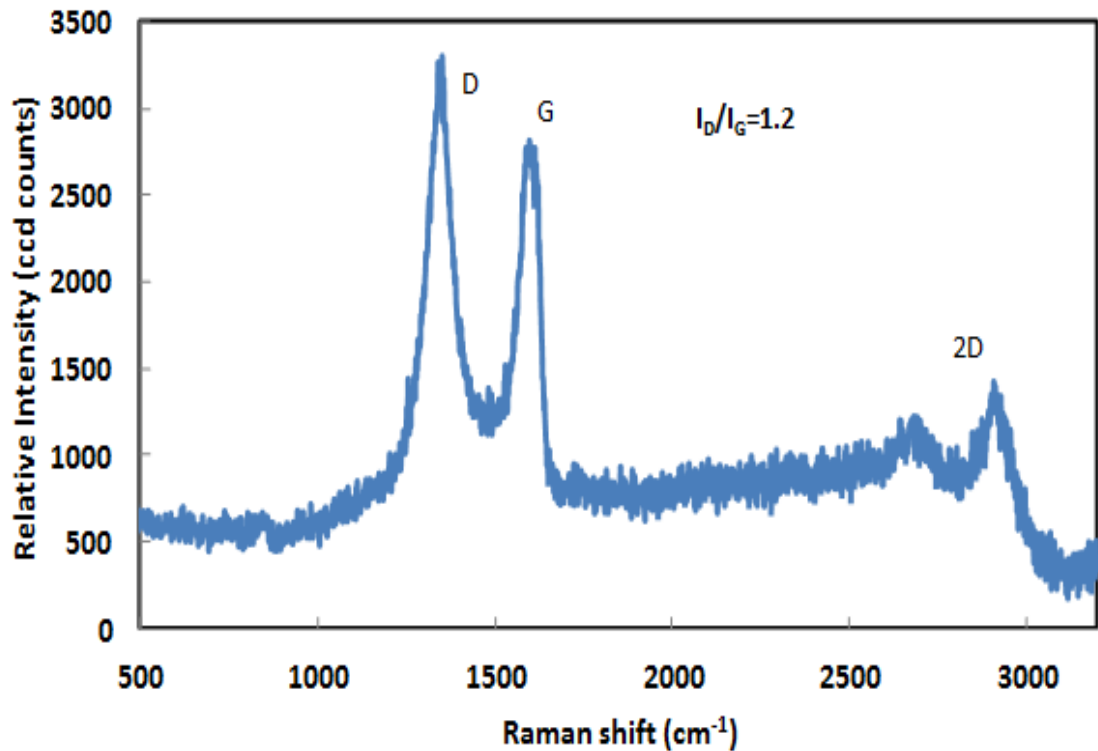


Figure 3.1: Raman spectrum of the fabricated SA

3.2.2 Experimental setup

Experimental set-up of proposed EDFL was illustrated in Figure 3.2 where the ring resonator consisted of a piece of EDF as the gain medium, wavelength division multiplexer (WDM), isolator, a graphene film based SA and 10 dB coupler. The SA was

fabricated by cutting a small part of the earlier prepared film ($2 \times 2 \text{ mm}^2$) and sandwiching it between two FC/PC fiber connectors, after depositing index-matching gel onto the fiber ends. The measured insertion loss and modulation depth of the SA were approximately around 2 dB and 2.6 % at 1550 nm. A 1480 nm laser diode was used to pump the EDF via the WDM. An isolator was incorporated in the laser cavity to ensure unidirectional propagation of oscillating laser. Output of the laser was collected from the cavity via a 10 dB coupler which retains 90% of light in the ring cavity to oscillate. Optical spectrum analyser (OSA, Yokogawa, AQ6370B) was used for spectral analysis of Q-switched EDFL with a spectral resolution of 0.02 nm whereas oscilloscope (OSC, Tektronix, TDS 3052C) was used to observe the output pulse train of Q-switched operation via a 1GHz bandwidth photo-detector. The performance of the laser for three different media was investigated. The media tested were 7 m long standard silica EDF with Erbium ion concentration of 400 ppm, 4.5 m long highly doped silica EDF with 2000 ppm Erbium ion concentration and 0.5 m long Bismuth EDF with Erbium ion concentration of 3000 ppm.

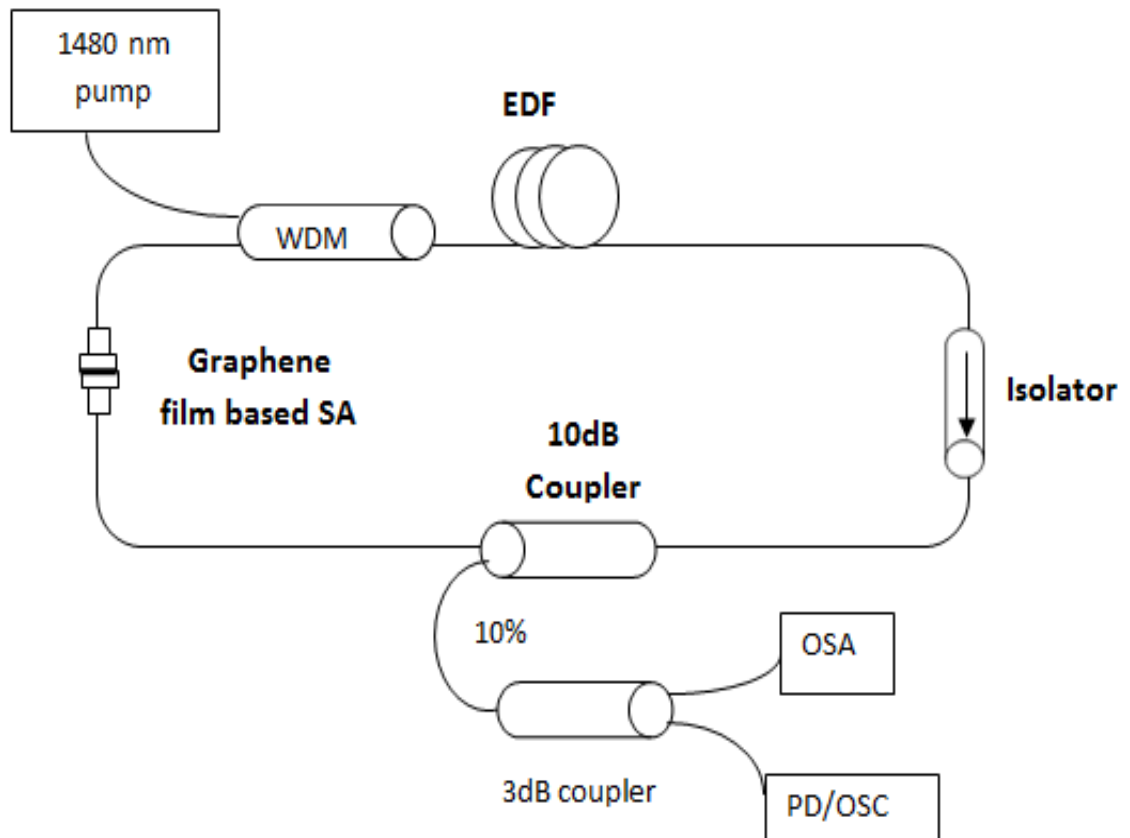


Figure 3.2: Schematic configuration of the Q-switched EDFL

3.2.3 Comparison of Q-switching performance at three different gain media

The Q-switching performance for the three different EDFLs is investigated by slowly increasing the 1480 nm pump power until a stable Q-switching pulse train is observed after the the pump power exceeds the lasing threshold. Stable and self-starting Q-switching operation is obtained at pump power thresholds of 33.7 mW, 98.5 mW and 59.5 mW for the EDFLs configured with 400 ppm silica EDF, 2000 ppm silica EDF and 3000 ppm Bismuth EDF, respectively. There is no lasing below the threshold pump power. Figure 3.3 shows the output spectra of these lasers at the threshold pump power. For 7 m long EDF with 400 ppm concentration, laser exhibits the lowest threshold pump power and operates at 1529 nm instead of 1559 nm. This is attributed to the length of the fiber which is reasonably short for 400 ppm Erbium concentration which resulted in insufficient population inversion for lasing at longer wavelength region. The

amount of Erbium ions increase by using higher concentration EDF (2000 ppm and 3000 ppm) and it absorbs the shorter wavelength photons to increase the population inversion at 1559 nm region. Since the loss is lower at longer wavelength region, lasing is initiated in this region which has a higher net gain. Output power is highest with Bismuth EDF since it provides the highest gain when it is pumped by 1480 nm laser diode. Spectral broadening is also observed especially with the silica EDF due to self-phase modulation (SPM) effect in the ring cavity.

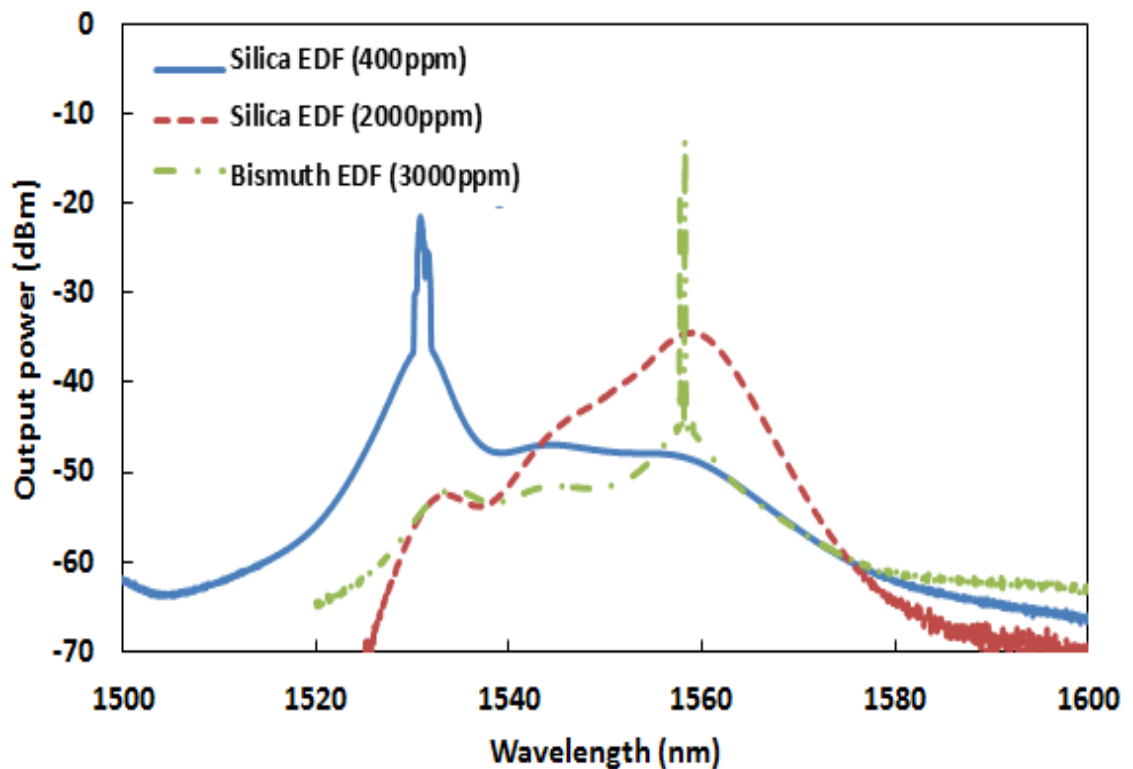


Figure 3.3: Optical spectrum of the Q-switched EDFLs when the pump is fixed at threshold power

In a passively Q-switched laser, cavity loss is modulated by the SA whose transmission/reflection depends on the light intensity. Basically, pulse is released when the cavity energy reaches a certain value determined by the absorber saturation fluence. Pulse repetition rate and pulse width therefore depend on the stored energy or pump power as described in Q-switching theory. Figures 3.4 and 3.5 show the repetition rate and pulse width, respectively against pump power for all three EDFLs. Repetition rate

of all Q-switched EDFLs has a monotonically increasing, near-linear relationship with pump power. On the other hand, pulse width of all EDFLs is inversely proportional with pump power, where the pulse duration becomes shorter as the pump power increases as shown in Figure 3.5. For instance, when the pump power is tuned from 59.5 to 107.9 mW, pulse train repetition rate varies from 22.5 to 57.3 kHz for EDFL configured with the Bismuth EDF. Meanwhile, pulse width of Bismuth EDFL drops from 5.01 μ s to 2.48 μ s. Pulse width is expected to decrease further if pump power can be augmented beyond 107.9 mW as long as it is still kept below the damage threshold of the graphene based SA. The shortest pulse width of 2.48 μ s is obtained with the EDFL configured with 0.5 m long Bismuth EDF. This is attributed to total cavity length used, which is shorter than the ones in the other two EDFLs configured with silica EDF. Laser from the 2000 ppm silica EDF displays the widest pulse width tunability whereby it can be tuned from 12.03 μ s to 4.58 μ s by varying pump power from 98.5 mW to 125.0 mW.

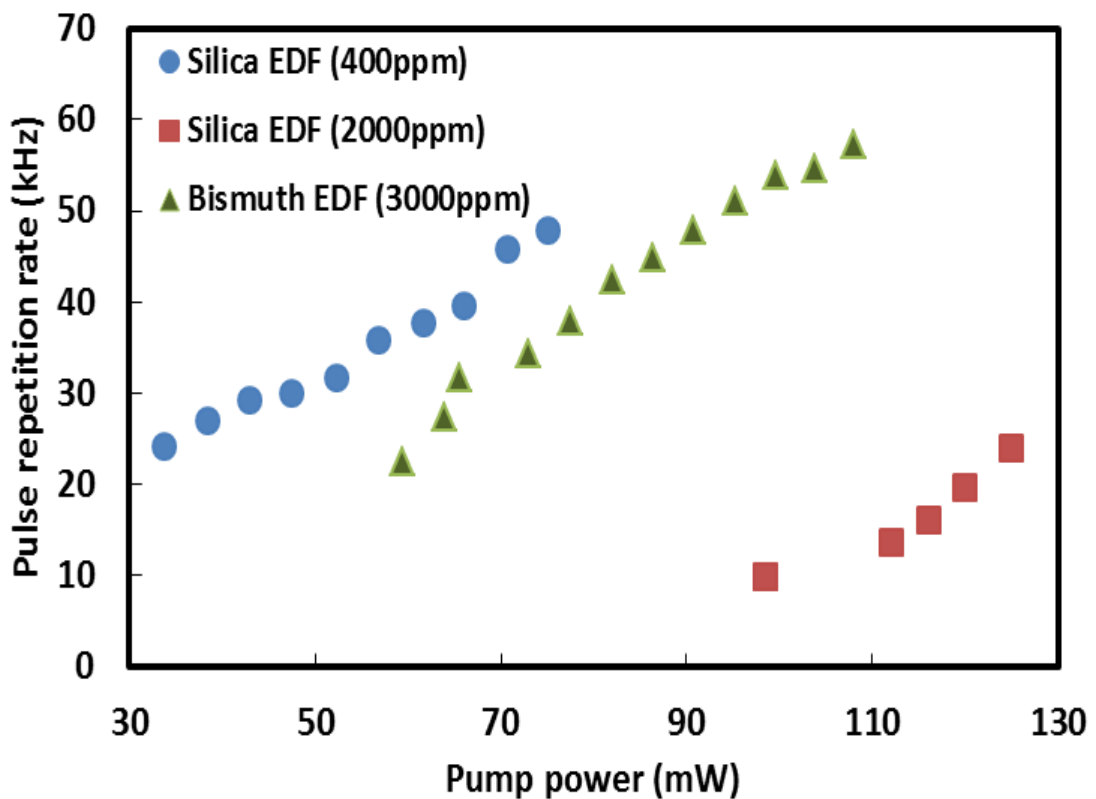


Figure 3.4: Pulse repetition rate against pump power for the EDFL configured with three different EDFs

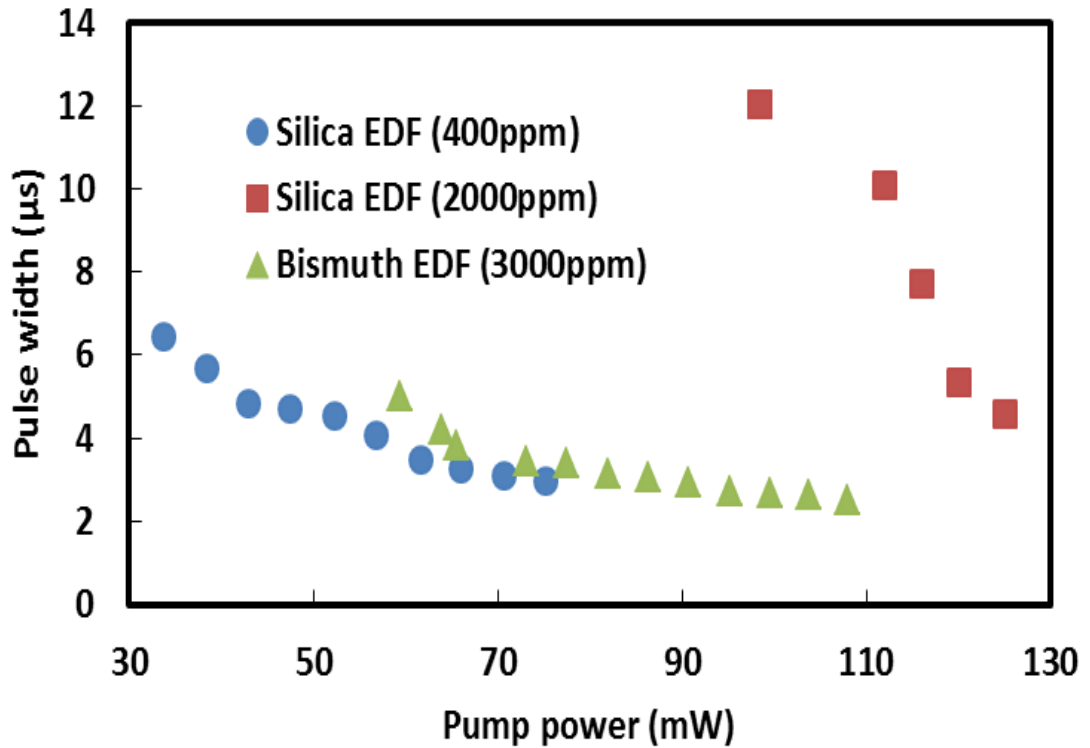
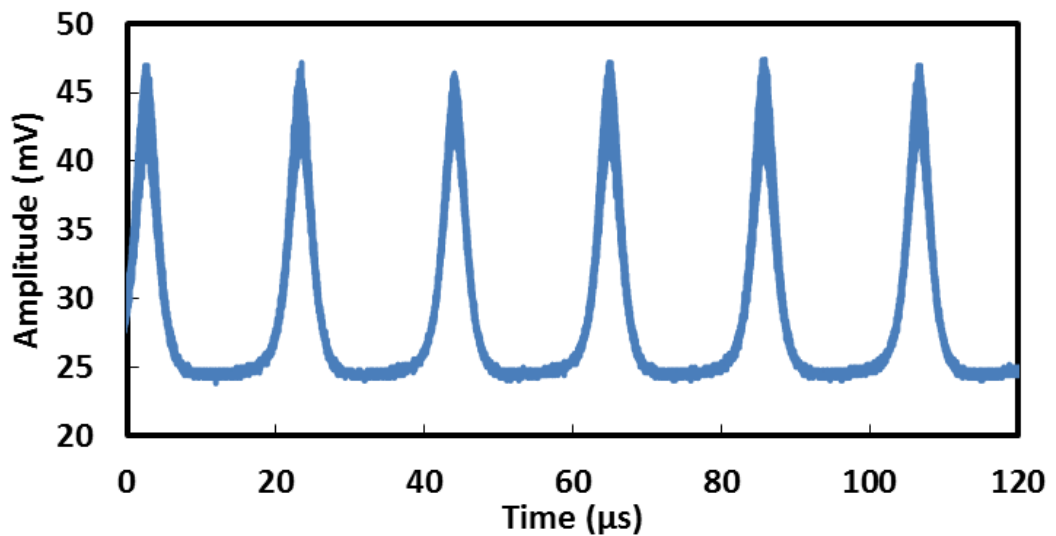


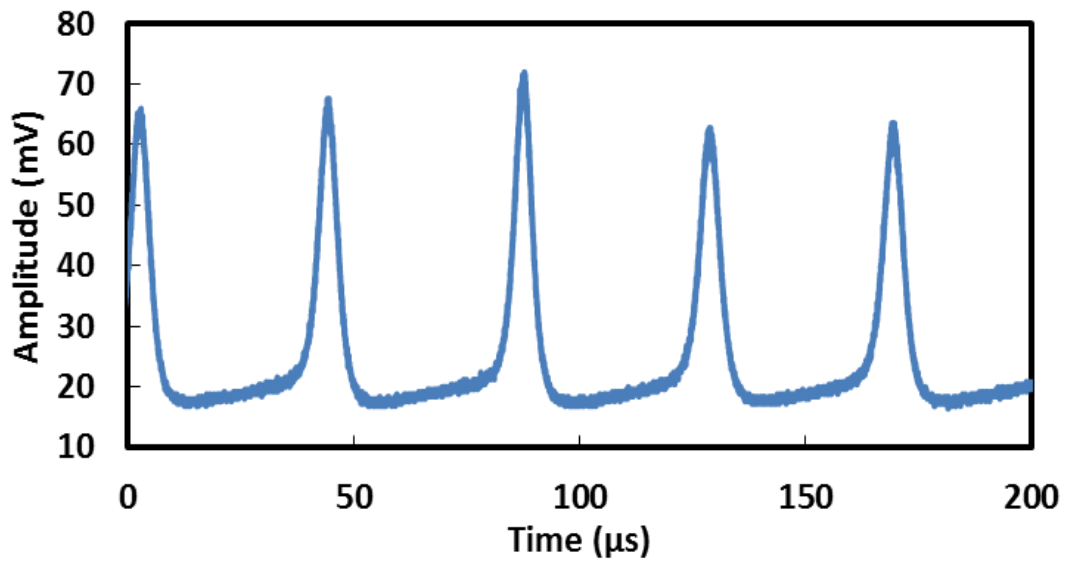
Figure 3.5: Pulse width versus pump power for the EDFL configured with three different EDFs

Figures 3.6 (a) - (c) show oscilloscope traces of Q-switched pulse train for EDFLs with 400 ppm, 2000 ppm and 3000 ppm EDFs, respectively at its highest repetition rates. There is no distinct amplitude modulation in each Q-switched envelop spectrum, which indicates that self-mode locking effect on Q-switching is weak. The highest repetition rate of 57.3 kHz is obtained with Bismuth EDF as pump power is fixed at 107.9 mW. Figure 3.7 and Figure 3.8 show the average output and pulse energy, respectively versus pump power for all EDFLs. As shown in Figure 3.7, the output power increases linearly with pump power for all EDFLs. For instance, the average output power of Bismuth EDFL increases from 372 μW to 788 μW as pump power increases from 59.5 to 107.9 mW. The slope efficiencies of 0.9%, 0.6% and 0.9% are obtained for Q-switched EDFL configured with 400 ppm, 2000 ppm and 3000 ppm, respectively. On the other hand, pulse energy shows an increasing trend with pump power for EDFL configured with 400 ppm EDF while the pulse energy of the two

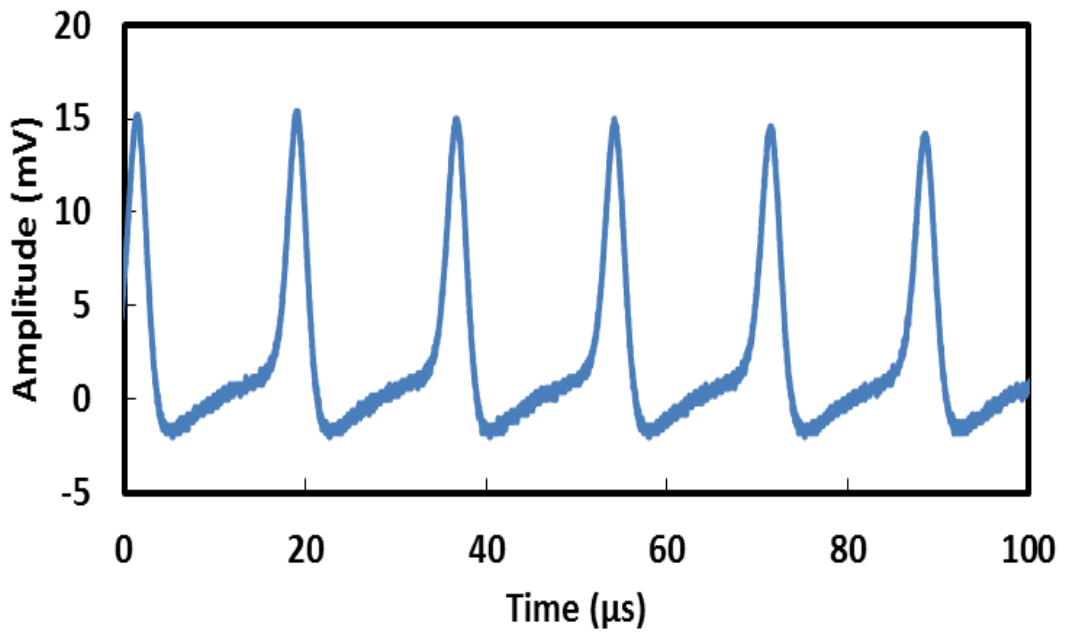
highly doped EDFs exhibits the opposite trend. It is also observed that pulse energy of EDFs with Erbium concentrations of 400 ppm and 3000 ppm are almost constant and difference of the maximum and minimum pulse energy is less than 3 nJ. For 2000 ppm silica EDF, the pulse energy of the Q-switch EDFL drops from 40.69 nJ to 22.74 nJ as pump power increases from 98.5 mW to 112 mW. This is predictable due to efficiency of this laser is lowest as shown in Figure 3.7. This laser exhibits a slow increasing rate of output power against pump power. However, pulse energy is directly proportional to the ratio of output power over repetition rate. Thus, this laser shows significantly decreasing pulse energy. Pulse energy performance of all tested lasers could be improved by reducing insertion loss of SA and optimizing the laser cavity. The performances of these lasers are summarized in Table 3.1.



(a)



(b)



(c)

Figure 3.6: Pulse train of maximum pulse repetition rate at three different gain medium (a) Silica EDF (400 ppm) (b) Silica EDF (2000 ppm) and (c) Bismuth EDF (3000 ppm)

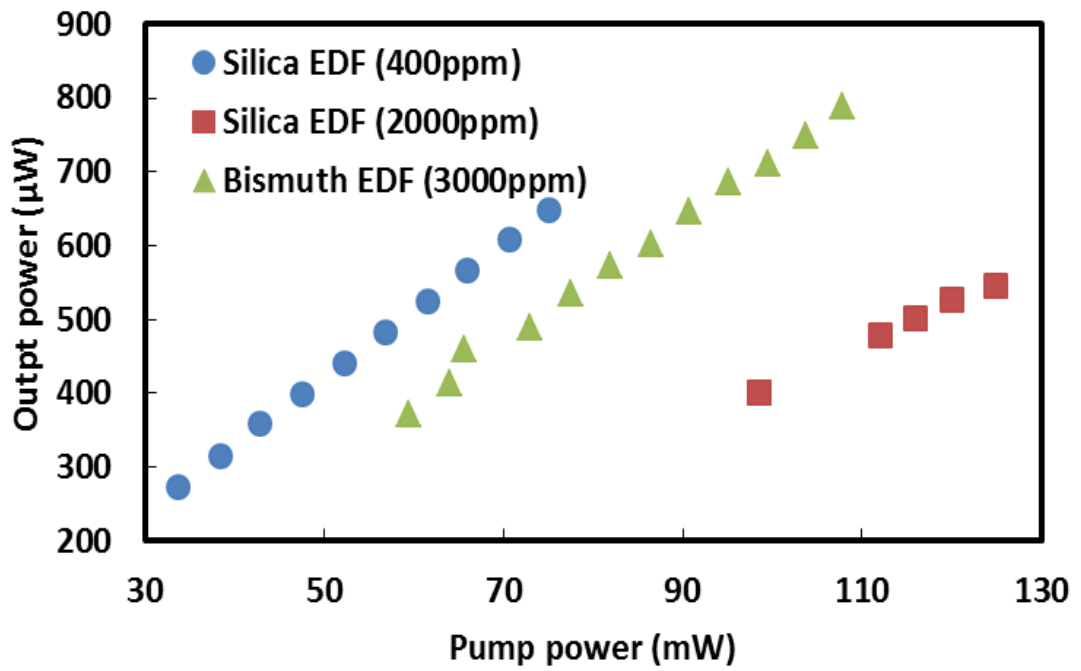


Figure 3.7: Output power against pump power for three different gain medium

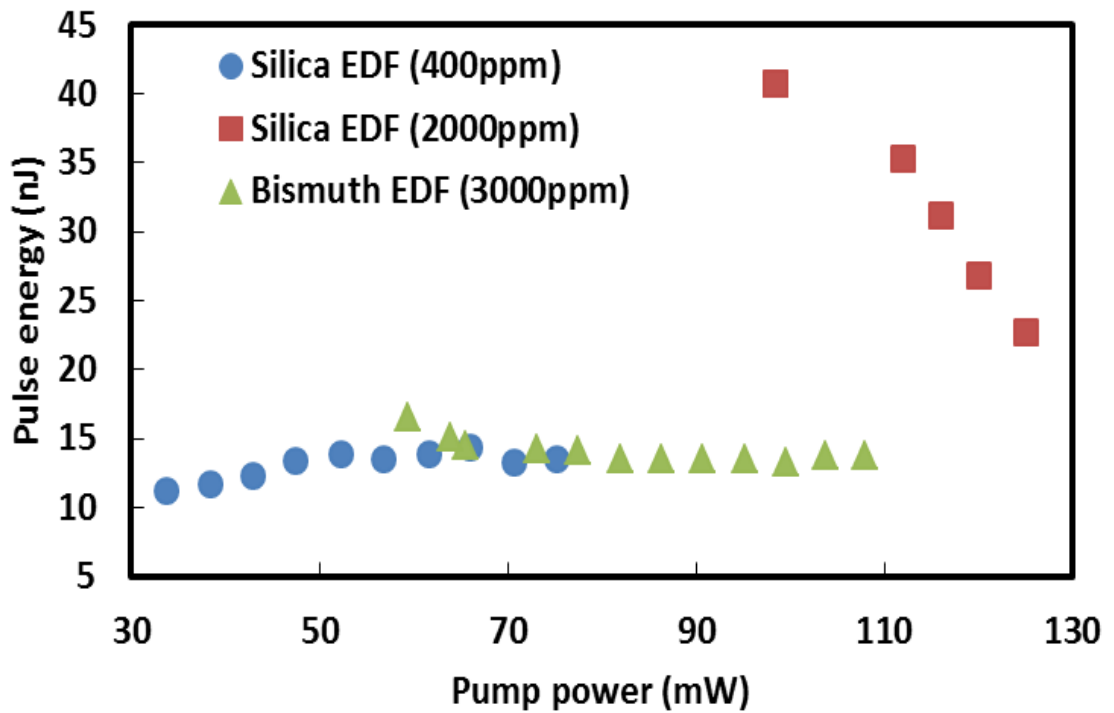


Figure 3.8: Pulse energy against pump power for three different gain medium

Parameters	Silica EDF (400 ppm)	Silica EDF (2000 ppm)	Bismuth EDF (3000 ppm)
Pump Power (mW)	33.7-75.14	98.5-125	59.5- 107.9
Output Power (μ W)	272-648	400-546	372-788
Pulse Energy (nJ)	11.22-14.32	22.74-40.69	13.75-16.55
Pulse Repetition rate(kHz)	24.24-47.93	9.83-24.01	22.5-57.3
Pulse Width (μ s)	6.43-2.98	12.03-4.58	5.01- 2.48

Table 3.1: Summary of laser performance for three different gain media

3.3 Q-switched EDFL using a solid state Thulium-doped Fiber SA

Besides film based graphene SA, modulation of the Q-factor can also be realized using solid-state SA fibers. The advantages of the solid-state SA fibers are their ability to hold enormous gain excited in the gain fiber from lasing and their high damage threshold for high-power Q-switched pulses. Only a few SA fibers have been demonstrated in the literature, and most are for Ytterbium-doped fiber lasers (YDFLs) (Isomäki & Okhotnikov, 2006). The energy transition $^3H_6 - ^3F_4$ of Tm^{3+} has a very broad emission wavelength range, from 1.6 to 2.1 μ m, and an absorption band from 1.5 to 1.9 μ m. It is reported that the absorption cross section of Tm^{3+} doped fibers (TDFs) are larger than the emission cross sections of EDF at 1.6 μ m region, suggesting a possible realization of a passively Q-switched EDFL using a TDF as a passive SA. In

this section, we have successfully demonstrated Q-switched EDFL by using a 2 m long TDF as a SA in a ring laser cavity.

3.3.1 Configuration of the proposed Q-switched EDFL using a TDF SA

The experimental set-up of the proposed Q-switched EDFL is illustrated in Fig. 3.9, where the ring resonator consists of a 3.5 m long EDF as the gain medium, a WDM, 3 dB output coupler, polarization controller (PC) and a short piece of TDF as a SA. The EDF used has an Erbium ion concentration of 2000 ppm, core diameter of 4 μm , mode field diameter of 6 μm and NA of 0.24. A 1480 nm laser diode is used to pump the EDF via the WDM. The TDF SA was a 2.0 meter long with an initial absorption loss of 6 dB at 1570 nm, numerical aperture of 0.16 and core diameter of 2.9 μm . A PC is used to adjust the polarization state of the oscillating light, which in turn controls the operating wavelength of the laser. The laser light is extracted from the cavity by a 3 dB fiber coupler which retains 50% of the light in the cavity for further oscillation. An OSA with wavelength resolution of 0.02 nm is used to capture the output laser spectrum while a 350 MHz oscilloscope in conjunction with 1 GHz bandwidth photo-detector is used to detect the pulse train.

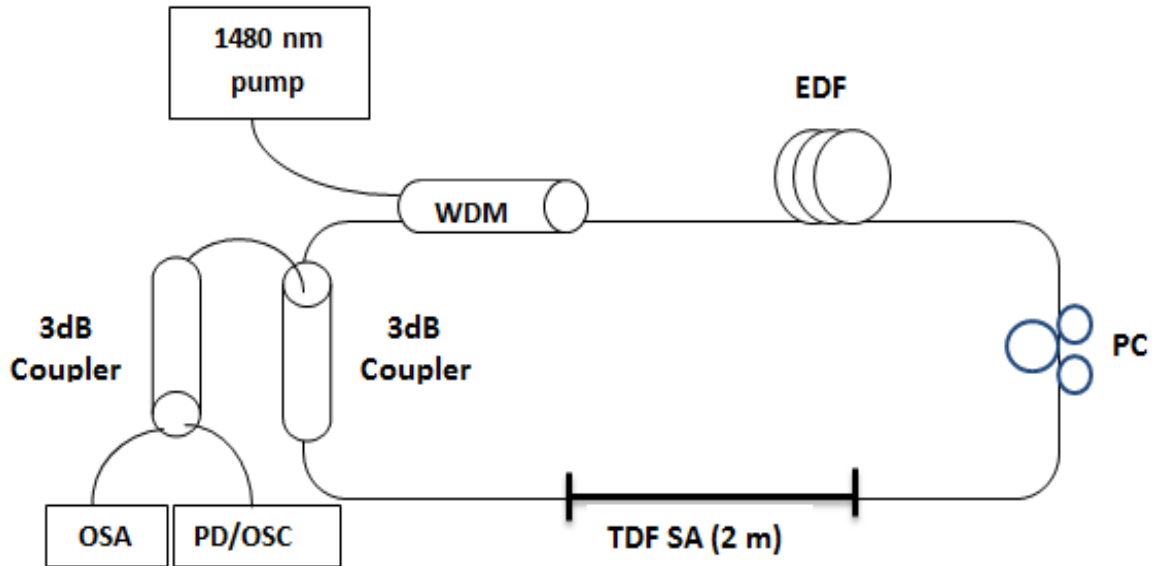


Figure 3.9: Schematic configuration of the proposed thulium fiber based Q-switched EDFL

3.3.2 Q-switching performance

The oscillator started to operate at Q-switching regime after reaching the launched pump power of 20 mW. Stable self-starting Q-switched pulses were observed as shown in Fig. 3.10 by carefully adjusting the PC when the launched pump power was varied from 20 to 33.7 mW. However, as the pump power further increases, the pulse train becomes unstable and disappears. As shown in Fig. 3.10, the time interval between pulse reduces while the pulse amplitude increases as the pump power increases from 20 to 33.7 mW. The Q-switching pulse generation is due to gain-switching action provided by the Thulium ions interaction with the oscillating Erbium laser. The high cavity loss induced by Thulium causes large amount of energy is stored in the gain medium. When the cavity reached the saturation state, cavity loss rapidly reduce and allow efficient extraction of stored energy by the laser pulse. Fig. 3.11 shows the output spectra of the EDFL with and without the TDF SA when the pump power is fixed at 33.7 mW. Without the TDF SA we observed a stable CW operation of EDFL at 1572 nm. After

incorporating a 2 m long TDF inside the cavity, pulsing operation is observed. The operating wavelength of the pulsed laser shifts to 1557.6 nm due to the cavity loss which increases with the incorporation of TDF. The laser operates at a shorter wavelength which has a higher gain to compensate for the loss.

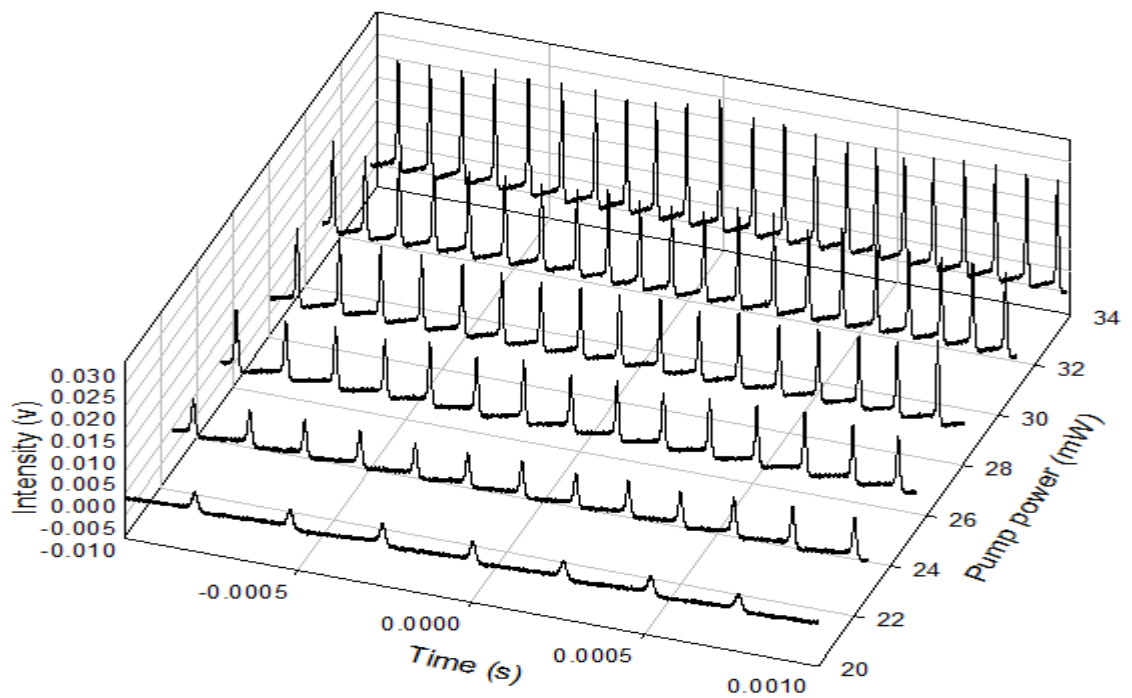


Figure 3.10: Q-switched pulse evolution of the proposed Q-switched EDFL against pump power

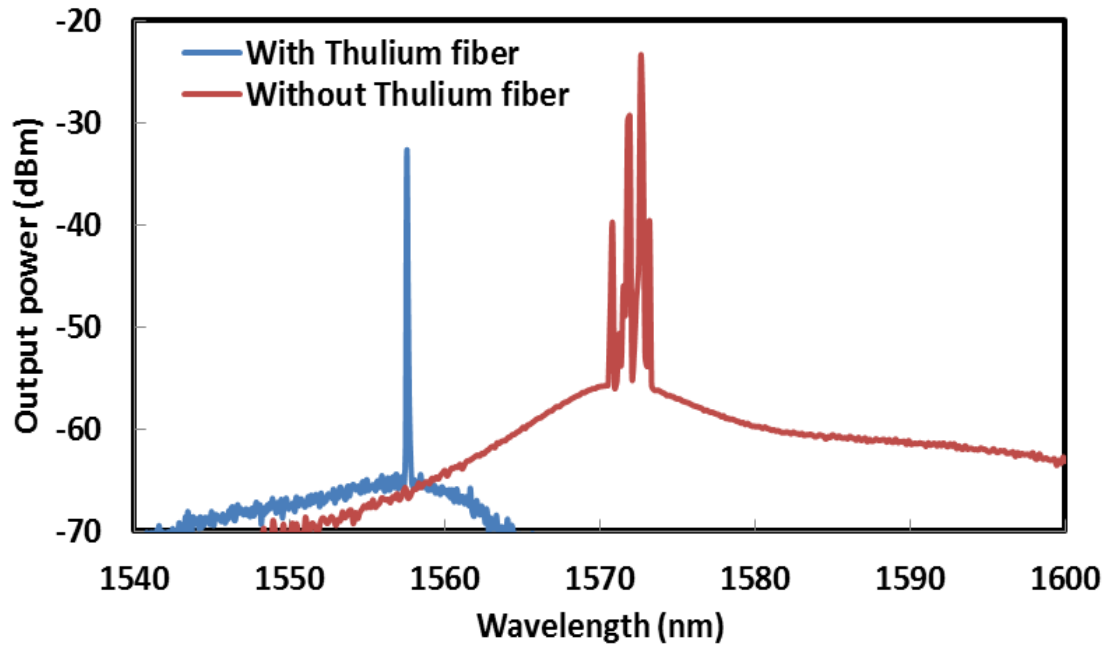


Figure 3.11: Optical spectrum and of the proposed Q-switched EDFL when the pump is fixed at 33.7 mW

Figure 3.12 shows how repetition rate and pulse width are related to the pump power. The dependence of the pulse repetition rate can be seen to increase almost linearly with the pump power, whereas the pulse width decreases also almost linearly with the pump power. By raising the pump power into the cavity, it will speed up the gain population excitation process to achieve the saturation state. Thus, more pulses with narrower pulse width are generated in a same period of time. This agrees well with the passive Q-switching theory with the passive SA. The pulse repetition rate of the Q-switched EDFL can be widely tuned from 3.9 kHz to 12.7 kHz by varying the pump power from 20.0 mW to 33.7 mW. On the other hand, the pulse width reduces from 20.6 μ s to 7.4 μ s as the pump power increases in the range of Q-switching operation. It is observed that the pulse train becomes unstable and disappears as the pump power is increased above 33.7 mW. This is due to the TDF SA could not recover in time after a pulse and less gain population was excited before the next pulsing. Based on the pulse repetition rate at the maximum pump power, the relaxation lifetime (3F_4) of the thulium

fiber should be near and less than 0.079 ms and that was the inversion of the largest repetition rate before the disappearing.

We also measured the average output power and calculated the corresponding single-pulse energy. Fig. 3.13 shows the relationship of average output power and pulse energy of the Q-switched EDFL against pump power. As shown in the figure, average output power almost linearly increased from 180 μW to 240 μW as the pump power increases from 20.0 mW to 33.7 mW. Besides, pulse energy exhibited decreasing trend from 22.8 nJ to 9.4 nJ at the same pump power range. The decrement of pulse energy is most probably due to TDF SA does not fully recover in time after a pulse and less gain population was excited before the next pulsing. This pulse energy is relatively higher with the previously reported carbon nanotubes based Q-switched EDFL. Energy characteristics of the laser allow one to apply it for technological processes as marking, trimming, micromachining etc. Moreover, it can be used in medicine due to the relatively high absorption by biological tissue. It should be noted that the output power and energy can be further increased through the optimization of cavity design and SA.

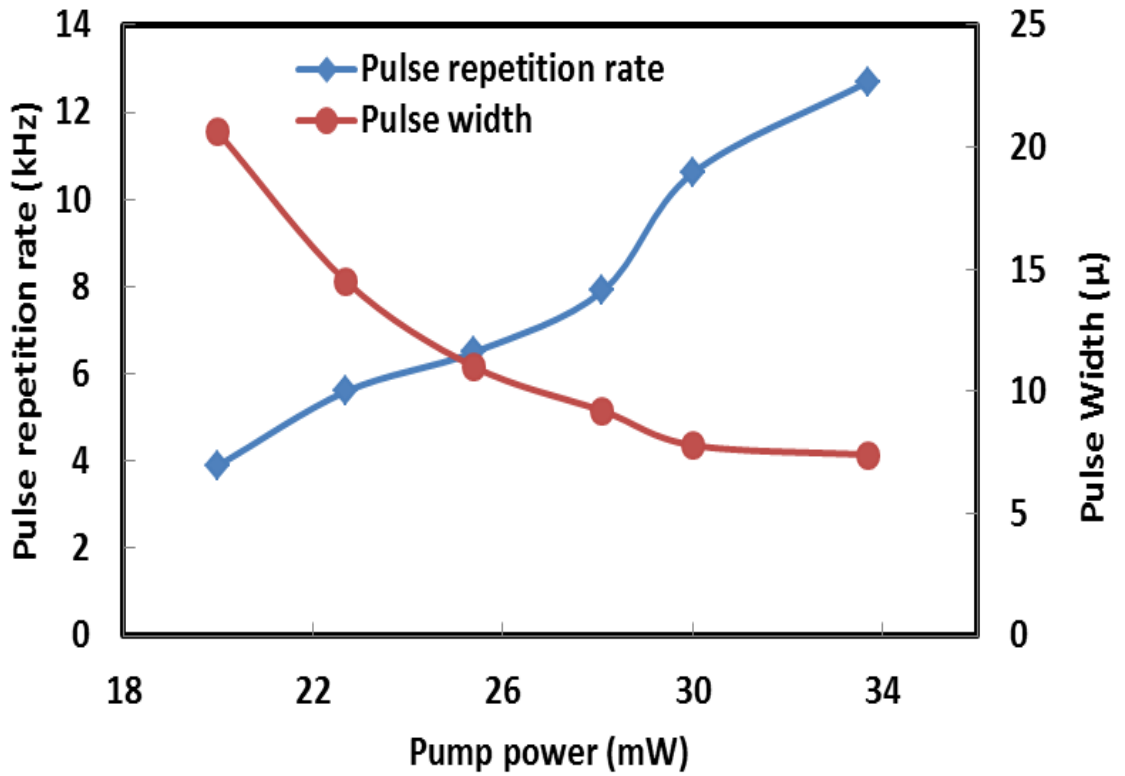


Figure 3.12: Repetition rate and pulse width of the proposed Q-switched EDFL against the pump power

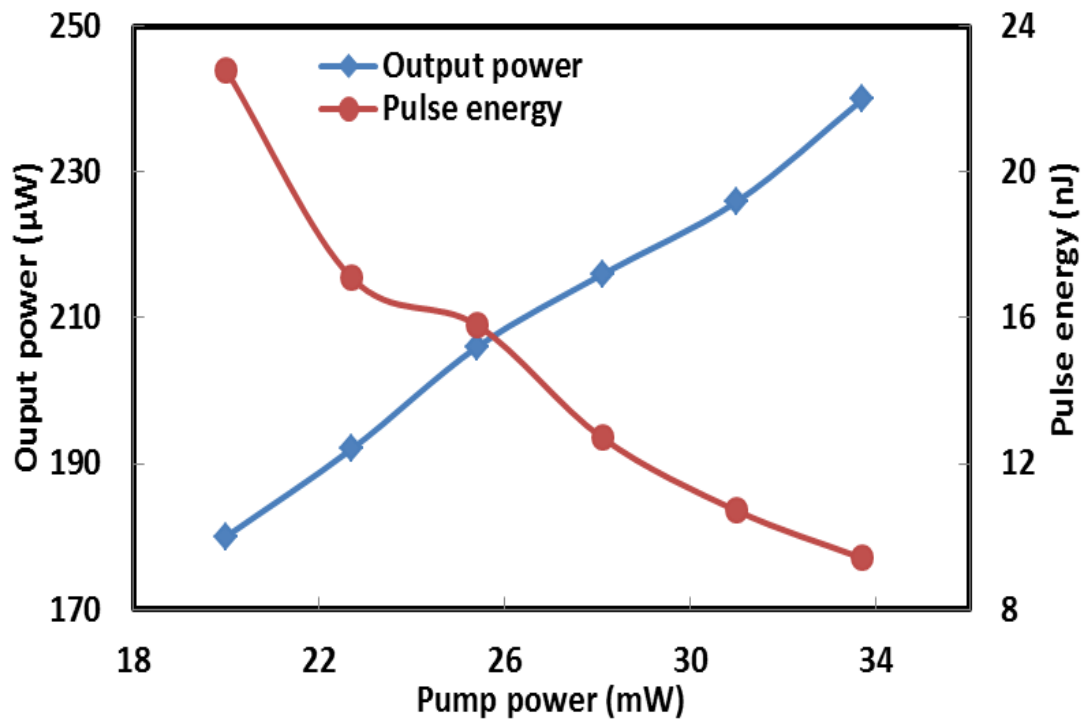


Figure 3.13: Output power and pulse energy of the proposed Q-switched EDFL against the pump power

3.4 Q-switching pulse generation using nonlinear polarization rotation technique

As discussed in the previous sections and many literatures, passive SAs based on various materials such as graphene, carbon nanotubes, semiconductor (SESAM) and TDF have shown promising result to realize a stable Q-switched fiber laser. However, fabrication of these SAs involved complicated chemical processes. Beside these SAs, Q-switching pulse can also be realized by using an artificial SA based on nonlinear polarization rotation (NPR) technique. Compared to the real SAs, Q-switched fiber lasers by NPR are easier to implement as they only use common optical components. Recently, photonic crystal fibers (PCFs) have been reported as one of the promising nonlinear medium to initiate NPR. The large contrast of refractive index between silica and air has cause the nonlinearity of PCFs to easily achieve 10 – 100 times higher compare to normal single-mode silica fiber. In this section, a Q-switched EDFL is proposed and demonstrated by using the NPR technique with an assistance of 50 m PCF. A Q-switching operation in the proposed laser is realized at the threshold power as low as 12.1 mW.

The experimental set-up of the proposed EDFL is illustrated in Fig. 3.13. The ring resonator consists of a piece of EDF as the gain medium, WDM, PDI, PC, 50 m long PCF and 3 dB couplers. A 1480 nm laser diode is used to pump the 3.5 m long EDF with 2000 ppm Erbium concentration via the WDM. A polarization dependent isolator (PDI) and PC are incorporated in the laser cavity to ensure unidirectional propagation of the oscillating laser. PCF is incorporated into the cavity as the birefringent fiber. The combination of PCF-PDI-PC will act as an artificial SA to initial Q-switching operation in the cavity. The output of the laser is collected from the cavity via a 3 dB coupler which retains 50% of the light in the ring cavity to oscillate. The

OSA is used for spectral analysis of the Q-switched EDFL whereas oscilloscope is used to observe the output pulse train of the Q-switched operation via a 1 GHz bandwidth photo-detector.

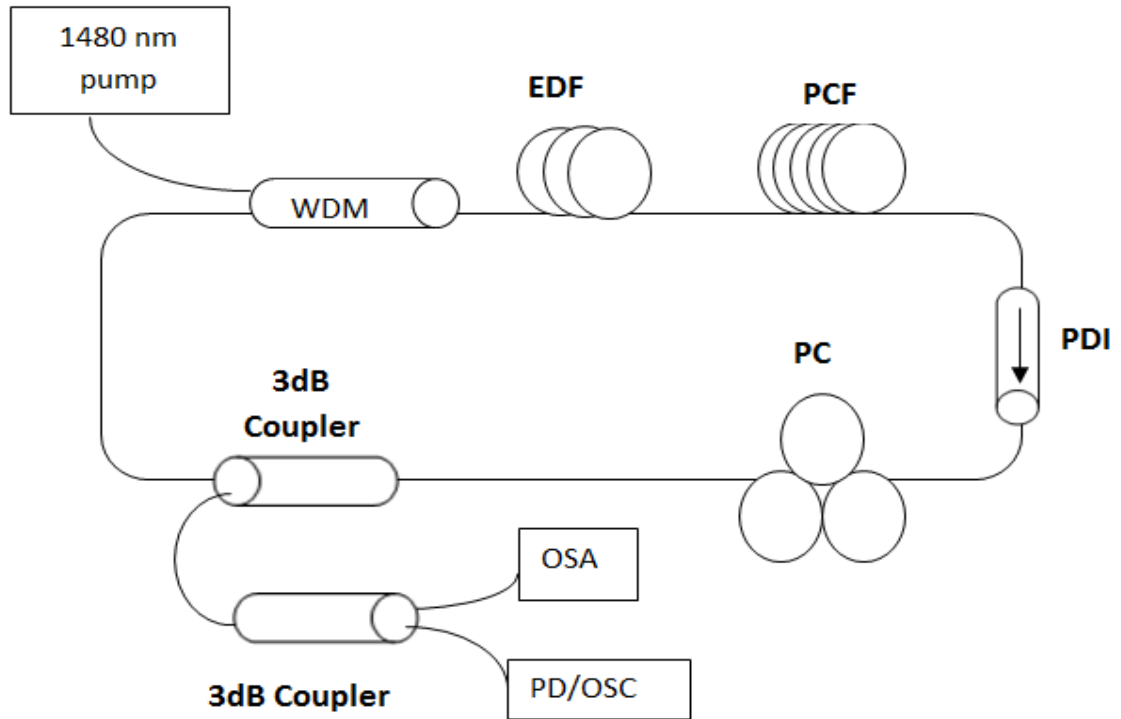


Figure 3.14: Schematic configuration of the proposed Q-switched EDFL

In this experiment, Q-switching pulse generation is self-started at a very low threshold power of 12.1 mW. However, this pulse starts to disappear as the pump power is increased above 15.1 mW. The pulse evolution against pump power is shown in Fig. 3.15. As shown in the figure, the pulse repetition rate increases with the increment of pump power. Fig. 3.16 shows the output spectrum of the Q-switched EDFL at pump power of 12.1 mW. It is shown that Q-switched laser also produces an unstable amplitude lines with free spectral range (FSR) of 0.48 nm, which is most probably due to the longitudinal modes interference in the laser cavity. FSR of 0.48 nm is determined by the length and the effective group indices of the PCF. The unstable multi-wavelength generation is due to the intensity dependent loss induced by NPR. The role of PCF is to

increase the nonlinear effect as well as to constitute an inline periodic filter with the PDI.

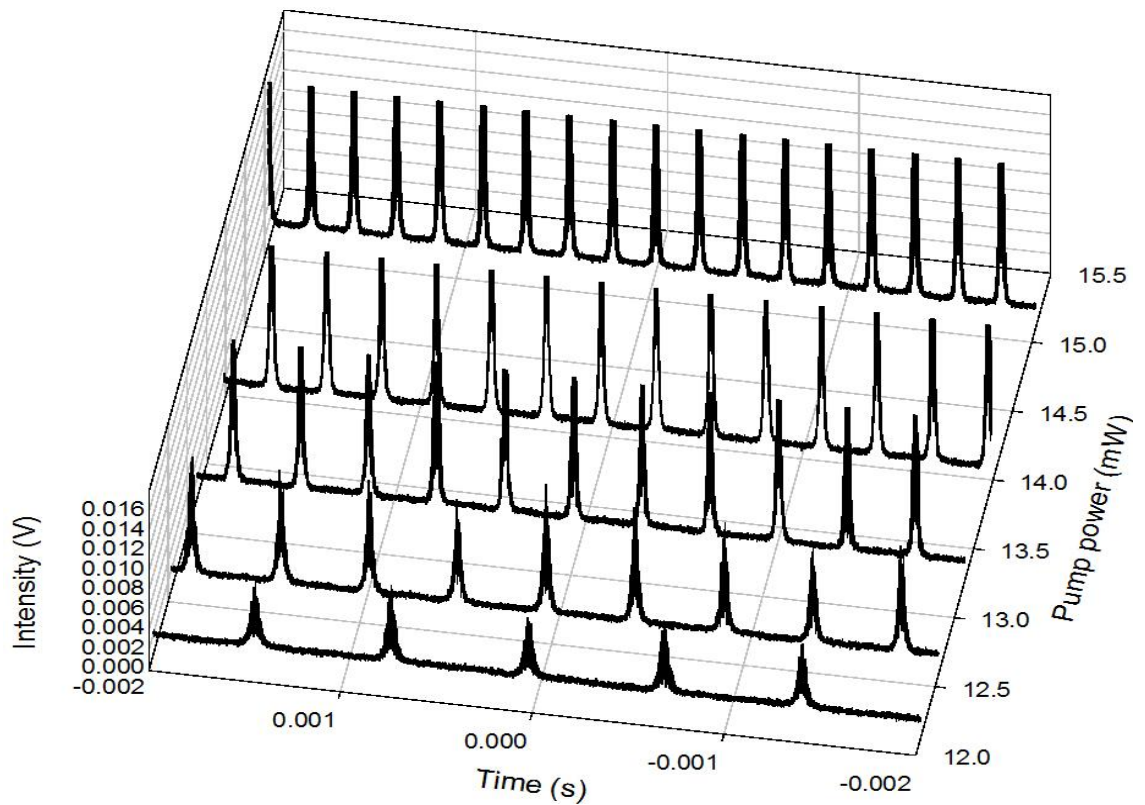


Figure 3.15: Pulse evolution of the proposed Q-switched EDFL against pump power

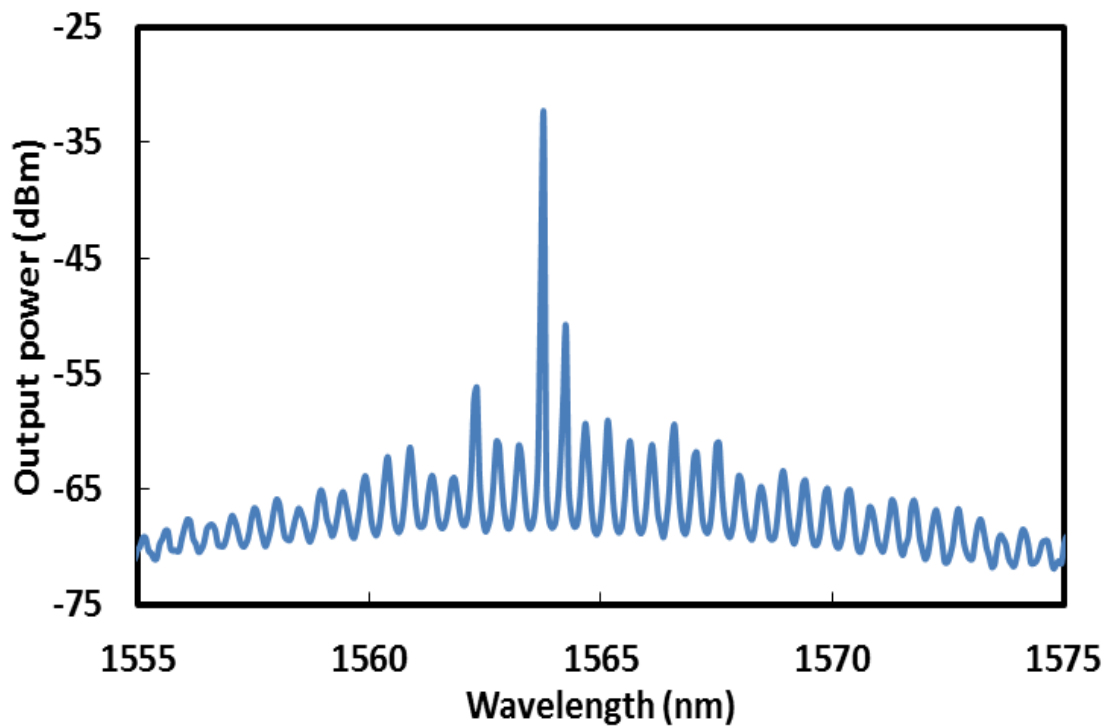


Figure 3.16: Optical spectrum for the Q-switched EDFL at threshold pump power

Fig. 3.17 shows how an average output power and pulse energy of the Q-switched EDFL when varied with the pump power. As shown in the figure, average output power increases almost linearly increased from 12.5 μW to 58.0 μW as the pump power increases from 12.1 mW to 15.1 mW. The pulse energy also increased from 9.0 nJ to 12.4 nJ as the pump power increases from 12.1 mW to 15.1 mW. Fig. 3.18 shows the relation between repetition rate and pulse width with the pump power. Pulse repetition rate can be seen to increase almost linearly with the increment of pump power, while the pulse width shows decreasing trend with the pump power. The pulse repetition rate of the Q-switched EDFL can be tuned from 1.4 kHz to 4.7 kHz by increasing the pump power from 12.1 mW to 15.1 mW. On the other hand, the pulse width reduces from 20.6 μs to 5.1 μs as the pump power increases in the range of Q-switching operation. The combination of PC-PDI-PCF acted as a SA based on the NPR effect. With proper adjustment of PC, the cavity loss can reach a higher level. Lasing radiation was too weak to pass through the PDI and PCF which act as polarizer in the cavity. Hence, a mass of inverted populations was accumulated at the upper energy level in the EDF. When the accumulation reached a sufficient level, the lasing radiation became strong enough to propagate through the polarizer. Then, the inverted populations in EDF exhausted abruptly and cavity loss became too high to allow the lasing radiation to propagate through. Therefore, the Q-switched pulse train was formed. Erbium ion saturation time can be further decreased with a higher pump power, provided that the erbium ion life time is much longer than the round trip time in the cavity. As shown in Fig. 3.18, the pulse repetition rate is directly proportional to the pump power, which is well agreed with NPR Q-switching theory. Moreover, accumulation rate and exhaustion rate of inverted populations in EDF increased with the increment of pump power. Hence, pulse width behaves inversely proportion to pump power as shown in Fig. 3.18.

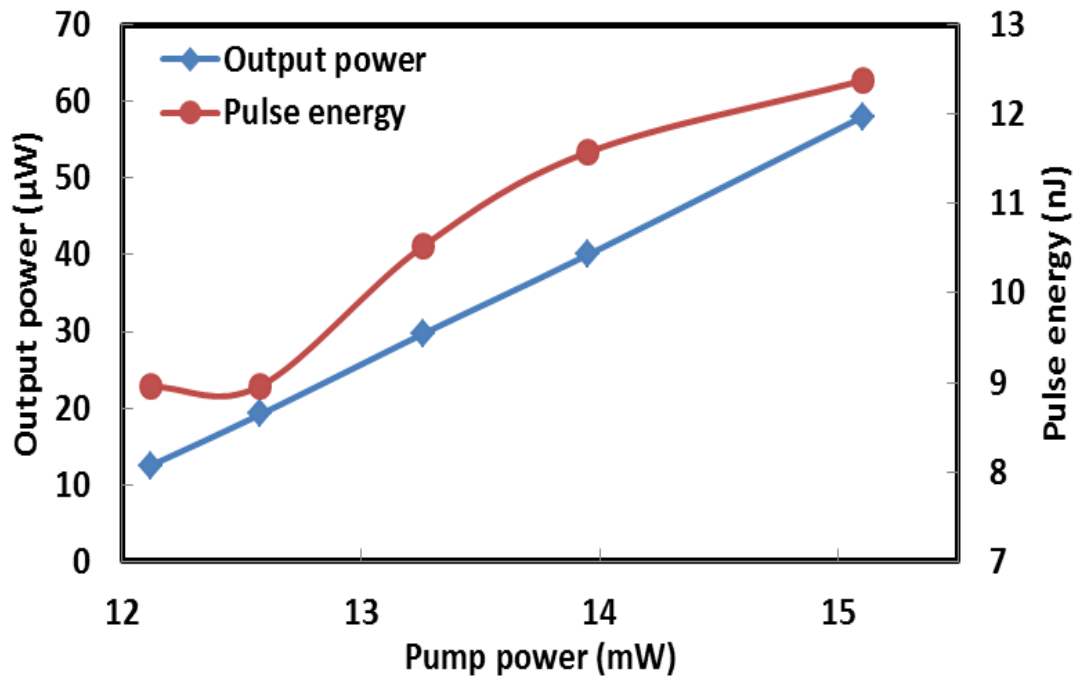


Figure 3.17: Output power and pulse energy of the proposed Q-switched EDFL against pump power

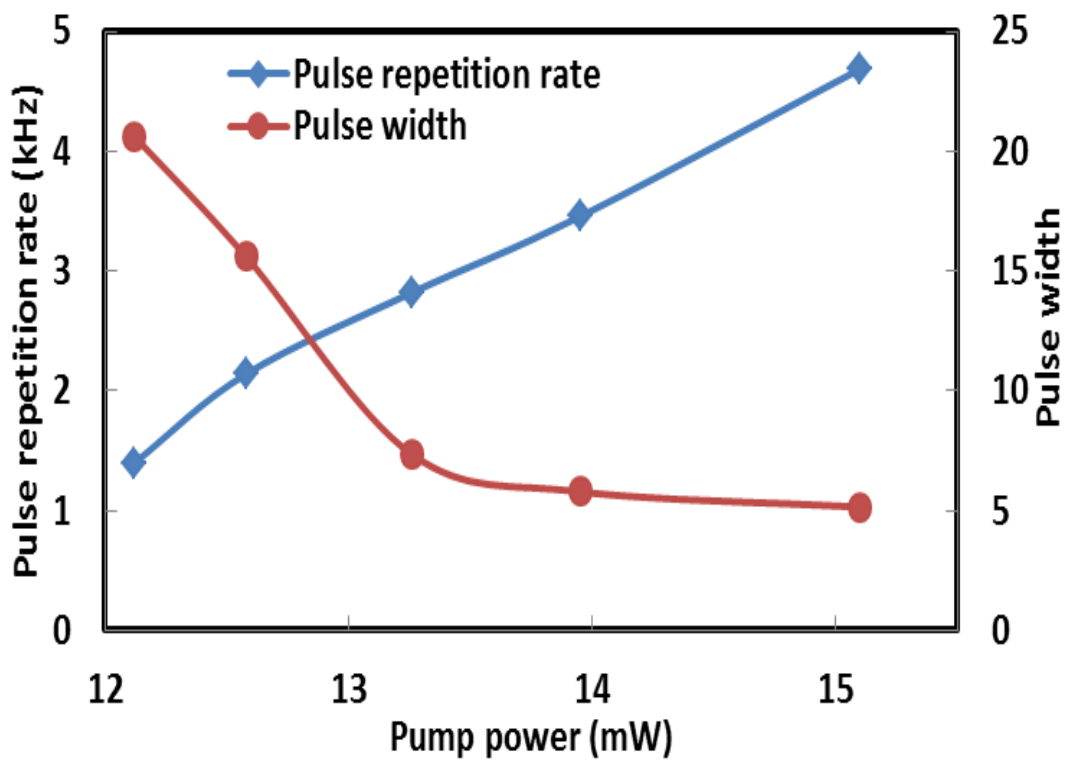


Figure 3.18: Repetition rate and pulse width of the proposed Q-switched EDFL against pump power

3.5 Multi-wavelength Q-switched Generation With Graphene Based SA

Both multi-wavelength and Q-switched EDFLs have wide applications in optical communications, sensors and instrumentations. Multi-wavelength laser can be achieved at room temperature by using various methods such as cascaded stimulated Brillouin scattering (Fok & Shu, 2006) and four-wave mixing (FWM) (Han et al., 2006). Recently, nonlinear polarization rotation (NPR) technique is also proposed for multi-wavelength generation based on intensity dependent loss in the cavity (Feng, Tam, & Wai, 2006). On the other hand, a Q-switched EDFL has been successfully demonstrated by using a graphene based SA as described in section 3.2. It was observed that the Q-switching performance is superior especially in terms of pulse energy with the use of highly doped silica-based EDF (2000 ppm) as gain medium compared to that of other fibers. In this section, a Q-switched multi-wavelength EDFL is demonstrated by integrating a graphene SA in an EDFL cavity comprising an additional nonlinear gain medium. The SA is obtained by sandwiching the graphene film between two fiber connectors. 50 m long PCF is used as the nonlinear gain medium to activate the NPR effect and thus allows the generation of a stable multi-wavelength pulse train.

The experimental set-up of the proposed multi-wavelength Q-switched EDFL is illustrated in Figure 3.19. The ring resonator consists of a 4.5 m long EDF as the gain medium, WDM, PDI, PC, 50m long PCF, a graphene-based SA and 10 dB output coupler. A 1480 nm laser diode is used to pump the EDF via the WDM. A PDI and PC are incorporated in the laser cavity to ensure unidirectional propagation of the oscillating laser and to act as a polarizer. A PC was also utilized to tune the polarization state of light in the laser cavity. The output of the laser is collected from the cavity via a 10 dB coupler which retains 90% of the light in the ring cavity to oscillate. The OSA is

used for the spectral analysis while the oscilloscope is used to observe the output pulse train via a photodetector.

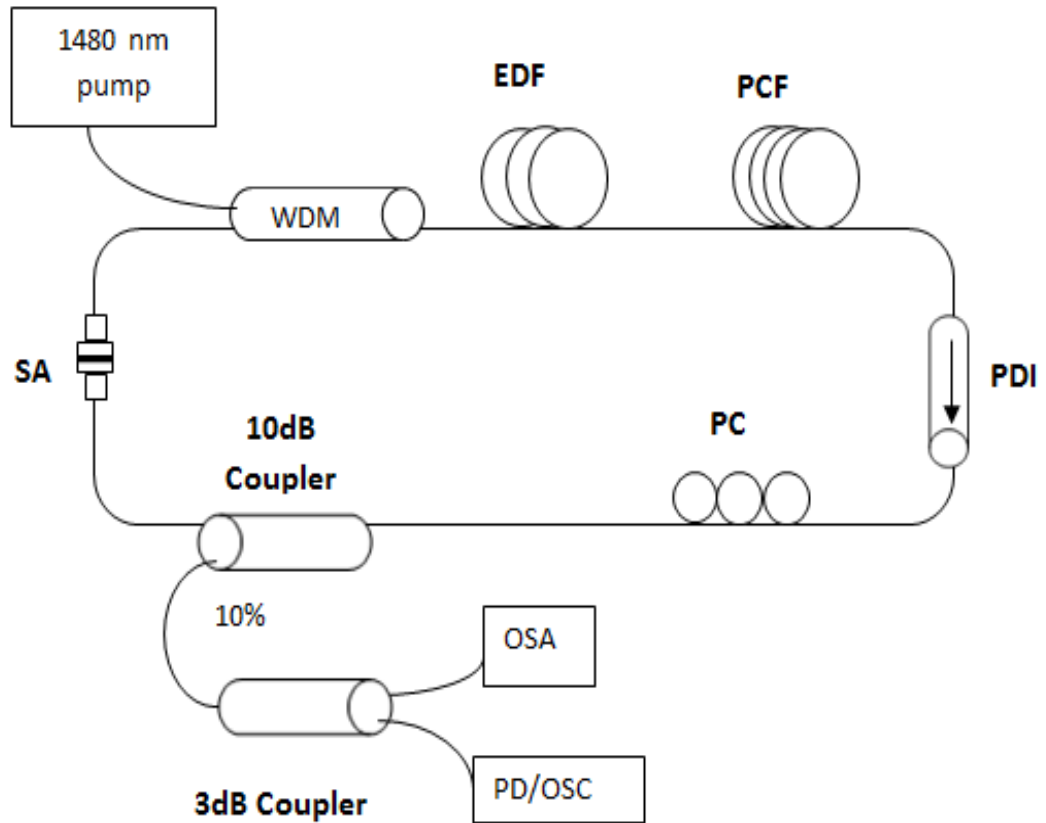
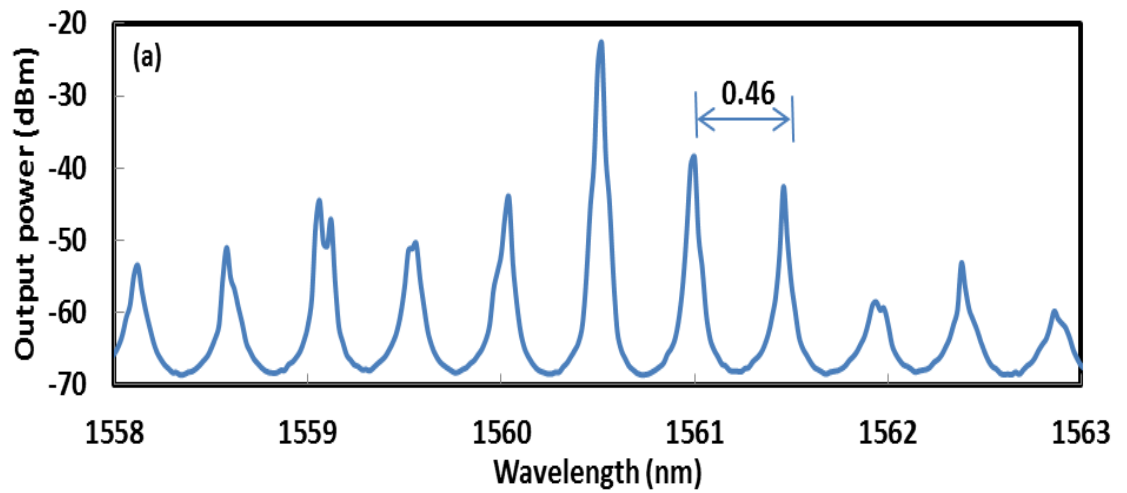


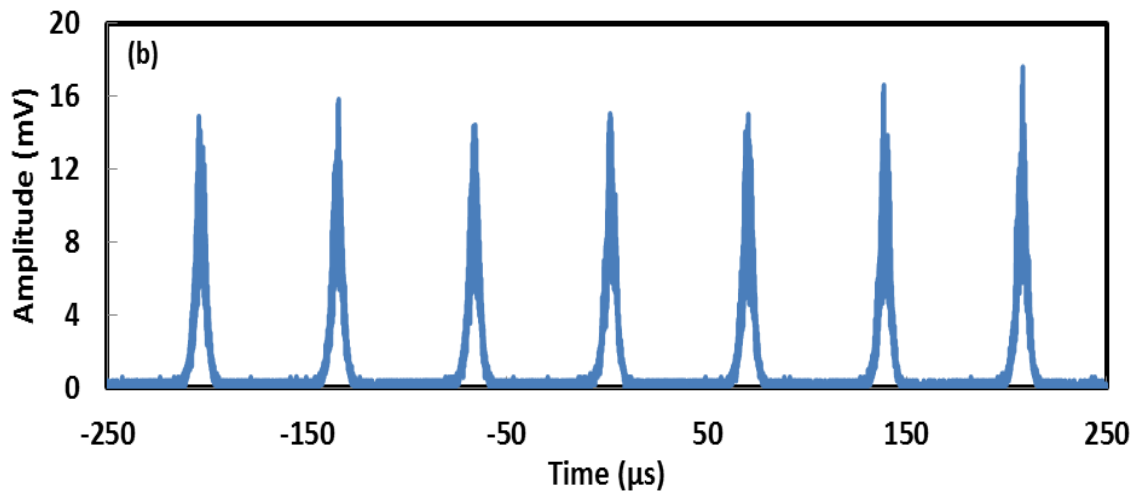
Figure 3.19: Schematic configuration of the proposed multi-wavelength Q-switched EDFL

To realize the multi-wavelength Q-switched lasing operation, the laser cavity must have two important components; interferometer and SA. The interferometer functions to generate multiple resonance peaks for multi-wavelength generation while SA with a wideband optical absorption range is required to provide saturable absorption, which covers all the multi-wavelength region. In this work, a stable multi-wavelength laser with Q-switching operation was obtained as the pump power reaches the threshold pump power of 39.6 mW with a proper tuning of PC. Figures 3.20 (a) and (b) show the output optical spectrum and the typical pulse train of the proposed multi-wavelength Q-switched EDFL respectively, when the pump is fixed at the threshold

pump power. As shown in Figure 3.20 (a), the Q-switched laser produces at least 10 lines with free spectral range (FSR) of 0.46 nm, which is determined by the length and the effective group indices of the PCF. At the threshold pump power of 39.6 mW, the multi-wavelength laser produces a Q-switched pulse train with repetition rate of 14.6 kHz and pulse width of 1.52 μ s as shown in Figure 3.20 (b).



(a)



(b)

Figure 3.20: (a) Optical spectrum and (b) typical pulse train of the proposed multi-wavelength Q-switched EDFL when the pump is fixed at the threshold pump power of 39.6 mW

The multi-wavelength generation can be described as follows. The light is split into two orthogonal modes, which experience different nonlinear phase shift as they propagate inside the PCF owing to the Kerr effect. Then the polarization orientation of the light rotates in the PCF with the angle of rotation is correlative with the light intensity. The signal passes through the PDI, which the transmittivity is dependent on the rotation of the polarization or the oscillating light intensity. The combination of the PCF and PDI functions as an intensity equalizer, which produces an intensity dependent inhomogeneous loss and thus alleviates the mode-competition. As a result, the balance between the inhomogeneous loss induced by NPR and the mode competition effect of the EDF can lead to a stable multiwavelength oscillations. When the polarization state is selected properly by adjusting the PC, multi-wavelength laser can be easily obtained as shown in Figure 3.20. Figure 3.21 shows the evolution of the output spectra against the pump power. As shown in the figure, the number of lines and its peak power increases with the pump power. However, the wavelength spacing is maintained at 0.46 nm for all pump powers.

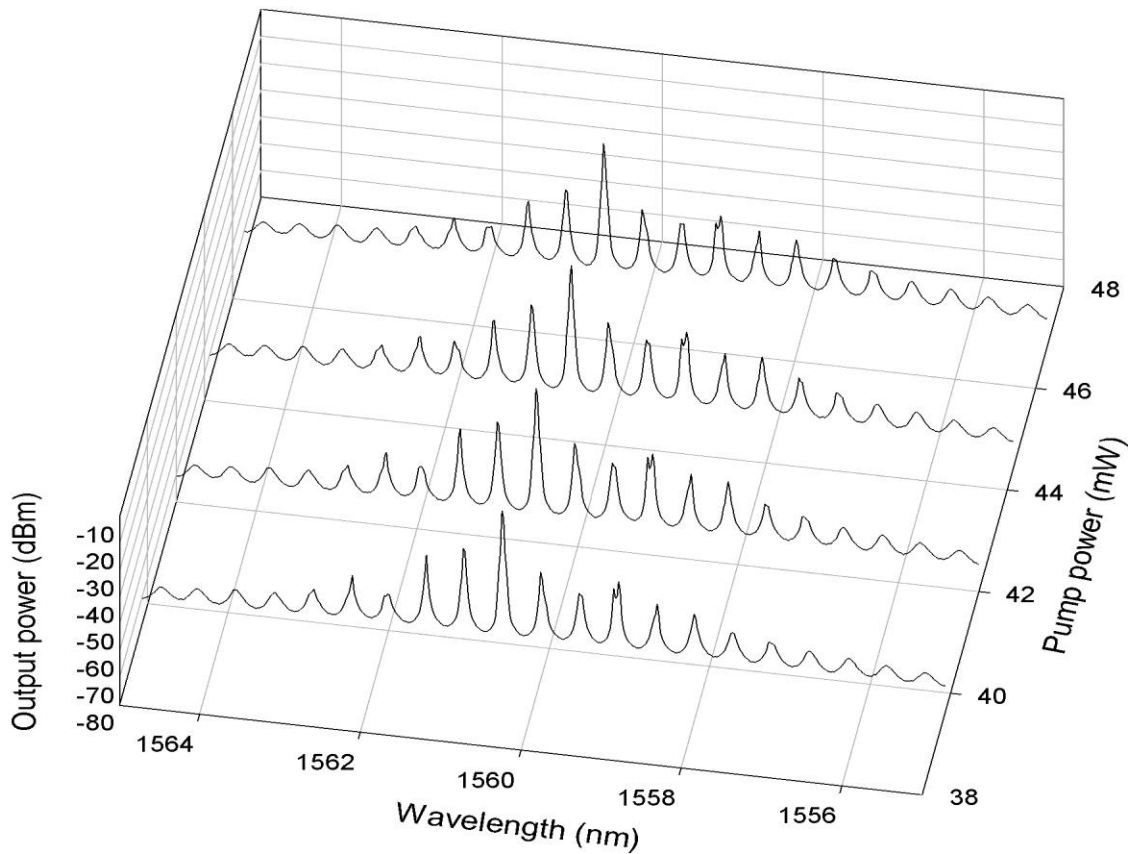


Figure 3.21: Output spectrum evolution of the proposed multi-wavelength Q-switched EDFL against pump power

Figure 3.22 shows the relationship of repetition rate and pulse width to the pump power. The dependence of the pulse repetition rate can be seen to increase almost linearly with the pump power, while the pulse width decreases also almost linearly with the pump power. The pulse repetition rate of the Q-switched EDFL can be tuned from 14.6 kHz to 16.3 kHz by varying the pump power from 39.6 mW to 46.8 mW. On the other hand, the pulse width reduces from 1.5 μ s to 1.2 μ s as the pump power increases from 39.6 mW to 46.8 mW. Figure 3.23 shows how the average output power and pulse energy are related with the pump power. As shown in the figure, average output power increased from 23.0 μ W to 23.5 μ W as the pump power increases from 39.6 mW to 46.8 mW while the pulse energy slightly decrease from 1.57 nJ to 1.43 nJ at the same pump power range. These results show that the graphene-based SA functions very well

as a typical SA to achieve the Q-switching while the highly nonlinearity of PCF has successfully induced NPR in the cavity to achieve multi-wavelength operation.

It should be noted that no Q-switched operation occurs without the graphene SA connected in the laser cavity. It is clear that the Q-switched operation is mainly induced by the SA. By removing the SA from the set-up, an unstable multi-wavelength laser with continuous wave operation is observed. Thus, we strongly believed that the incorporation of SA also improves the stability of the multi-wavelength lasing due to the nonlinearity of graphene-based SA that can induce both NPR and FWM effects in the laser cavity. The FWM effect functions to stabilize the multi-wavelength operation. The stability of the multi-wavelength laser is also investigated by monitoring the spectrum evolution of the laser against time at the threshold pump power of 39.6 mW as shown in Figure 3.24. In the experiment, the output spectrum is repeatedly scanned for every 5 minutes. As shown in the figure, the multi-wavelength Q-switched EDFL lases stably with power fluctuations of less than 1 dB over 20 minutes. It shows the combination of PCF with PDI and PC produces a very stable multi-wavelength laser based on the NPR mechanism.

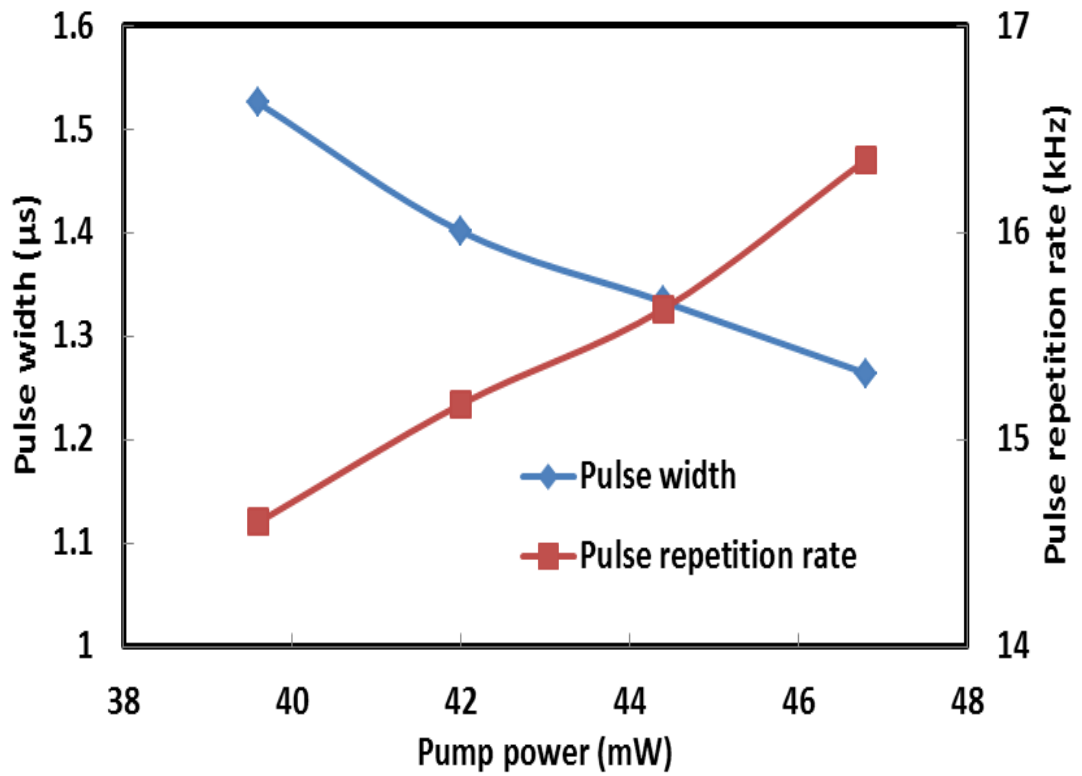


Figure 3.22: Repetition rate and pulse width of the proposed multi-wavelength Q-switched EDFL against pump power

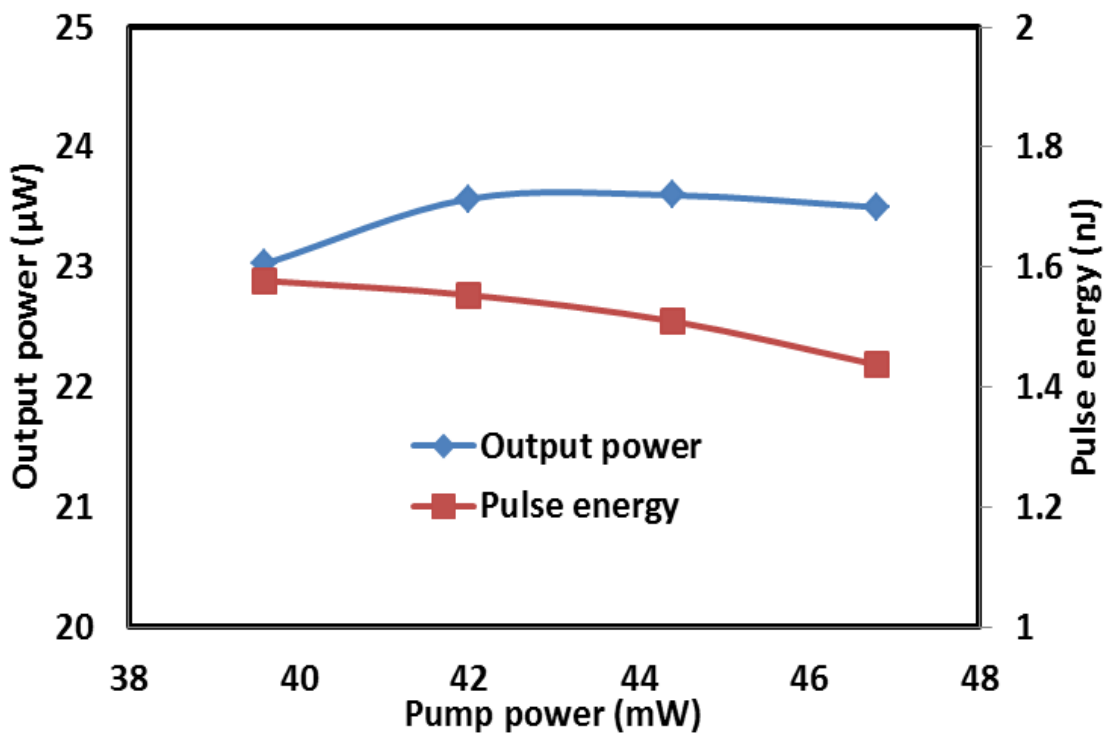


Figure 3.23: Output power and pulse energy of the proposed multi-wavelength Q-switched EDFL against pump power

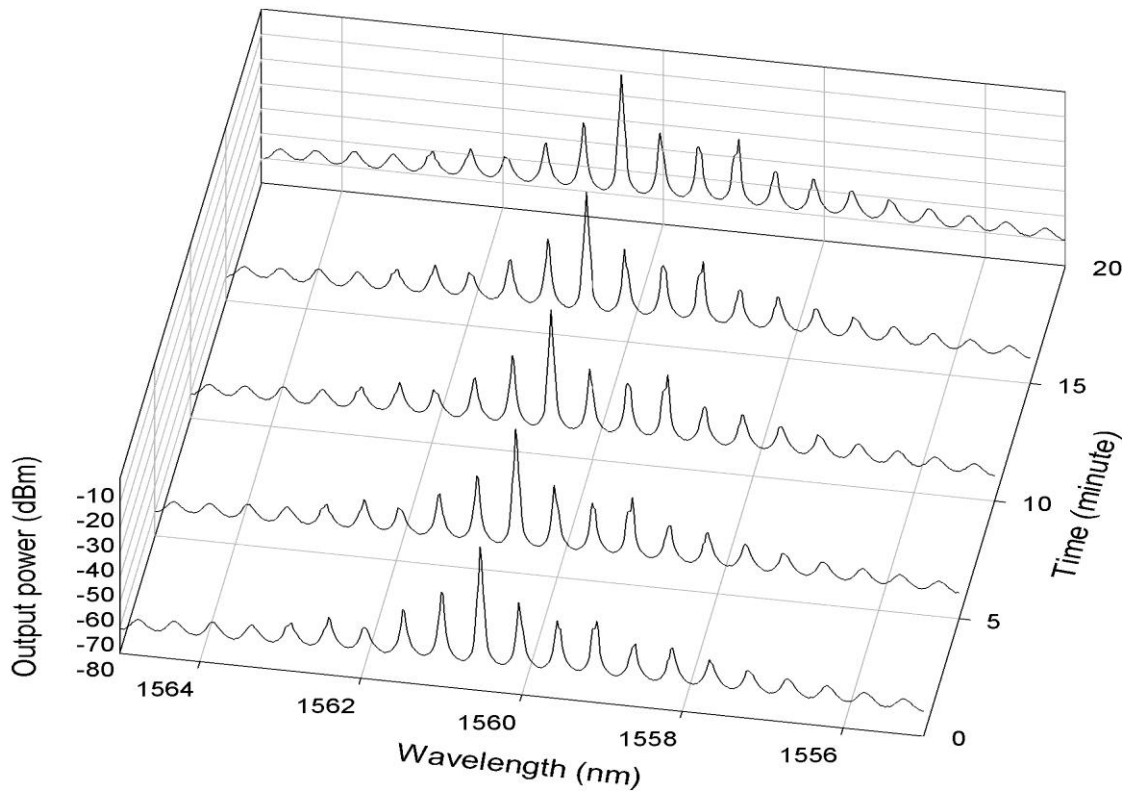


Figure 3.24: Output spectrum evolution of the proposed multi-wavelength Q-switched EDFL against time

3.6 Summary

In this chapter, three passive techniques for generating Q-switching pulse have been evaluated and demonstrated; graphene film based SA, solid state TDF SA and NPR. It is found that the NPR based Q-switching operation occurs at a relatively lower pump power of around 12 mW compared to other Q-switching techniques. Other techniques require higher pump power to initiate Q-switching operation mainly due to the device loss. For instance, Q-switched EDFLs based on graphene and solid state TDF SA has a threshold pump power in a range of 20 mW and 33 mW respectively. The NPR based Q-switched EDFL requires a lower pump power to initiate Q-switching due

to the incorporation of high nonlinearly of PCF, which induces sufficient phase shift in low pump power.

NPR technique proved its multi-functional operation to achieve both Q-switched and multi-wavelength operation. Furthermore, NPR also offers advantages such as tunable saturable absorption strength and ease of implementation with only conventional optical fiber components. Even though SAs can produce more stable Q-switched under laboratory environmental condition, but SAs are easily damage under high power operation. Since NPR technique is highly rely on the light polarization in the laser cavity, readjustment of polarization state is required in order to maintain the Q-switched operation whenever there is vibration or temperature fluctuation. However, the uncertainty of vibration and temperature fluctuation can be well controlled under laboratory environmental condition. Besides the advantages above, NPR technique exhibits a high potential to obtain different types of pulsed laser by only changing the polarization state. With these crucial advantages, NPR technique is chosen to be the most suitable method for further investigation in different type of pulsed laser. Several types of pulsed laser such as mode-locked and dark pulse are investigated in the following two chapters via NPR method.

CHAPTER 4

DEVELOPMENT OF PASSIVE MODE-LOCKED ERBIUM-DOPED FIBER LASERS

4.1 Introduction

Passively mode-locked fiber lasers are attractive for many applications because of their simplicity, compactness, efficient heat dissipation, and ability to generate high-quality pulses (Laubereau & Kaiser, 1974). For instance, mode-locked Erbium-doped fiber lasers (EDFLs), which are capable of generating ultra-short pulses in the telecommunication wavelength of about 1.55 μm , have promising applications in the next generation telecommunication systems (Kaiser & Huttel, 2007). Generation of ultra-short pulses has also attracted considerable attention in other areas of physics such as the ultrafast physics and nonlinear optics. The passively mode-locked lasers work by inducing a stable phase relationship between the longitudinal modes of the laser cavity. Under the optimum fixed-phase condition, interference between these modes produces stable ultra-short pulses. Among the different types of passively mode-locked techniques, nonlinear polarization rotation (NPR) has gained the significant interests in recent years. This is attributed to the NPR implementation, which can easily tune the phase shift in a laser cavity and thus different type of fix-phase condition in a laser cavity can be easily achieved.

In this chapter, several passively mode-locked fiber lasers are demonstrated using the NPR technique. At first, the mode-locked EDFL with three switchable operation states is proposed and demonstrated. Next, square pulse emission with ultra-low repetition rate is proposed and demonstrated by using long laser cavity. Finally, a

multi-wavelength mode-locked fiber laser is proposed and demonstrated using a figure-of-eight configuration.

4.2 NPR based mode-locked EDFL with three switchable operation states

Mode-locked EDFLs normally operates in the negative net cavity dispersion regime, where the nonlinear Kerr effect naturally balances the group velocity dispersion (GVD) of the cavity. This NPR effect results in the formation of stable soliton pulses with sub-picosecond pulse width. Other types of pulses such as stretched pulse (Haus et al., 1995), self-similar pulse (Renninger, Chong, & Wise, 2010), and dissipative soliton (DS) (Wu et al., 2009) have also been obtained successively in the recent years using the NPR technique. DSs have been investigated in large- or all-normal dispersion regime previously (Liu, 2009). It was found that the cavity gain and loss play essential roles in the formation of DSs, where various operation regimes can be realized by controlling both parameters. In this section, we experimentally demonstrate a new NPR based mode-locked EDFL which is capable to generate dissipative soliton pulse with switchable repetition rate. The EDFL operates in anomalous dispersion region. Three switchable operation states are obtained by varying the pump power and without disturbing the polarization state. The proposed laser generates nanosecond and microsecond pulses, where their energy can be easily amplified by the optical amplifiers. Such optical pulses could have many potential applications such as in laser range-finder and fiber sensors systems.

4.2.1 Experimental setup

The experimental setup of the mode-locked EDFL with switchable repetition rate is shown in Figure 4.1. The EDFL uses a ring configuration with a cavity length of about 6.9 km. A 3.5 m long EDF with doping concentration of 2000 ppm and group velocity dispersion (GVD) parameter of about -21.64 (ps/nm)/km was used as the gain fiber. The other fibers in the cavity are a 6.9 km long dispersion compensation fibers (DCFs) with GVD of about -4 (ps/nm)/km and a standard SMF, which constituted the rest of the ring. The cavity operates in large positive GVD where the net dispersion and fundamental repetition rate are estimated at -0.073 ps² and 29.0 kHz, respectively. The NPR technique was adopted for achieving the mode locking and thus a fiber pigtailed polarization dependent isolator (PDI) together with an inline polarization controller was employed to control the polarization of light in the cavity. The PDI is also used to ensure the unidirectional operation of the ring. The EDF was pumped by a 1480 nm laser diode through a wavelength-division-multiplexing (WDM) coupler. A 3dB fiber coupler was used to tap out the laser emission. All the components (isolator, WDM and fiber output coupler) in the resonator were made from standard SMF. An optical spectrum analyzer (OSA, Yokogawa, AQ6370B) and a 350MHz oscilloscope (Tektronix TDS 3052C) together with a 1 GHz photo-detector were used to simultaneously monitor the spectrum and output pulse train of the laser.

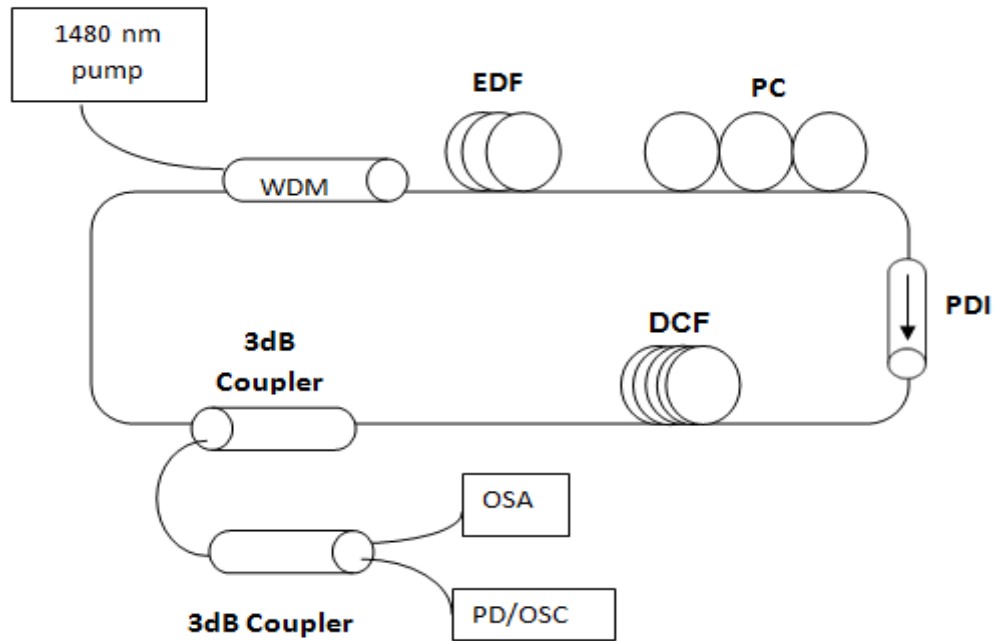


Figure 4.1: Schematic configuration of the mode-locked EDFL

4.2.2 Comparison of the three different mode-locked operation states

A major difference of the current fiber laser from those reported previously is that a long cavity was used, which increases the total normal cavity dispersion. Mode locking of the laser is always self-started, and depending on the pump strength, various modes of laser operation were observed, including fundamental and harmonic dissipative soliton. In particular, under low pumping power a stable square pulse emission mode was also observed. The square pulse trains is self-started at threshold pump power of 17.5 mW and transforms to fundamental dissipative soliton as the pump power increases above 34.3 mW. Figure 4.2 shows the typical oscilloscope traces of the observed square pulse emission at two different pump power of 17.5 and 34.3 mW. Both pulse trains have a repetition rate of 87.0 kHz, which indicates that the laser generates a third-order harmonic pulse. Inset of Figure 4.2 illustrates an envelope of a single pulse, which shows a rectangular pulse with a steep rising and falling edges. The

square (or rectangular) pulse duration increases with the pump strength, while the peak of the pulse reduces as the pump power increases. The pulse widths are obtained at 105 ns and 245 ns with the pump power of 17.5 and 34.3 mW, respectively. At pump power of 34.3 mW, the maximum single pulse energy of 11.3 nJ is achieved in our experiment without the appearance of pulse breaking. The square pulse operation of the laser can be explained as a result of the nonlinear polarization switching in the laser cavity. Due to the large nonlinearity of the DCF, the polarization switching threshold of the fiber laser is low. Consequently, the laser signal starts to have a square pulse shape for smaller peak power than that in a cavity with a smaller nonlinearity.

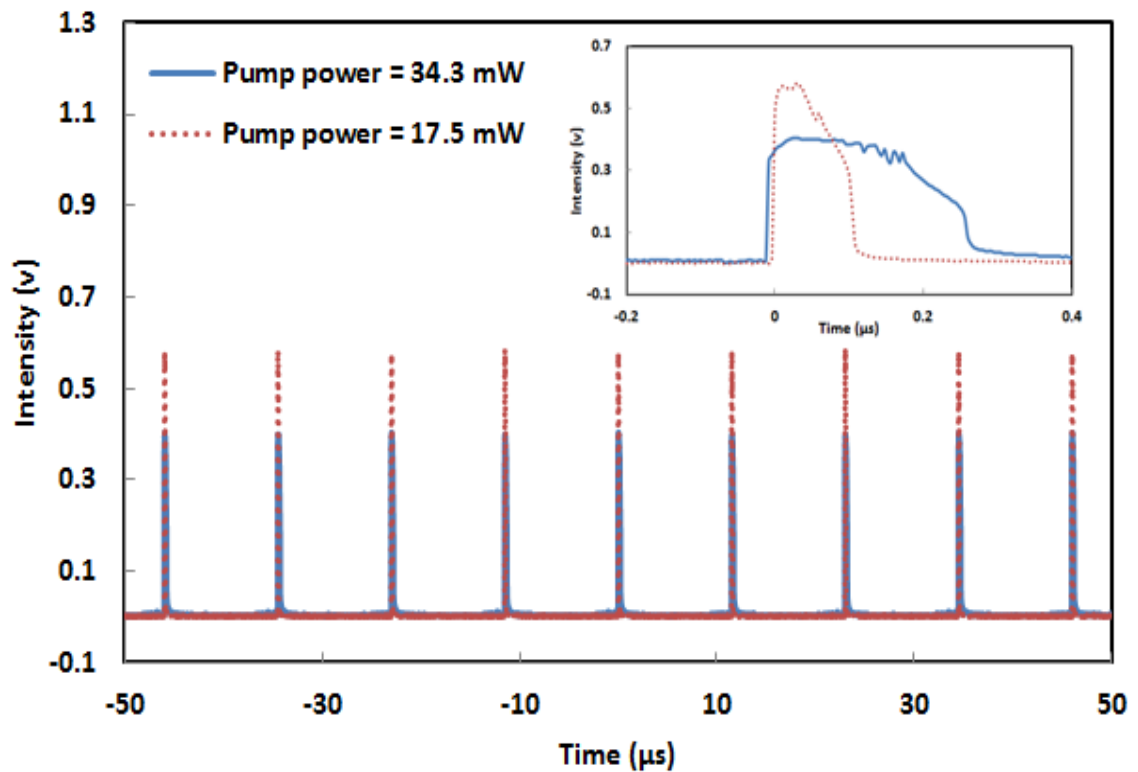


Figure 4.2: Typical pulse train of the proposed mode-locked EDFL at two different pump powers of 17.5 mW and 34.3 mW. Inset shows the corresponding single pulse envelopes

As the pump power is further increased above 48.2 mW, the pulse train switches to another stable operation state as shown in Figure 4.3. It operates at fundamental mode within a pump power range from 48.2 to 116.7 mW whereby the pulse width and

repetition rate of the generated dissipative soliton are maintained at $8.5 \mu\text{s}$ and 29 kHz respectively, throughout the pump power range. It is also observed that the average output power of the laser increases from 1.27 mW to 3.84 mW as pump power increases from 48.2 mW to 116.7 mW . Besides, pulse energy exhibits increasing trend from 43.5 nJ to 131.5 nJ in the same pump power range. When the pump power continues to increase beyond 116.7 mW , the pulse train experiences unstable oscillation before it reaches another stable operation state at pump power of 138.9 mW . Figure 4.4 shows the typical pulse train at two different pump powers of 138.9 and 145.0 mW . Within the pump power range, the laser operates in harmonic mode with a fixed pulse width and pulse repetition rate of $2.8 \mu\text{s}$ and 58 kHz respectively. As the pump power is increased from 138.9 mW to 145 mW , the output power increases from 5.9 mW to 6.2 mW while pulse energy improves from 101 nJ to 106.5 nJ . It was shown that the long-cavity laser can generate three different pulses in the same laser cavity. The interaction and evolution of multiple pulses in mode-locked fiber lasers are attributed to the phase shift, which corresponds to the instantaneous frequency at pulse peak to be nonzero.

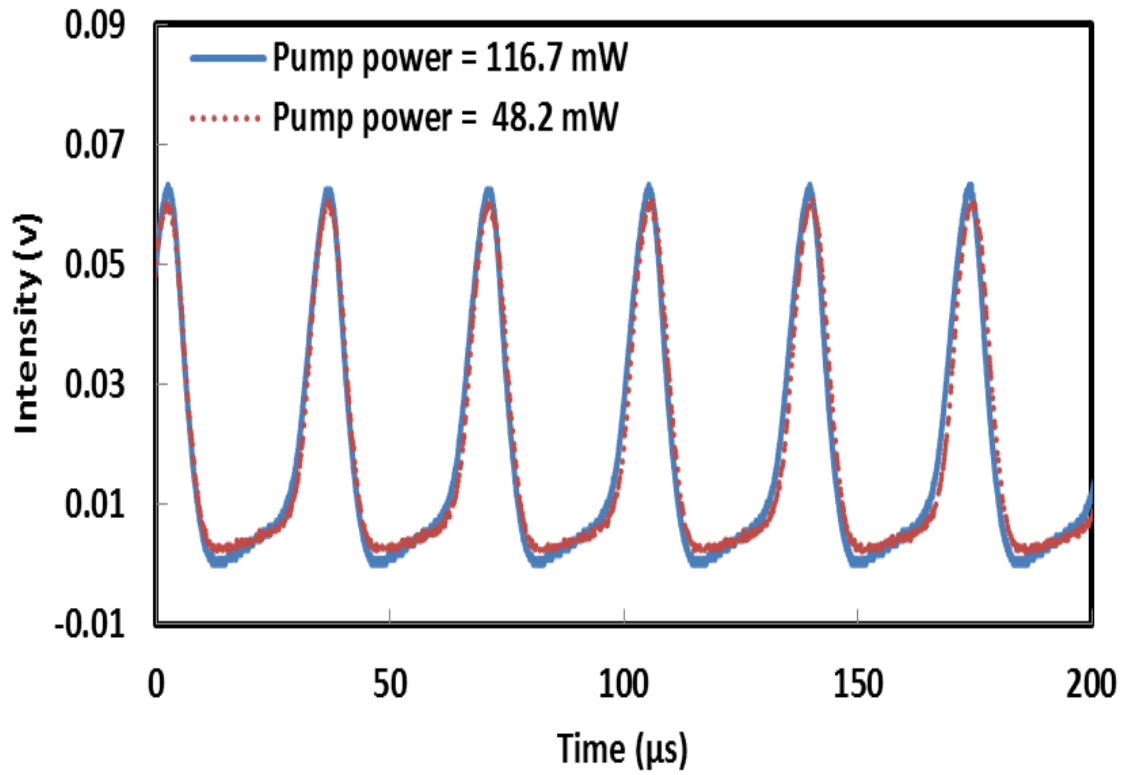


Figure 4.3: Typical pulse trains of the mode-locked EDFL at pump powers of 48.2 mW and 116.7 mW, which operate at fundamental mode

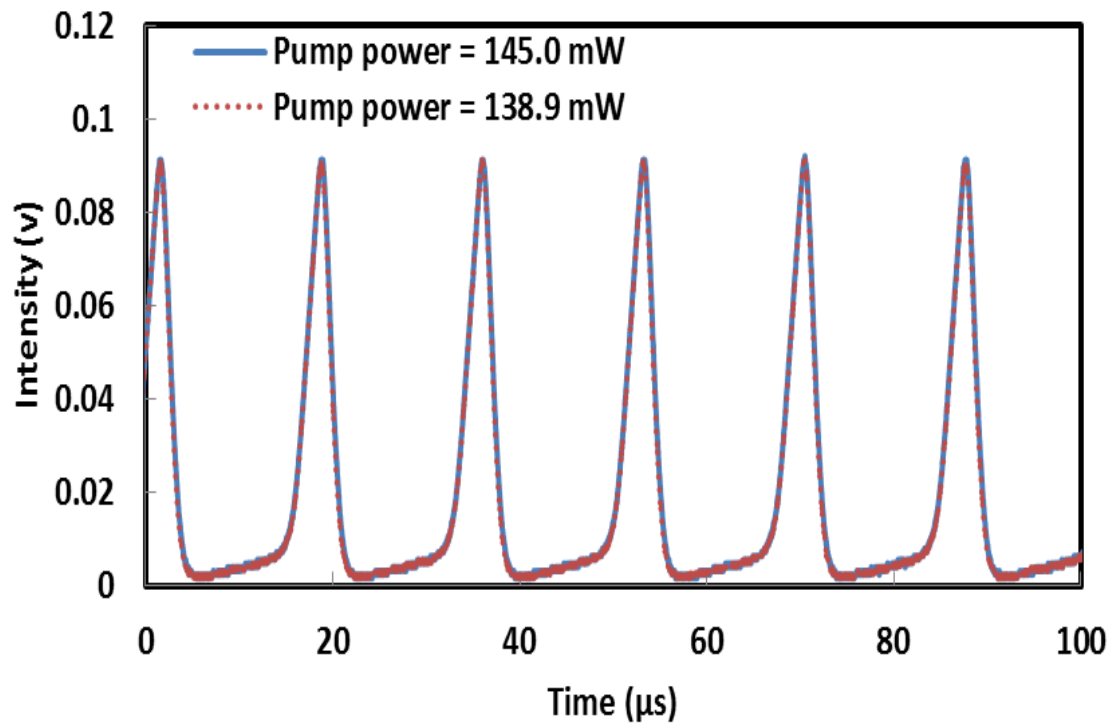


Figure 4.4: Pulse train obtained from proposed EDFL with pump power of 138.9 mW and 145 mW

Figure 4.5 shows the output spectrum of the mode-locked EDFL at different pump powers. The laser operates at a center wavelength of 1568 nm and the evolution of the output spectrum with the pump power can be explained by NPR phenomena. By adjusting the PC, the linear polarized light changes to elliptically polarized light. The elliptically polarized light splits into two orthogonal modes and experience different nonlinear phase shift as it propagates through DCF and EDF owing to Kerr effect. The direction of elliptically polarized light rotates due to the intensity difference. Rotated degree for central part of noise pulse can be different with leading and trailing edges. When it passes through PDI, only the central part can pass through with a low loss, whereas the leading and trailing edges are blocked. After many round trips, square pulse generation can be observed especially at a lower pump power. The square pulse duration increases with the pump strength. As shown in Figure 4.5, the optical spectrum has no characteristic sharp spectral edges as that of the dissipative solitons, but resembles that of the amplified spontaneous emission (ASE) of the EDF with the spectral centre shifted to the longer wavelength side. It is also found that the proposed laser here works on the stable operation when the pump power is from 17.5 to 34.3 mW, 48.2 to 116.7 mW, and 138.9 to 145.0 mW, respectively. In the other regime, the laser works unstably. So this laser alternately evolves on the stable and unstable mode-locking states as a function of the pump strength.

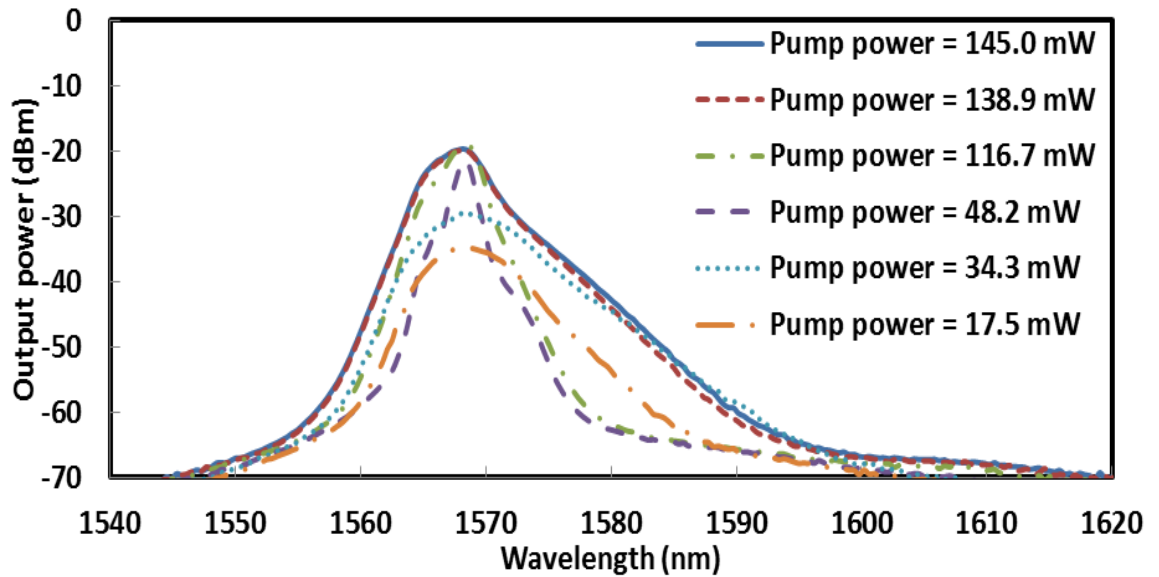


Figure 4.5: Optical spectrum of the mode-locked laser at various pump powers

4.3 Mode-locked square pulse emission with ultra-low repetition rate

Resonator with kilo-meters long offers lower fundamental repetition rate in the kilo-Hertz and hence allow the deliverance of higher pulse energy. However, there is a challenge that needs to be overcome if the oscillator is long. The combined action of both Kerr nonlinearity and dispersion generally leads to pulse break up (multi-pulse) after the accumulated nonlinear phase has exceeded a certain level. Pulse breaking leads to higher repetition rate and lower pulse energy compared to single pulse operation. Apart from the DS with steep spectral edges, a new approach, namely the dissipative soliton resonance (DSR) (Chang et al., 2008) has been suggested capable to increase the pulse energy from a fiber laser. The formation of DSR is based on certain parameters selection within the frame of complex Ginzburg-Landau Equation (CGLE) equation where its pulse energy can be increased infinitely. DSR is recognized as square pulse with flat top and steep edges and thus its pulse duration is rather broad. In this

section, nano-second DSR square pulse generation with an ultra-low repetition rate of 10.2 kHz is demonstrated by inserting a 20 km long SMF in a simple EDFL's ring resonator. It is worth noting that although the cavity length is significantly long, the fiber laser still operates at its fundamental repetition rate without pulse breaking. By manipulating the polarization state in the cavity, the proposed laser can also be adjusted to operate in harmonic mode.

4.3.1 Configuration of the proposed mode-locked square pulse EDFL

The experimental setup of the proposed mode-locked fiber laser is schematically shown in Figure 4.6. It uses a 4.5 m long EDF with an erbium concentration of 2000 ppm, cut-off wavelength of 910 nm, a pump absorption coefficient of 24 dB/m at 980 nm and a dispersion coefficient of -21.64 ps/nm·km at $\lambda = 1550$ nm, as the gain medium. The EDF is pumped with a 1480 nm laser diode through a 1480/1550 nm WDM. A PDI is used to ensure unidirectional propagation of light in the cavity and at the same time to generate linear light polarization. A PC is employed to adjust the polarization of light. A 20 km spool of SMF constitutes the long cavity and also serves to increase the nonlinearity and dispersion. The dispersion parameter of the SMF is 17 ps/nm·km. 50% of the circulating light is taken out of the cavity via a 3 dB coupler and then fed into another 3 dB coupler. The second coupler splits the light for simultaneous monitoring, one part into an OSA and the other into an oscilloscope (OSC) and Radio Frequency Spectrum Analyzer (RFS) together with a high speed photo-detector. The cavity is operating in a large negative dispersion region due to the long SMF

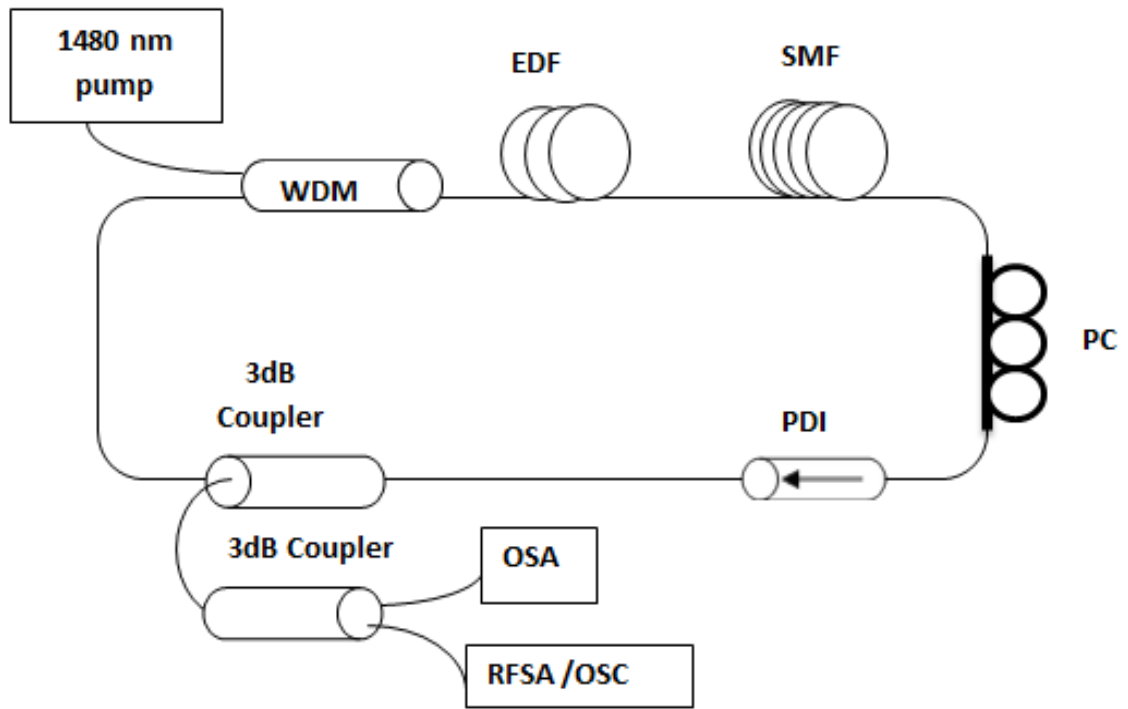


Figure 4.6: Experimental set-up of the proposed DSR laser

4.3.2 Mode-locked square pulse performance

The mode-locked laser is generated based on NPR effect in the ring cavity. The polarizing isolator placed besides the PC acts as the mode-locking element in the proposed laser. It plays the double role of an isolator and a polarizer such that light leaving the isolator is linearly polarized. Consider a linearly polarized pulse just after the isolator. The polarization state evolves nonlinearly during the propagation of the pulse inside the EDF and SMF due to SPM and cross phase modulation (XPM) effects in the ring cavity. The state of polarization is non-uniform across the pulse because of the intensity dependence of the nonlinear phase shift. The PC is adjusted so that it forces the polarization to be linear in the central part of the pulse. The polarizing isolator lets the central intense part of the pulse pass but blocks (absorbs) the low-intensity pulse wings. The net result is that the pulse is slightly shortened after one round trip inside the

ring cavity, an effect identical to that produced by a fast saturable absorber. In other words, the PDI, working together with the birefringence fibers generates an intensity dependent loss mechanism in the cavity that contributes to mode-locked square pulse generation in the cavity.

In this experiment, by careful adjustment of the PC, stable square pulse starts to form at pump power of 108 mW. Figure 4.7 shows the optical spectrum of the typical square pulse emission from the laser at three different pump powers of 108 mW, 112 mW and 125 mW. At the maximum pump power of 125 mW, the laser operates at 1568.7 nm with the peak power of -17.2 dBm and 3 dB bandwidth of about 1 nm. Figure 4.8 shows the oscilloscope trace of a square pulse train. The pulse train has an ultra-low repetition rate at 10.2 kHz as determined by the cavity length. Figure 4.9 focuses on a single pulse envelop at two different pump powers. As shown in the figure, the square pulse has distinct characteristic of steep leading and trailing edges and its pulse width can be tuned by changing the pump power. At 120 mW, the measured pulse width is 120.0 ns while at 125 mW pump power, the pulse width increases to 167.7 ns. At the maximum pump power, the pulse still has a square shape while keeping the peak power almost constant. With the orientations of the wave-plates fixed, it is observed that the peak power of the square pulse is maintained while the pulse width increases with pump power. The ripple structures on the top of the pulse are probably due to insufficient gain to compensate for the loss in the ultra-long cavity. A cleaner square pulse structure is expected at higher pump power.

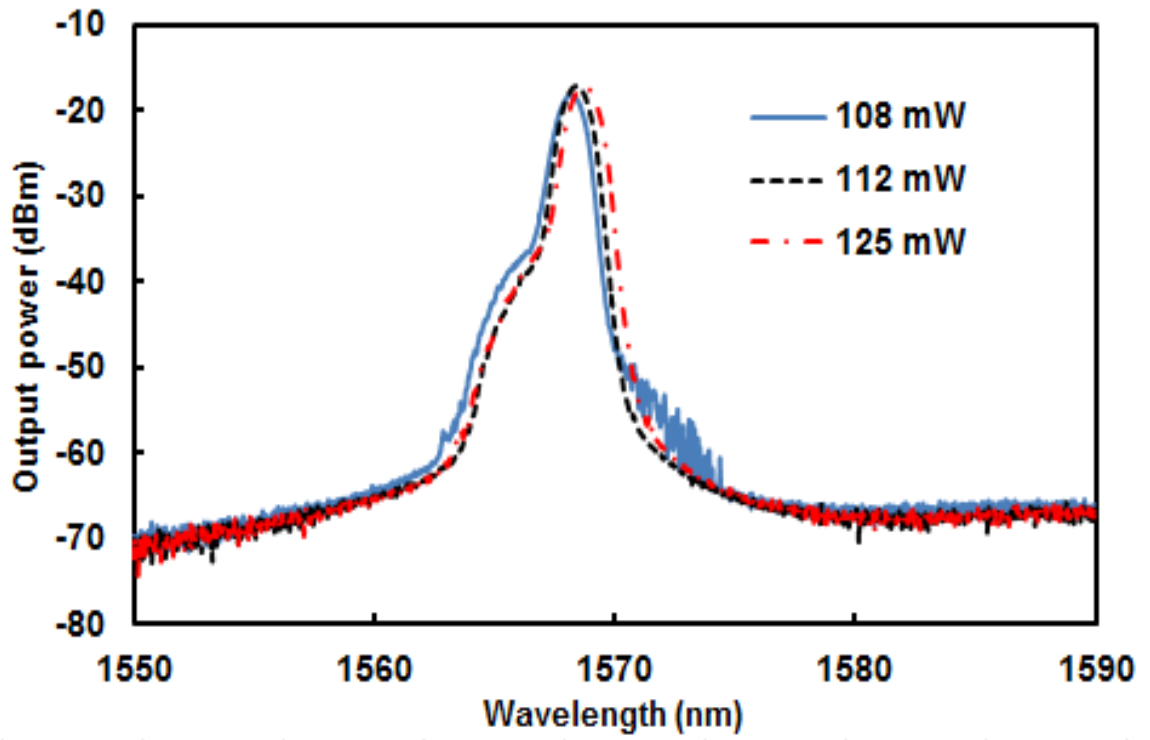


Figure 4.7: Optical output spectra of pulse laser at three different pump powers

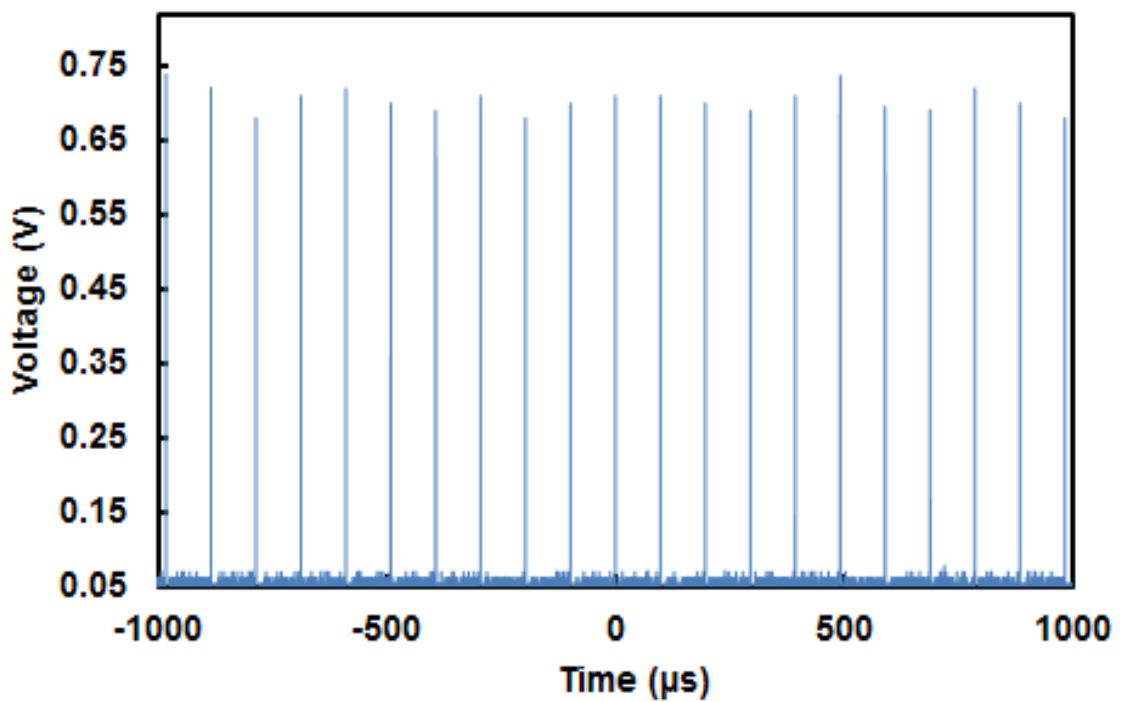


Figure 4.8: Typical pulse train with a fundamental repetition rate at 10.2 kHz

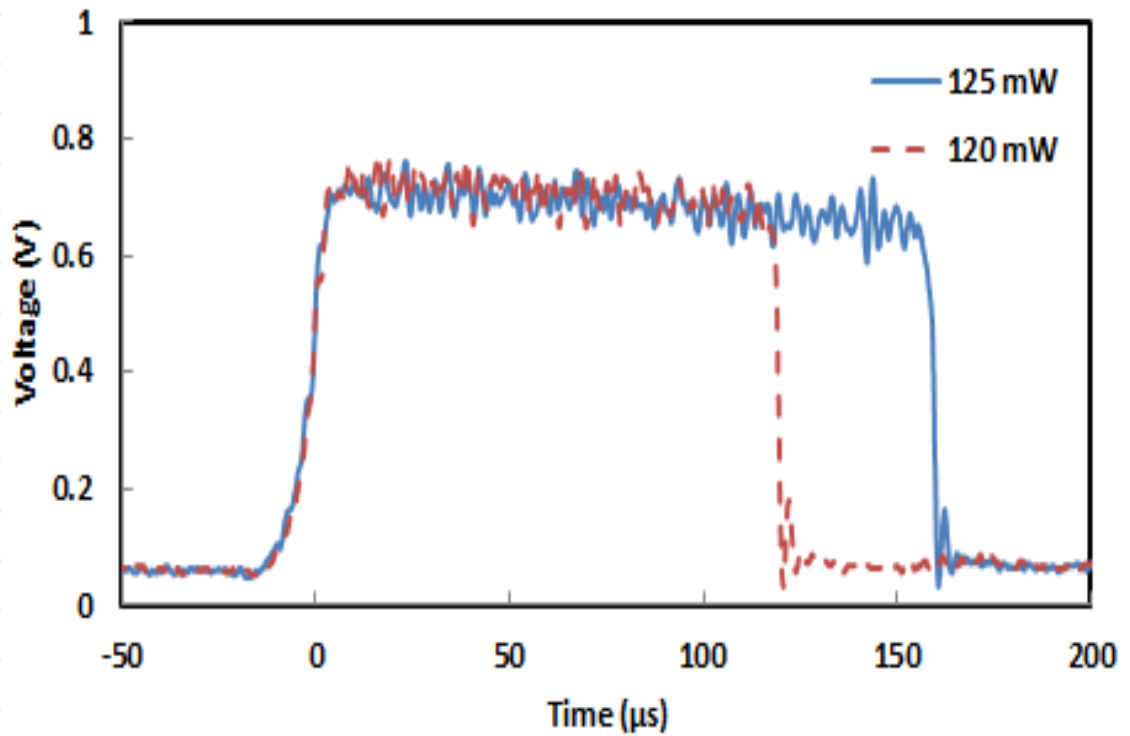


Figure 4.9: Oscilloscope trace of the single square pulse envelop at two different pump powers

As shown in Figure 4.7, the shape and 3 dB bandwidth of the mode-locked spectra are almost invariable with pump power. It is believed that the square pulse formed here has the characteristic of square shape which undergoes pulse broadening with constant peak power and also invariable 3 dB optical bandwidth spectra which resembles the DSR theory. The theory of DSR indicates that the pulse energy could be boosted up to an infinitely large value while the square pulse duration will broaden with increasing pump power while pulse amplitude converges to a given plateau value when the cavity parameters are chosen near to the resonance curve.

The evolution of pulse width with respect to pump power is presented in Figure 4.10. The pulse width can be tuned from 28.2 ns approximately to 167.7 ns without pulse breaking by increasing pump power from 108 mW to 125 mW. The generation of square pulse in the long cavity is most probably due to the DSR phenomenon in the long cavity laser. After the generation of square pulse, the peak amplitude is kept almost

constant and does not increase with pump power anymore. The excess power circulating in the cavity now accounts for the increase in the pulse width rather than the peak intensity. Due to the increment of pulse width, the pulse energy could be increased greatly as opposed to other soliton operation regions.

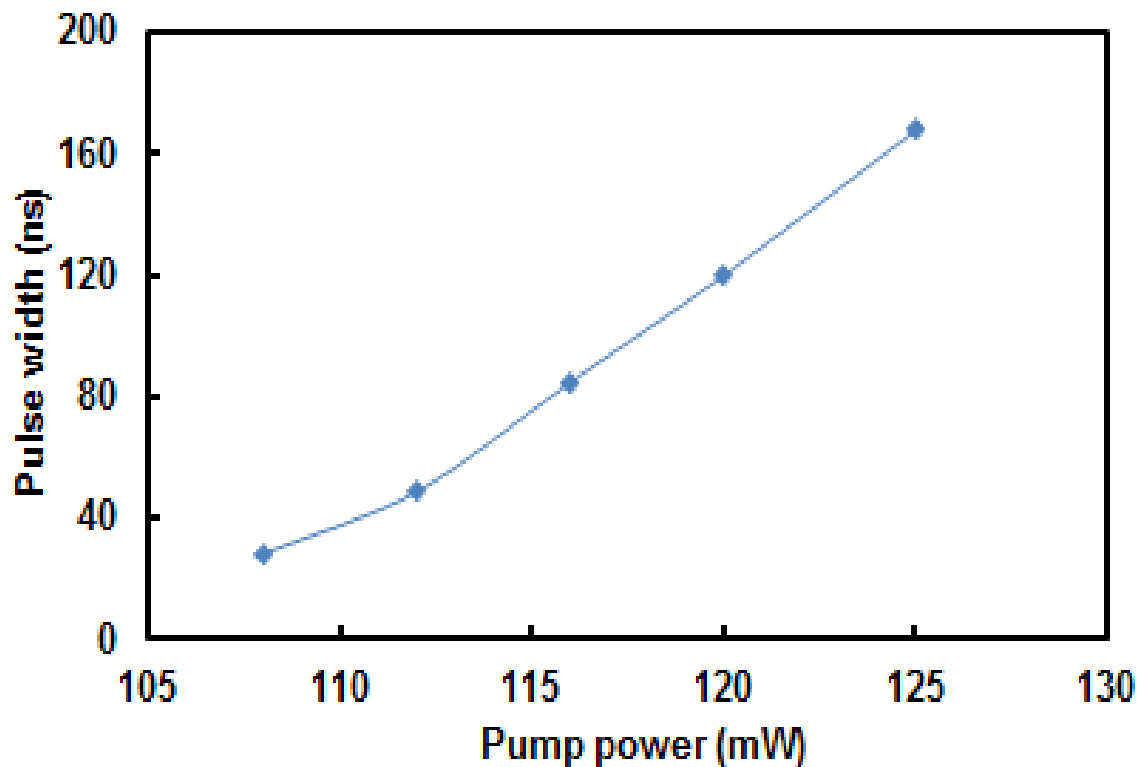
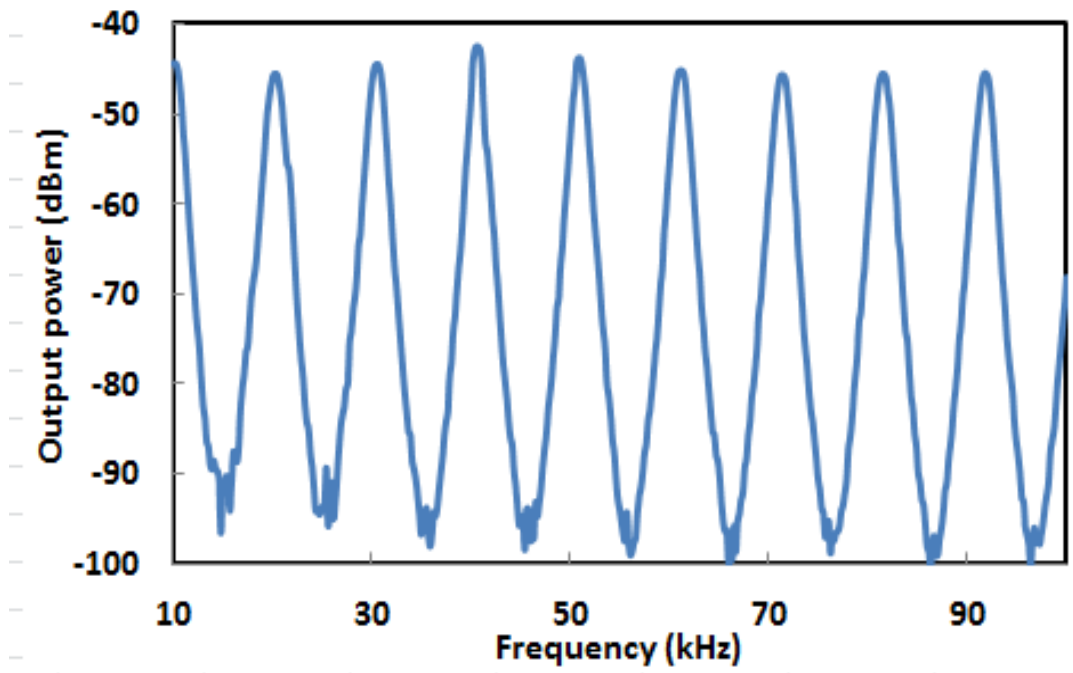
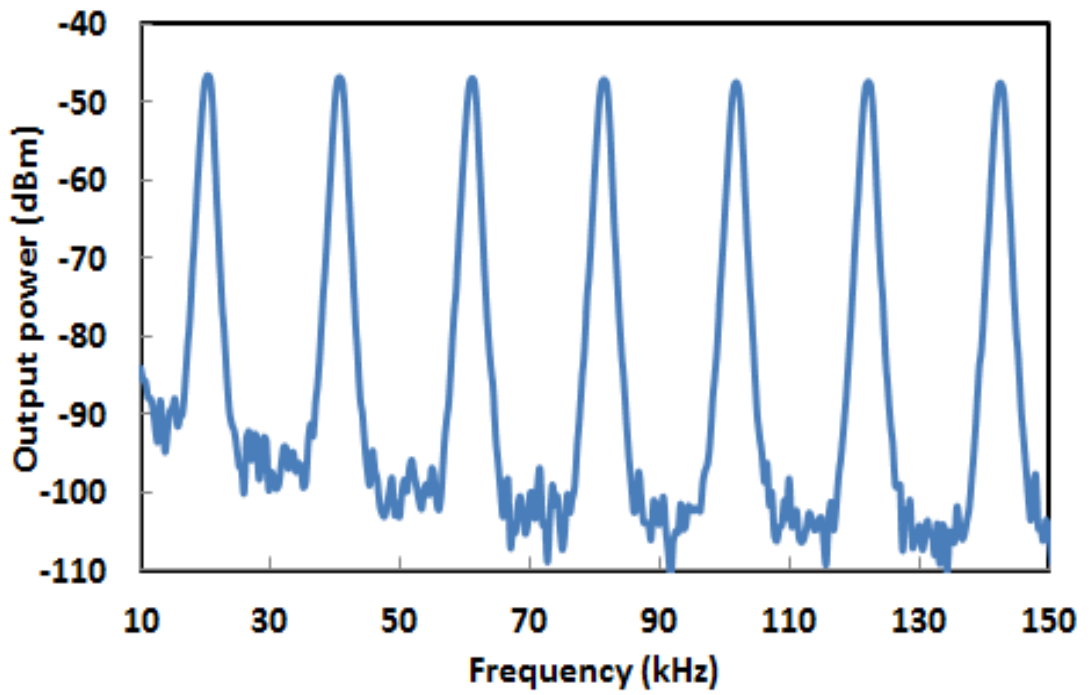


Figure 4.10: Pulse width of the square pulse versus pump power

Figure 4.11 shows the radio frequency (RF) spectrum for both the square and harmonic pulse (at pump power of 125 mW), which reveals the repetition rate of 10.2 kHz and 20.4 kHz respectively. The signal to noise ratio (SNR) is obtained from the intensity ratio of the fundamental peak to the pedestal extinction for both pulses are estimated to be approximately 42 dB and 44 dB, which indicates the stability of the laser. However, the SNR value is lower compared to other mode-locked fiber laser, which usually has a SNR of around 50 dB. This is attributed to the cavity length used which is significantly longer.



(a)

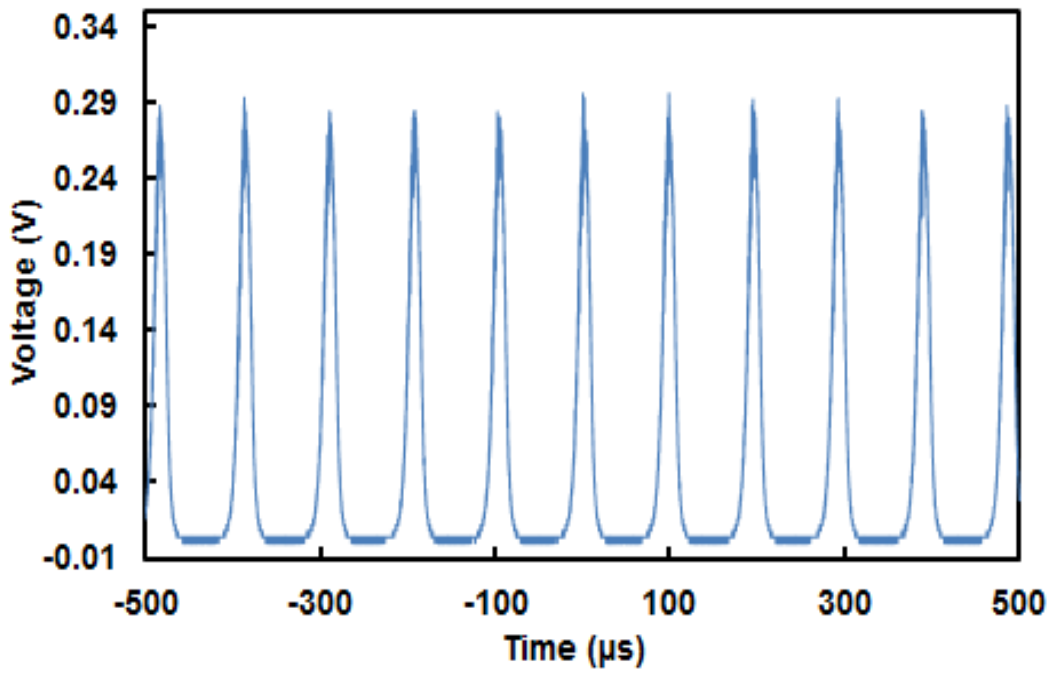


(b)

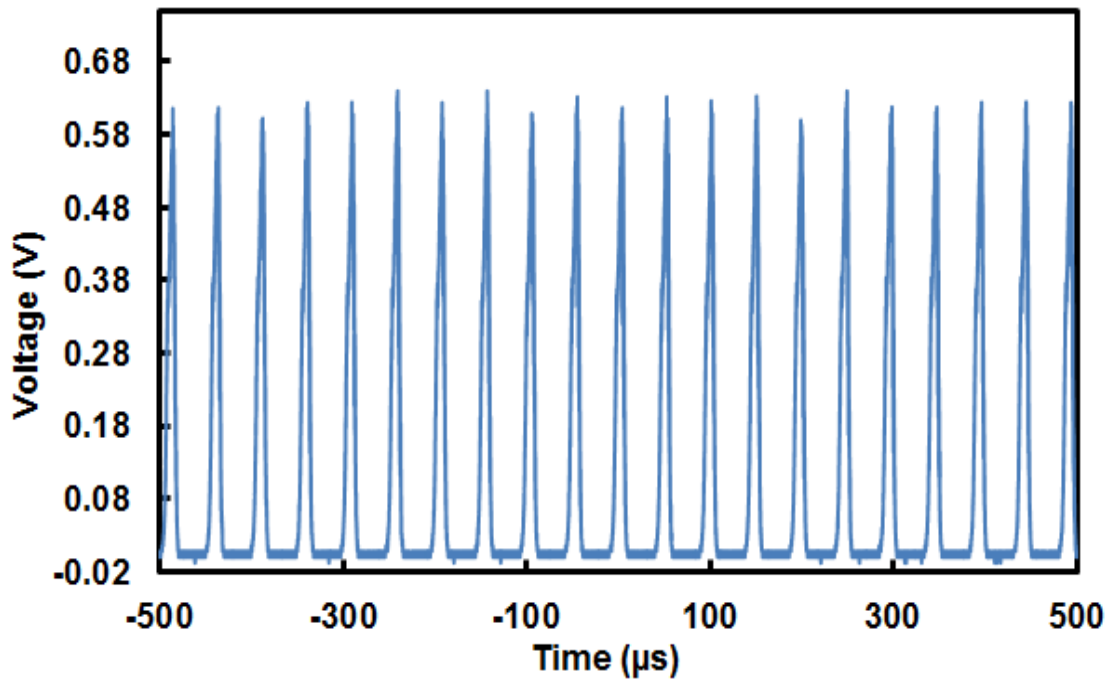
Figure 4.11: RF spectrum of the generated pulses: (a) square pulse and (b) harmonic pulse

The square pulse can be switched to harmonic pulse operating in micro-second region by careful adjustment of the PC while maintaining all other cavities' parameters. Self-starting harmonic mode-locking can be realized by an appropriate adjustment of polarization of light and at an adequate pump power. When pump power is raised to approximately 100 mW, mode-locked pulse is formed with repetition rate of 10.2 kHz which corresponds to the fundamental frequency.

As the pump power is increased to 108 mW, pulse breaking is observed where its repetition rate doubles to 20.4 kHz, representing the second harmonic order pulse. Harmonic mode-locking is regarded as a phenomenon when a single circulating pulse breaks into multiple pulses with constant temporal spacing. This technique is often adopted for high repetition rates in multi-GHz fiber lasers. The typical pulse train of the mode-locked fiber laser is shown in Figure 4.12 for two different pump powers of 100 mW and 108 mW. The attainable pulse widths are 14.2 μ s and 8.1 μ s at 100 mW and 108 mW, respectively. The optical spectrum of the harmonic pulse is illustrated in Figure 4.13 when the pump power is set at 125 mW. As shown in the figure, the harmonic laser operates at 1569.36 nm with peak output power of -18.4 dBm and 3 dB bandwidth of 1.7 nm.



(a)



(b)

Figure 4.12: Typical pulse train of the mode-locking pulse at two different pump powers: (a) 100 mW and (b) 108 mW

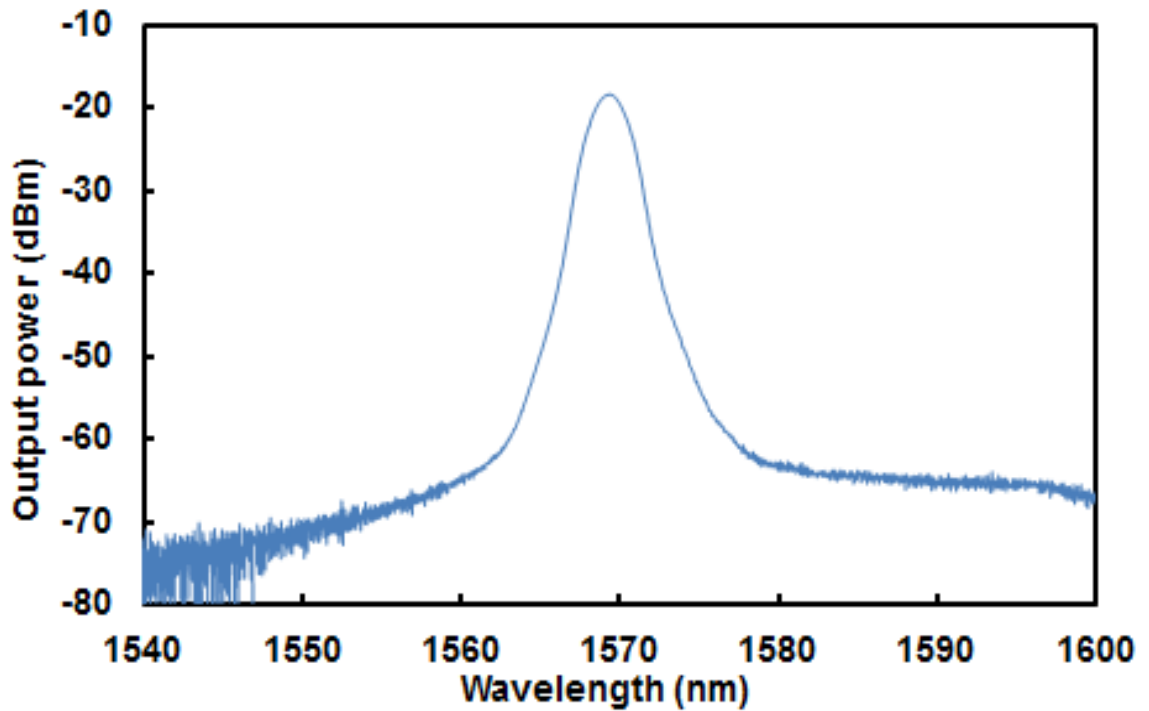


Figure 4.13: Output spectrum of the harmonic mode-locked EDFL

Figure 4.14 depicts the relationship between the output power and pump power for both DSR and harmonic pulses obtained from the proposed mode-locked EDFL of Figure 4.6. The output power is measured at the 50% port of second 3 dB coupler which channels the output light into OSA. It is observed that the output power increases linearly with pump power for both lasers. As expected, the square pulse recorded higher output power compared to harmonic pulse. The output power for square pulse varies from 2.19 mW to 2.54 mW as the pump power increases from 108 mW to 125 mW. On the other hand for harmonic pulse, the highest measured output power is 2.39 mW at 125 mW. Figure 4.15 shows how the pulse energy changes with the increment of pump power for both lasers. Both square and harmonic pulses exhibit relatively high pulse energy in the nano-Joule range due to the long cavity length used in the laser setup. Pulse energy of both lasers is found to be increasing with pump power. By increasing the pump power from 108 mW to 125 mW, the pulse energy increases in a range of 215.3 nJ to 249.8 nJ and 0.215 pJ to 0.249 pJ for the square and harmonic pulse,

respectively. It is observed that the pulse energy reduces drastically from 188.7 nJ (100 mW) to 100 nJ (108 mW) as the fundamental pulse breaks into the second harmonic order pulse. When the fundamental pulse breaks, the repetition rate doubles from 10.2 kHz to 20.4 kHz. This will reduce the pulse energy as the pulse energy is inversely proportional to repetition rate. Consequently, the pulse energy of square pulse can be further increased by optimizing the laser parameters and employing higher pump power.

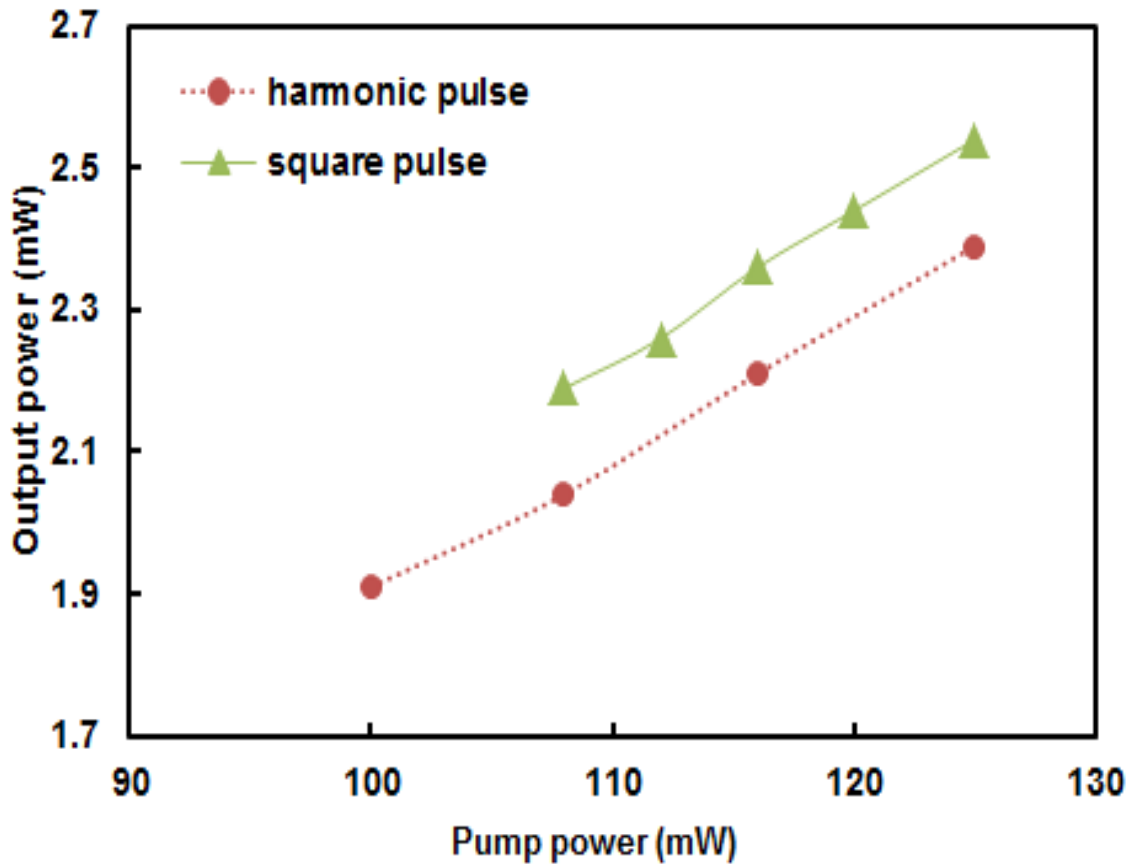


Figure 4.14: Measured output power for square and harmonic pulse at various pump powers

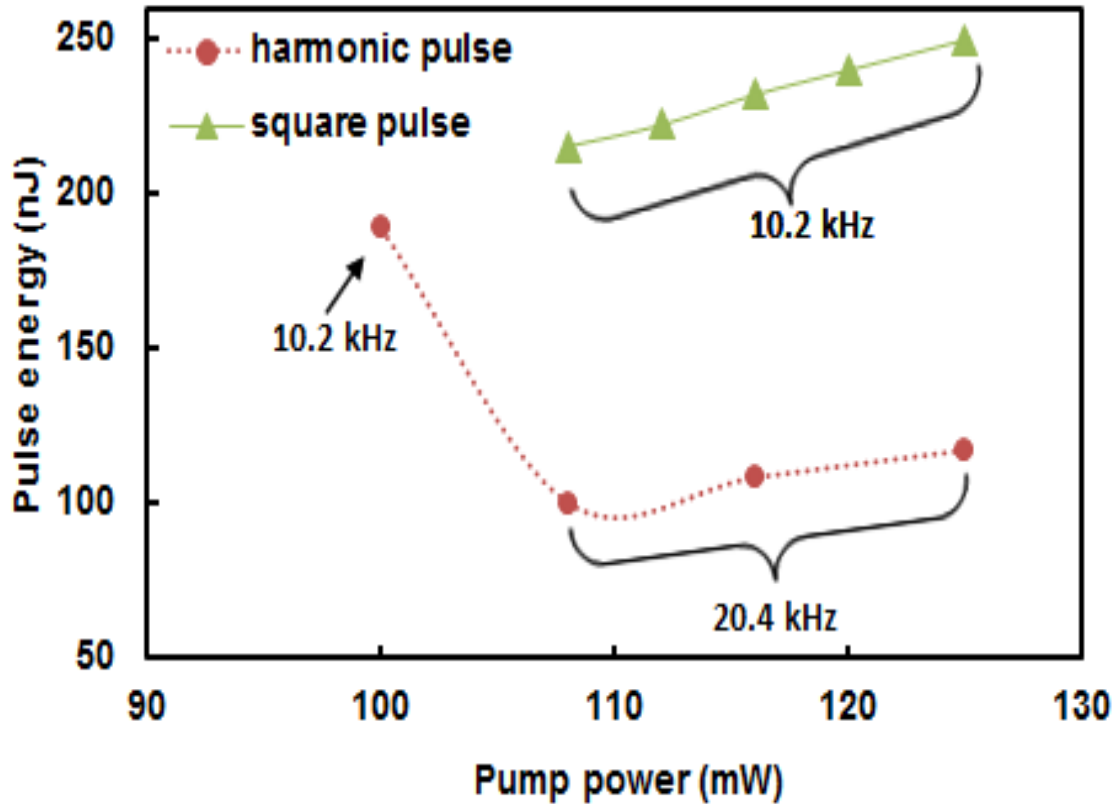


Figure 4.15: Pulse energy of produced pulse for square and harmonic pulse

The maximum attainable pulse energy for the square pulse is higher than second harmonic pulse by 53.1%. Lower pulse energy is observed for harmonic pulse due to the occurrence of pulse breaking phenomena where a single pulse breaks into many pulses; two pulses in this experiment. After a single pulse is formed and traverses in the cavity, it encounters high nonlinear effects and dispersion, introduced by the long SMF. A single pulse will break into many pulses where overtaking of different parts of a pulse will lead to optical wave breaking. It can be concluded that a laser should remain single pulse operation in order to realize high pulse energy. Square pulse which has steeper leading and trailing edges along with flat top in the temporal domain can withstand pulse breaking compared to the Gaussian or sech^2 shape pulse. This can be presumed that the square pulse has very low frequency chirps across the central region of pulse and has nonlinear pulse chirping at the pulse edges. The nonlinear chirp at the pulse edges can resist the dispersion and nonlinearity effects in the cavity and thus can

maintain its wave breaking free pulse. Neither square pulse nor harmonic pulse is observed when the 20 km long SMF is removed. Without the long SMF, only the conventional pulse with Kelly side-bands is obtained. The insertion of 20 km long SMF brings the cavity's parameter near to the resonance curve, thereby producing wave breaking free square pulse. From the experimental results, the laser operates in two different operating regimes; harmonic and square pulse by changing the pump power and also the polarization of light. The change of light polarization leads to different saturable absorption strength and intrinsic spectral filtering which affects the intra-cavity nonlinear gain and transmittivity. As a result, various kinds of pulse shapes can be formed. Both square and harmonic pulses generated by the mode-locked EDFL are stable. If there is no perturbation introduced to the laser, both square and harmonic pulse EDFL can last several hours under normal laboratory condition.

4.4 Multi-wavelength mode-locked EDFL in figure-of-eight cavity

Both multi-wavelength and mode-locked EDFLs have wide applications in optical communications, sensors and instrumentations (Brackett, 1990; Yoo et al., 2009). There are many different methods that have been proposed to achieve multi-wavelength lasing at room temperature such as cascaded stimulated Brillouin scattering (Ippen & Stolen, 1972), incorporating a semiconductor optical amplifier or raman amplifier and four-wave mixing (FWM) (Harun et al., 2009). Besides the application of pulsed laser generation, nonlinear NPR which can induce intensity dependent loss in the laser cavity is also widely used for multi-wavelength laser generation. In this section, a multi-wavelength mode-locked EDFL is demonstrated using figure-of-eight set up by incorporating 50 m long photonic crystal fiber (PCF) and 20 km long SMF.

4.4.1 Configuration of the proposed multi-wavelength mode-locked EDFL

The experimental set-up of the proposed multi-wavelength mode-locked EDFL is illustrated in Figure 4.16, which the ring resonator consists of a 3.5 m long EDF as the linear gain medium, wavelength division multiplexer (WDM), polarization-dependent isolator (PDI), polarization controller (PC), 50 m long PCF, 20 km long SMF, 2 x 2 coupler and 3 dB couplers. The EDF used has an Erbium ion concentration of 2000 ppm, core diameter of 4 μm , mode field diameter of 6 μm and NA of 0.24. A 1480 nm laser diode is used to pump the EDF via the WDM. A PDI and PC are incorporated in the laser cavity to ensure unidirectional propagation of the oscillating laser and to act as a polarizer. 20 km long SMF is placed between the PDI and PC to function as a nonlinear gain medium. The figure-of-eight is achieved by a 2 x 2 coupler connected with PCF to form another ring. The output of the laser is collected from the cavity via a 3 dB coupler which retains 50% of the light in the ring cavity to oscillate. The optical spectrum analyser (OSA, Yokogawa, AQ6370B) is used for the spectral analysis of the proposed EDFL with a spectral resolution of 0.02 nm whereas the oscilloscope (OSC, Tektronix, TDS 3052C) is used to observe the output pulse train of the mode-locked operation via a 1 GHz bandwidth photo-detector.

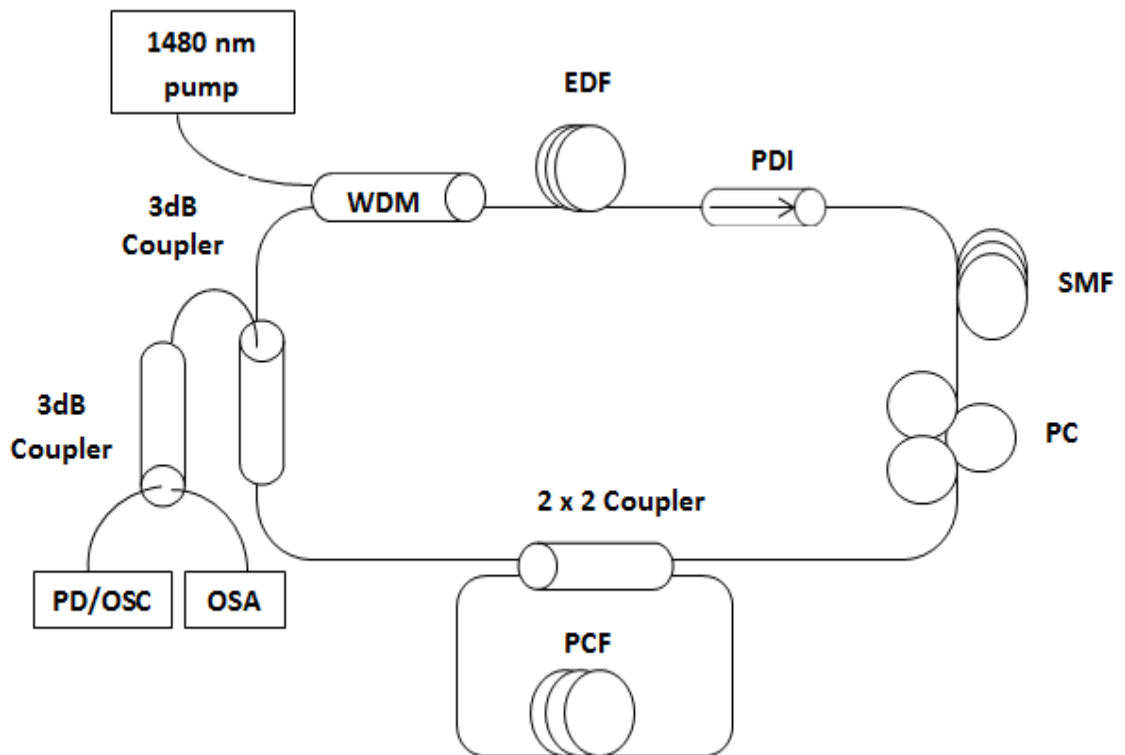
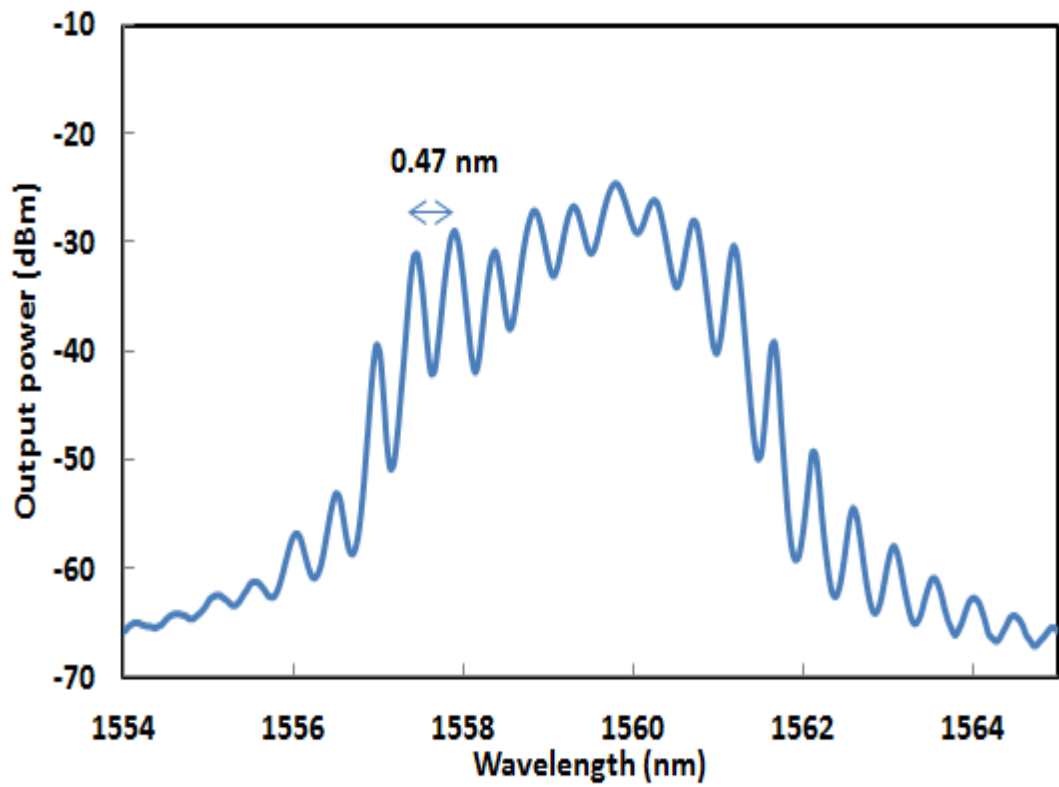


Figure 4.16: Schematic configuration of the proposed multi-wavelength mode-locked EDFL

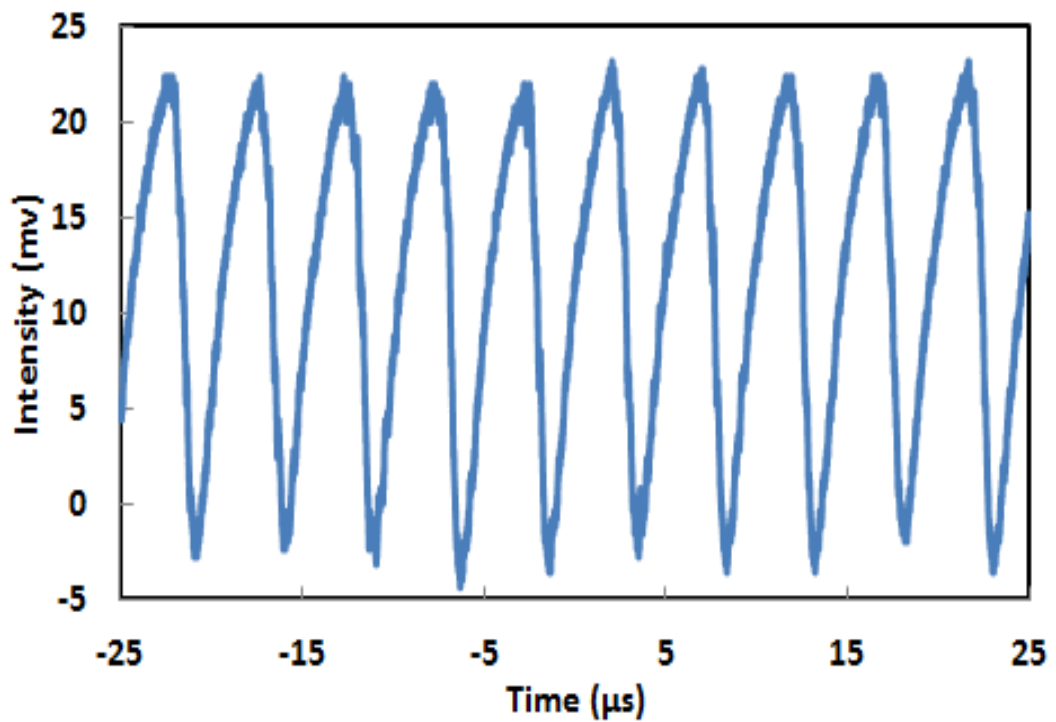
4.4.2 Multi-wavelength mode-locked performance

The multi-wavelength mode-locked operation is observed as the pump power is fixed within 137 mW to 146 mW. Figures 4.17(a) and (b) show the measured multi-wavelength output spectrum and typical mode-locked pulse train of the laser respectively, at pump power of 146 mW. As shown in Figure 4.17(a), the laser produces at least 11 lines with free spectral range (FSR) of 0.47 nm, which is determined by the length and the effective group indices of the PCF. The multi-wavelength generation is due to the intensity dependent loss induced by the NPR effect in the cavity. The role of 20 km long of SMF and 20 m of PCF is to increase the nonlinear effect as well as to constitute an inline periodic filter with the PDI. The multi-wavelength laser also

produces a mode-locked pulse train with repetition rate of 185 kHz and pulse width of 1.87 μs as shown in Figure 4.17(b). Multi-wavelength generation can be described as follows. The light source is split into two orthogonal modes, which experience different nonlinear phase shift as they propagate inside SMF and PCF owing to the Kerr effect. Then the polarization orientation of light rotates in these fibers with the angle of rotation is correlative with light intensity. The signal passes through the PDI, which the transmittivity is depended on the rotation of polarization or oscillating light intensity. Combination of the nonlinear gain media and PDI functions an intensity equalizer, which produces an intensity dependent inhomogeneous loss and thus suppresses the mode-competition. As a result, the balance between the inhomogeneous loss induced by NPR and the mode competition effect of the EDF can lead to a stable multi-wavelength oscillation. Moreover, figure-of-eight set up allows multiple oscillations of light inside the PCF, which further enhance the NPR effect in the cavity. If the polarization state is selected properly by adjusting the PC, multi-wavelength laser can be easily obtained. Figure 4.18 shows the spectrum of the multi-wavelength laser against the pump power. As shown in the figure, peak power increases with the pump power from 137 mW to 146 mW. However, the wavelength spacing is maintained at 0.47 nm throughout the multi-wavelength mode-locked tuning range.



(a)



(b)

Figure 4.17: Output of the proposed multi-wavelength mode-locked EDFL at pump power of 146 mW: (a) Optical spectrum and (b) typical mode-locked pulse train

As observed from the pulse train characteristic, pulse repetition rate doesn't change with the pump power and is maintained at 185 kHz throughout the experiment, which crucially indicates the mode-locking operation. By increasing the pump power 137 mW to 146 mW, the output power can be increased from 348 μ W to 369 μ W, whereas the pulse width remains at 1.87 μ s. By taking average output power divided by pulse repetition rate, maximum pulse energy of 2 nJ is obtained at the maximum pump power of 146 mW. The mode-locking operation is generated based on the NPR phenomena as well. By adjusting the PC, the linear polarized light changes to elliptically polarized light. The elliptically polarized light splits into two orthogonal modes and experience different nonlinear phase shift as it propagates through SMF and EDF owing to Kerr effect. The direction of elliptically polarized light rotates due to the intensity difference. Rotated degree for central part of noise pulse can be different with leading and trailing edges. When it passes through PDI, only the central part can pass through with a low loss, whereas the leading and trailing edges are blocked. After many round trips, stable mode-locked pulse can be generated as observed in Figure 4.17(b). The stability of the mode-locked is further studied by RF spectrum analyzer. Figure 4.18 shows the result from RF spectrum, where the SNR is measured to be about 40 dB. Besides, the frequency is obtained at around 185 kHz, which is well tally with the pulse repetition rate of Figure 4.17(b).

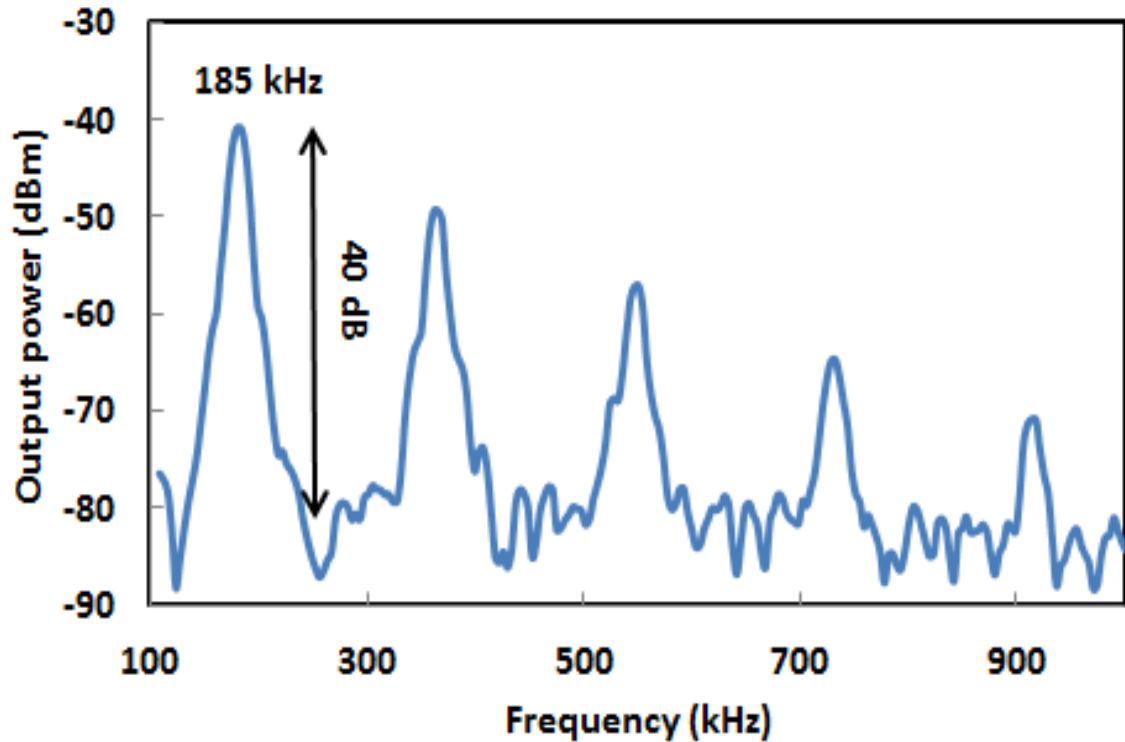


Figure 4.18: RF spectrum of the proposed multi-wavelength mode-locked EDFL

4.5 Summary

In this chapter, various types of mode-locking operations have been demonstrated based on NPR techniques, which included mode-locked EDFL with three switchable operating states, mode-locked square pulse EDFL and multi-wavelength mode-locked EDFL. It is found that the NPR based mode-locking operations are highly relied on the polarization state. Different mode-locking operation can be generated in a same cavity with the change of polarization state as shown in section 4.2 and section 4.3. Besides, pump power also plays an important role to induce mode-locking operation. Different mode-locking states require different threshold pump power. Under a sufficiently high pump power, mode-locked experiences pulse breaking process to generate square pulse or higher order harmonic mode-locked. Under NPR based mode-locked, the pulse repetition rate is constrained by the cavity length. Therefore, higher

order harmonic mode-locked is a solution to achieve higher pulse repetition rate and narrower pulse width mode-locked. On the other hand, the balance between the inhomogeneous loss induced by NPR and the mode competition effect leads to stable multi-wavelength oscillations. Throughout the experiment, multi-wavelength mode-locked is not achievable in a single loop cavity such as the set-up in section 4.2 and section 4.3. This is because mode-locked and multi-wavelength required different NPR mechanism to induce the phenomena. However, in figure-of-eight set-up, the main loop induces the mode-locking operation, whereas another loop induces the multi-wavelength operation to ‘slice’ the spectrum of the cavity.

The results shown in chapter 3 and chapter 4 are all operate in bright pulse regime. Besides the bright pulse regime, there is another type of operation regime, called dark pulse regime. Dark pulse regime is represented as a narrow intensity dip under a strong CW laser emission background. In the following chapter, several types of dark pulse lasers are investigated via NPR method.

CHAPTER 5

GENERATION OF DARK PULSES IN ERBIUM-DOPED FIBER LASER CAVITY USING NONLINEAR POLARIZATION ROTATION APPROACH

5.1 Introduction

Soliton formation is an attractive topic that has been extensively investigated in recent years due to its many applications in optical communications, sensors and instrumentations (Buryak et al., 2002). To date, most of the reported works on soliton mode-locked lasers are operating under the bright pulse regime. In addition to the bright pulse, fiber lasers can also generate the so-called dark solitons that are also a solution of the nonlinear Schrödinger equation (NLSE) (Radhakrishnan & Lakshmanan, 1995). These solitons can also be theoretically explained by the complex Ginzburg-Landau equation (CGLE). The dark pulses can be classified into two types; domain-wall (DW) and NLSE depending on their formation mechanisms. The difference between DW and NLSE type dark pulses is relied on their spectrum profile. The spectrum of the NLSE type dark pulse has only a single peak whereas the DW pulse produces an output spectrum with multiple peaks. The generation of DW pulse can be realized in both normal and anomalous dispersion while the standard NLSE type dark pulse could only be produced by a normal dispersion cavity. However, if the incident light field propagates in a medium with strong non-Kerr nonlinearities, it is possible to generate another type of dark pulse so-called Cubic-quintic nonlinear Schrödinger equation (CQNLSE) (Zhang & Dai, 2005) in anomalous dispersion cavity.

In this chapter, several passively mode-locked Erbium-doped fiber lasers (EDFLs) operating in dark pulse regime are demonstrated using NPR technique. At first, the generation of three different types of dark pulses; NLSE, DW and CQNLSE are demonstrated. Then, a multi-wavelength mode-locked fiber EDFL, which generates a dark pulse train is proposed and demonstrated by using long laser cavity. Finally, generation of the dark pulse train is demonstrated in Q-switched mode-locked EDFL based on NPR technique.

5.2 Harmonic NLSE dark pulse emission in EDFL

Most of the mode-locked lasers are reported to operate in bright pulse regime. However, fiber lasers can also generate the so-called dark pulses (Kivshar & Luther-Davies, 1998), which are normally referred to a train of intensity dips in a CW background of the laser emission. The existence of dark solitons is explained by both NLSE and CGLE. In this section, we experimentally demonstrated a NLSE dark pulse emission in EDFL cavity based on NPR technique. The operating regime of the proposed dark pulse laser can be tuned from fundamental to 5th order harmonic under appropriate polarization orientation and pump power.

5.2.1 Experimental setup

The experimental set-up of the proposed EDFL is illustrated in Figure 5.1, which comprises of two loops in figure of eight configuration. The main loop consists of a 3.5 m long EDF as the gain medium, wavelength division multiplexer (WDM), polarization-dependent isolator (PDI), polarization controller (PC), 10 km long

dispersion shifted fiber (DSF) and two 3 dB couplers. The EDF used has a doping concentration of 2000 ppm and group velocity dispersion (GVD) of about -21.64 ps/nm.km. This fiber was pumped by a 1480 nm laser diode via the WDM. The secondary loop consists of a 100 m long highly nonlinear fiber (HNLF), which is connected to the main loop by a 3 dB coupler. The HNLF has a dispersion of 0.15 (ps/nm)/km at 1550nm and effective area of $12.3 \mu\text{m}^2$. A PDI was used in the cavity to force a unidirectional operation of the ring, and an in-line PC was inserted in the cavity to adjust the linear birefringence of the cavity. A 2×2 3 dB fiber coupler was used to form a figure-of-eight structure with a piece of HNLF inserted in the new loop. The output of the laser was collected from the cavity via a 3 dB coupler which retained 50% of the light in the ring cavity to oscillate. The optical spectrum analyser (OSA, Yokogawa, AQ 6370B) was used for spectral analysis of the proposed EDFL with a spectral resolution of 0.02 nm whereas the oscilloscope was used to observe the output pulse train of the dark pulse emission via a 1 GHz bandwidth photo-detector.

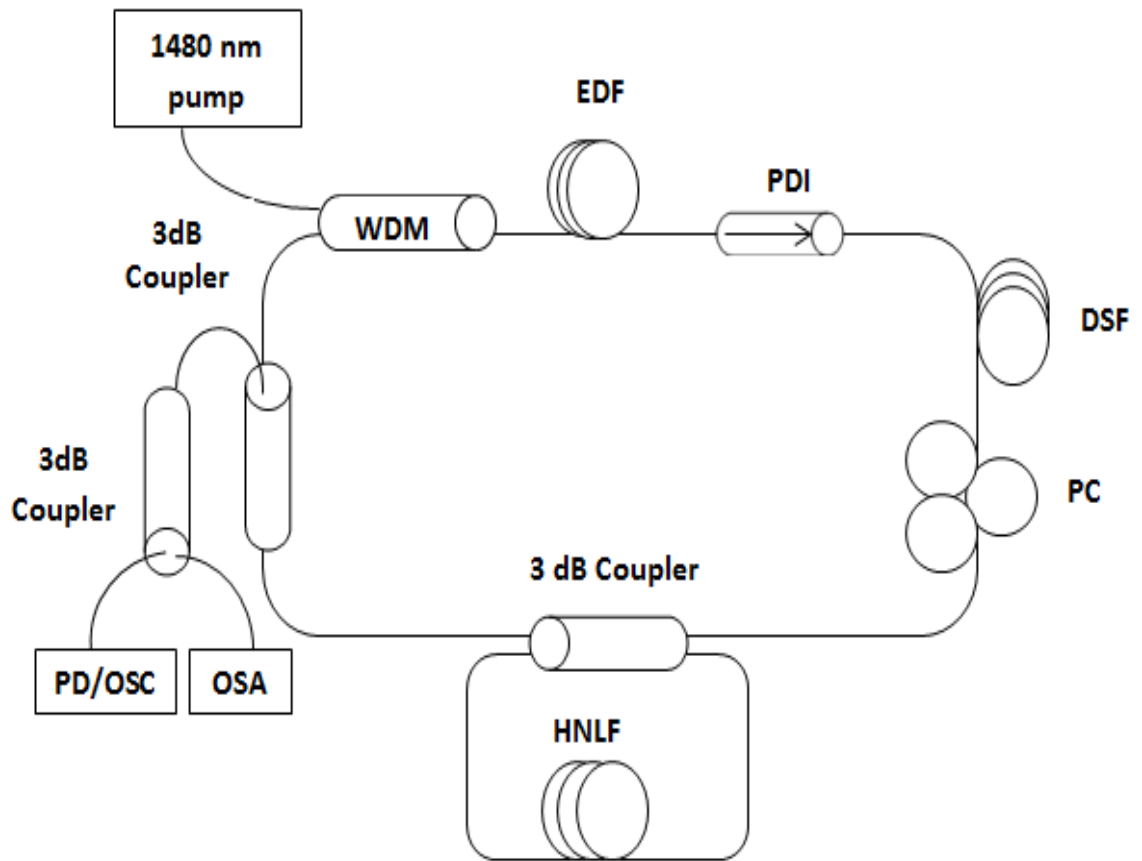
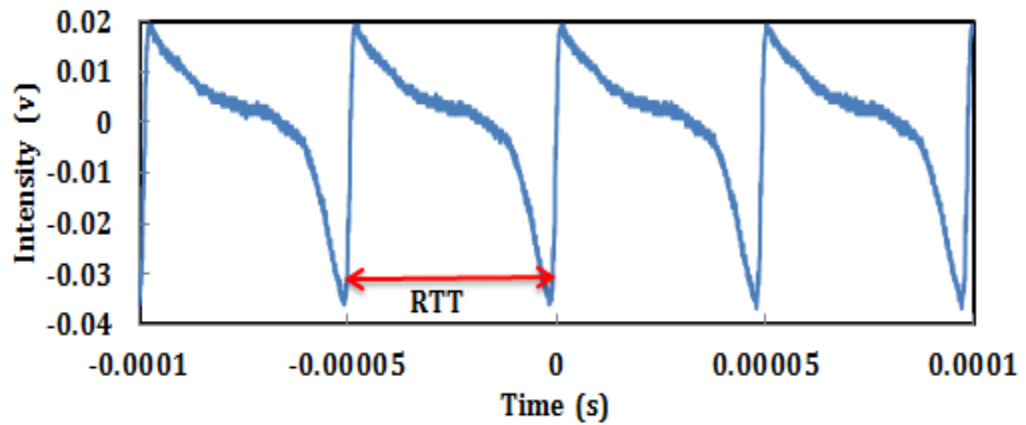


Figure 5.1: Schematic configuration of the proposed dark pulse EDFL

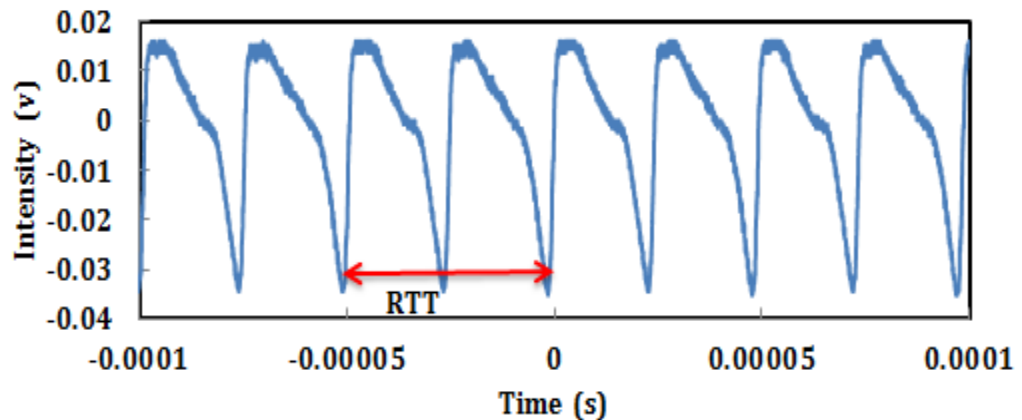
5.2.2 NLSE dark pulse performance

By carefully adjusting the PC orientation, dark pulse emission operating in fundamental repetition rate of 20 kHz could be observed at pumping threshold power of 29 mW. The typical pulse train of the fundamental dark pulse is shown in Figure 5.2(a). As shown in the figure, the dark pulse was represented as a narrow intensity dip in the strong CW laser emission background. When the 10 km DSF was removed from cavity, we were still able to observe dark pulse formation. However, the dark pulse train was random and unstable. To obtain a stable dark pulse train of laser emission, it was necessary to have a sufficient nonlinear gain in the cavity. Therefore, a 10 km DSF is incorporated in the proposed laser cavity to provide a nonlinear gain, which is required for the NPR process.

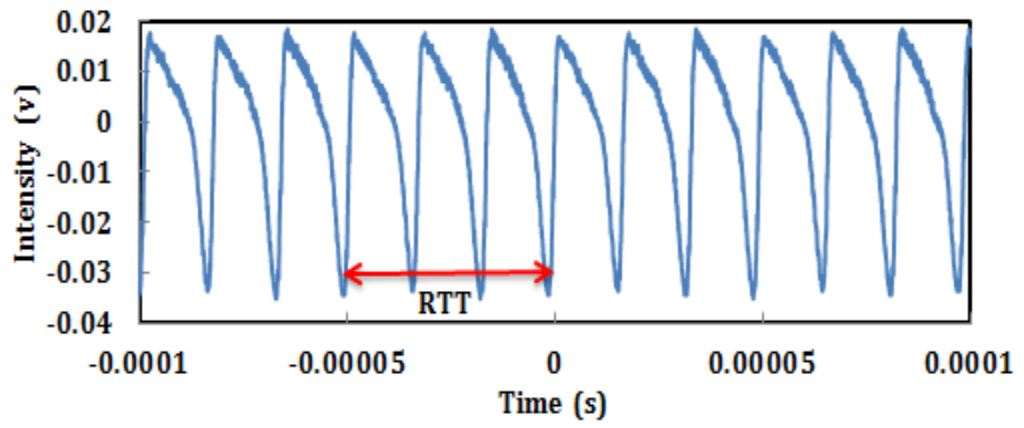
In addition, figure-of-eight setup also induced competition between two cavity modes and cavity feedback, which played an important role in the stability of the dark pulses in the laser. A harmonic dark pulse can also be formed in round trip time (RTT), where the harmonic's order can be tuned by increasing the pump power as shown in Figure 5.2(b)-(e). By carefully adjusting the PC, the operating frequency of the dark pulse trains were shifted to 2nd order, 3rd order, 4th order and 5th order harmonic as the pump power was increased to 34 mW, 50 mW, 59 mW and 137 mW respectively. The 2nd, 3rd, 4th and 5th harmonics correspond to repetition rates of 40 kHz, 60 kHz, 80 kHz and 100 kHz, as shown in Figure 5.2(b), (c), (d) and (e) respectively.



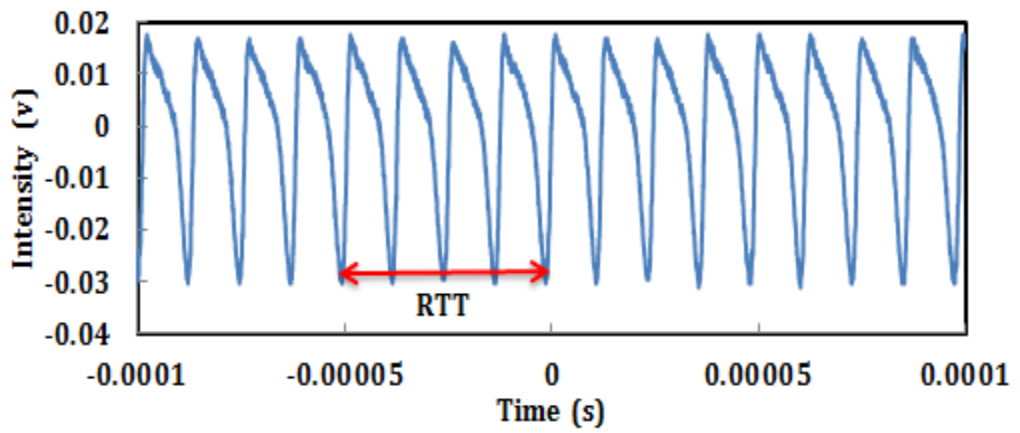
(a)



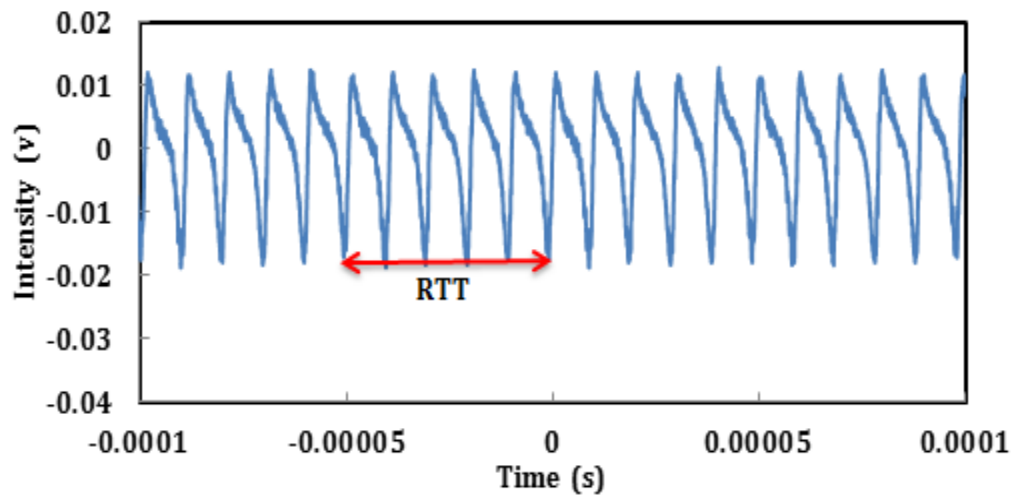
(b)



(c)



(d)



(e)

Figure 5.2: Dark pulse emission of the proposed EDFL at different orders of harmonic: (a) fundamental, (b) 2nd, (c) 3rd, (d) 4th, and (e) 5th

Figure 5.3 shows threshold pump power to achieve different order of harmonics and its corresponding output power at the threshold pump power. The fundamental repetition rate is observed at 29 mW, whereas the 2nd, 3rd, 4th and 5th order harmonics are obtained at pump power of 34 mW, 50 mW, 59 mW and 137 mW respectively. As the pump power is further increased to 150 mW and above, no higher harmonic order is observed. This may be caused by the gain limitation which constrained the pulse from further breaking beyond the 5th order harmonic. In the presence of relatively high pumping power, a single pulse circulating in the cavity can be split into several pulses. In such regime, pulses are usually randomly located in the cavity. However, under certain conditions they can self-arrange to create a stable and well organized pulse train with repetition rates far beyond the fundamental mode spacing. It is observed that the harmonic order increased as we increased the pump power. The output power also increased from 0.86 mW to 2.86 mW as the harmonic order was changed from the fundamental to the 5th order harmonic. This was attributed to the pump power used which was larger for the higher harmonic order.

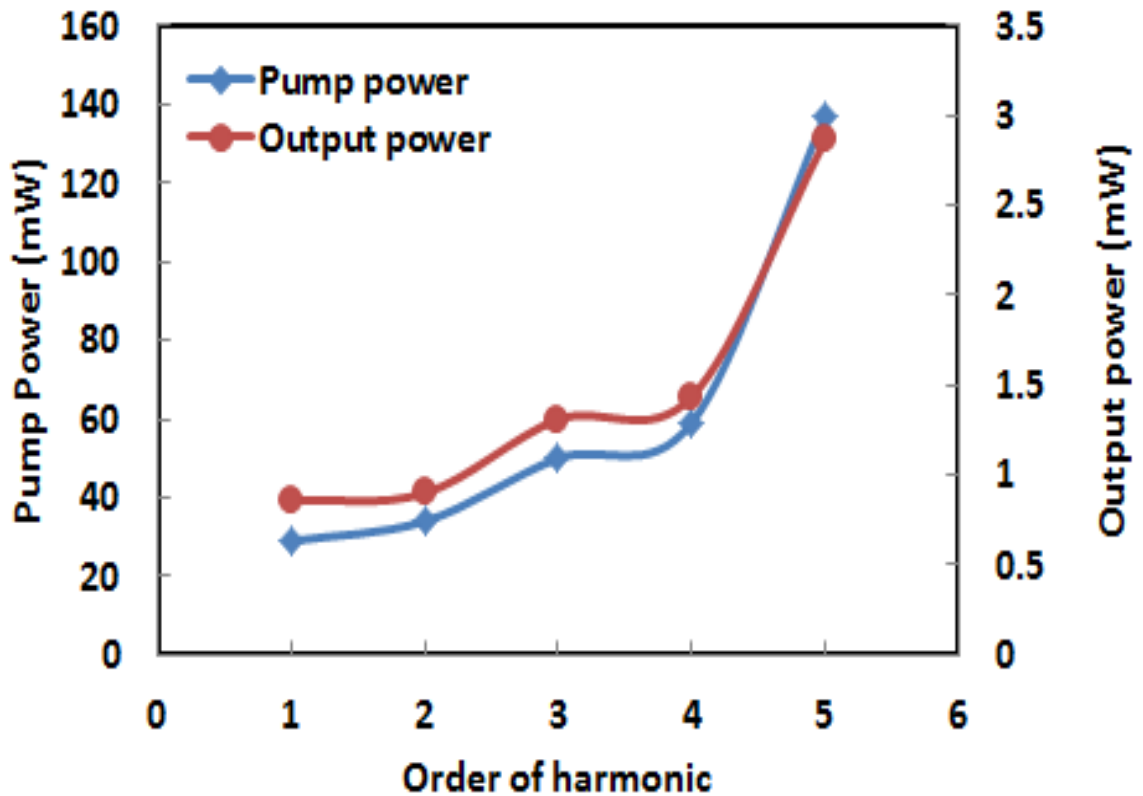


Figure 5.3: Threshold pump power and output power at different order harmonic

Figure 5.4 shows the relationship of pulse width and pulse energy against harmonic orders. Pulse width of the fundamental, 2nd order, 3rd order, 4th order and 5th order harmonic are obtained at 6.0 μ s, 3.6 μ s, 2.6 μ s, 2.3 μ s, and 2 μ s respectively. The pulse width reduces with the increment of harmonic order due to the higher pump power used to achieve higher harmonic order. On the other hand, the pulse energy at threshold pump power of different harmonic order fluctuates between 42.6 nJ to 17.8 nJ as shown in Fig. 5.4. Figure 5.5 shows the output spectra of the EDFL at different harmonic orders. It is observed that the operating wavelength of the laser is blue-shifted as the harmonic order increases. This is attributed to the pump power, which is stronger at higher order harmonic and thus the laser operates at a shorter wavelength due to the Erbium gain saturation. It is observed that the operating wavelength of the laser shifts from 1565 nm to 1560 nm as the operation changes from the fundamental repetition rate, to the 5th order harmonic.

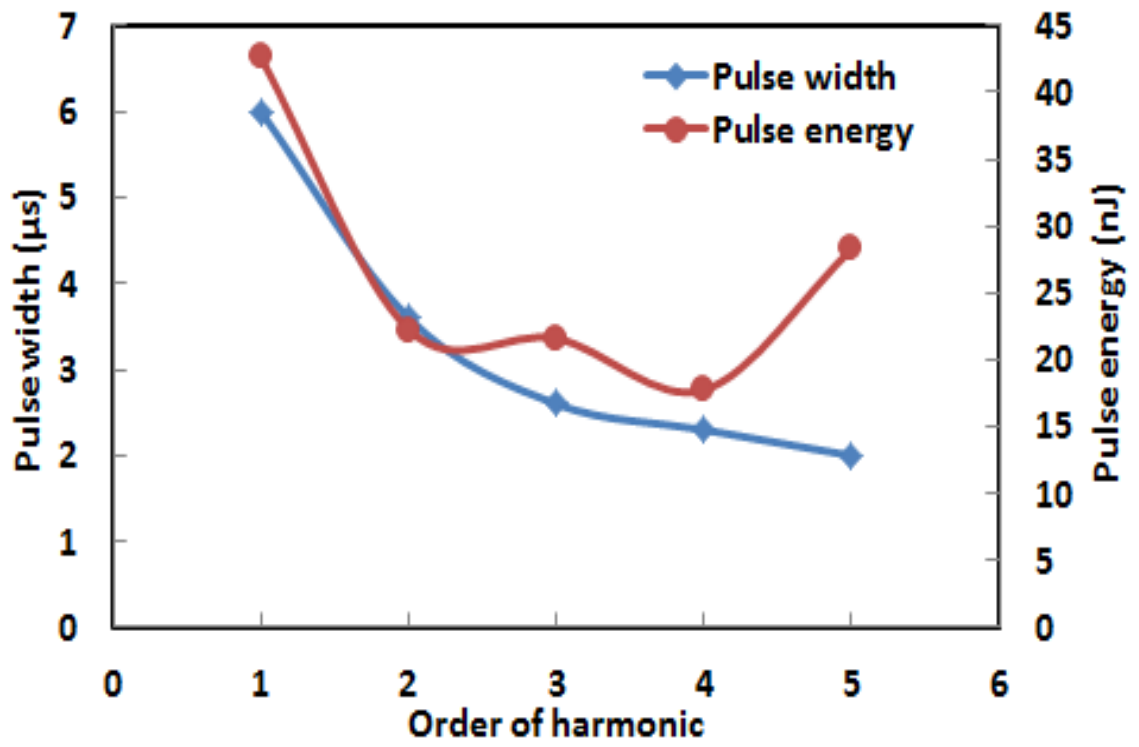


Figure 5.4: Pulse width and pulse energy against different order harmonic

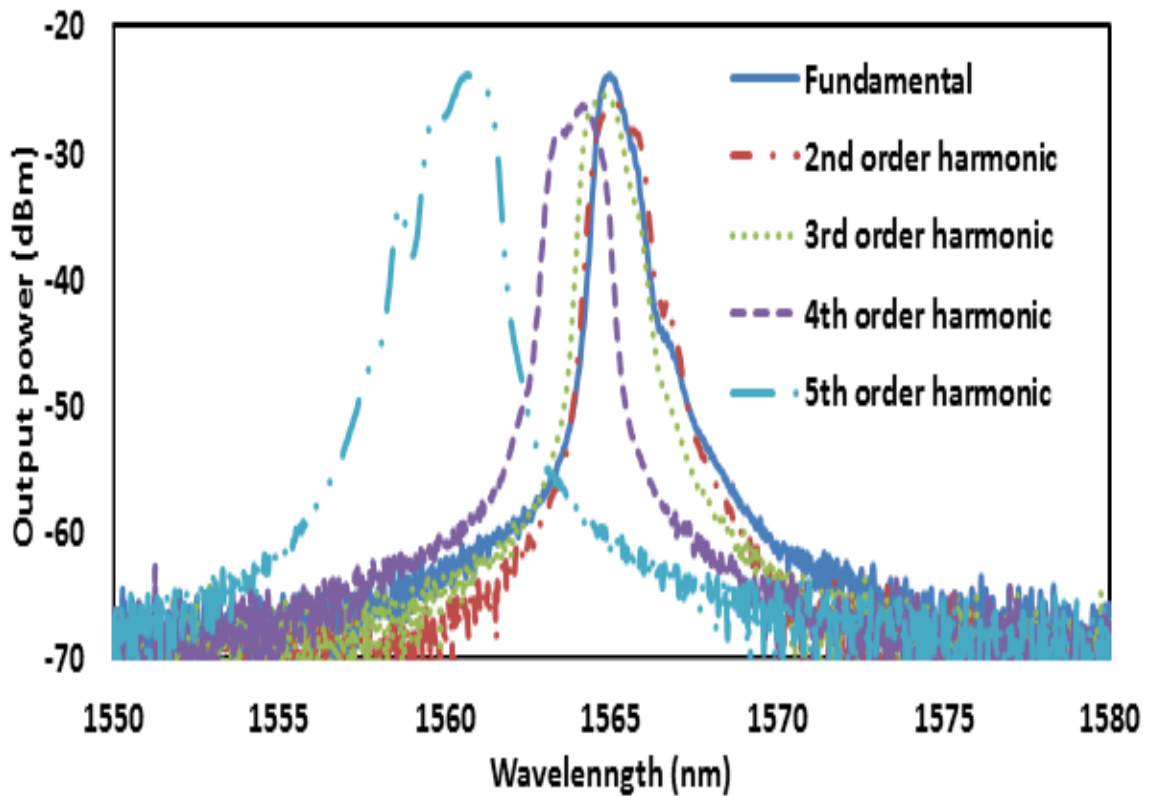


Figure 5.5: Output spectra of the dark pulse train at different order harmonics

5.3 Generation of switchable DW and CQNLSE dark pulse

The generation of NLSE dark pulse is normally determined by the amount of Kerr nonlinearities inside the cavity. However, if the cavity consists of a highly nonlinear medium, non-Kerr nonlinearities may dominate the Kerr nonlinearities inside the cavity (Yang & Zhang, 2005). Under this circumstance, generation of dark pulse is relied on cubic-quantic nonlinearity. Therefore, generation of dark pulse is possible in anomalous dispersion cavity. On the other hand, another type of dark pulse in anomalous dispersion cavity, called domain. The fundamental of domain wall dark pulse is interpreted by topological defects in temporal domain due to mutual coupling of two different wavelengths. In this section, a switchable DW and CQNLSE type dark pulse is experimentally demonstrated by adjusting the polarization state of the oscillating light. The demonstration of DW and CQNLSE type dark pulse emissions are based on the same anomalous dispersion laser cavity configuration.

5.3.1 Configuration of the switchable DW and CQNLSE dark pulse EDFL

The experimental set-up of the proposed EDFL is illustrated in Figure 5.6, which is configured with the same EDF and HNLF with the previous laser of Figure 5.1. The ring resonator consists of a 3.5 m long EDF, a WDM, a PDI, a PC, a 100 m long HNLF and a 95:5 output coupler. The HNLF is used to significantly increase nonlinearity of the cavity. The EDF is pumped by a 1480 nm laser diode via the WDM. A standard SMF with dispersion of 18 (ps/nm)/km constitutes the rest of the ring. The total cavity length is around 130 m. Unidirectional operation of the ring was achieved with the use of a PDI while an in-line PC was used to fine-tune the linear birefringence of the cavity. The output of the laser is collected from the cavity via a 95:5 coupler which retains 95%

of the light in the ring cavity to oscillate. The OSA with a spectral resolution of 0.02 nm is used to analyze the spectrum of the proposed EDFL whereas the oscilloscope (OSC) is employed in conjunction with a 1 GHz bandwidth photodetector to capture the output pulse train of the dark pulse emission.

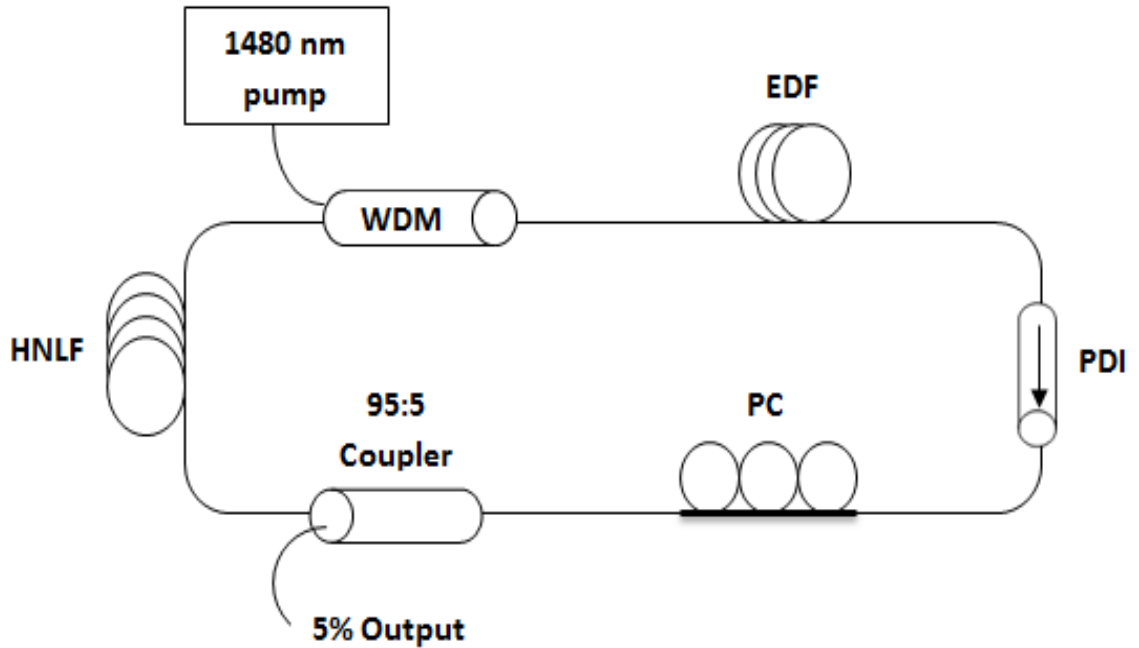


Figure 5.6: Experimental set-up of the proposed mode-locked EDFL, which capable for generating a switchable DW and NLSE dark pulse train

5.3.2 DW dark pulse performance

In this work, NPR technique is used to generate a pulse train operating in dark regime. The proposed laser operates in anomalous dispersion regime and the dark pulse emission was considered as topological defects in temporal domain due to mutual coupling of two different wavelengths. Under the optimum polarization setting, a DW type dark pulse emission could be achieved as pump power is increased above the pumping power threshold of 80 mW. The dark pulse train can be sustained until the cavity's maximum pump power of 140 mW. Figure 5.7 shows the typical dark pulse

emission of the proposed laser, which operates at fundamental repetition rate of 1.52 MHz. As shown in the figure, the dark pulse is represented by a narrow intensity dip, which exists in the strong continuous wave (CW) and the pulse width of the dark pulse is measured to be about 203 ns. At the maximum pump power of 140 mW, the average output power measured is about 3.4 mW, which can be translated to pulse energy of 2.24 nJ.

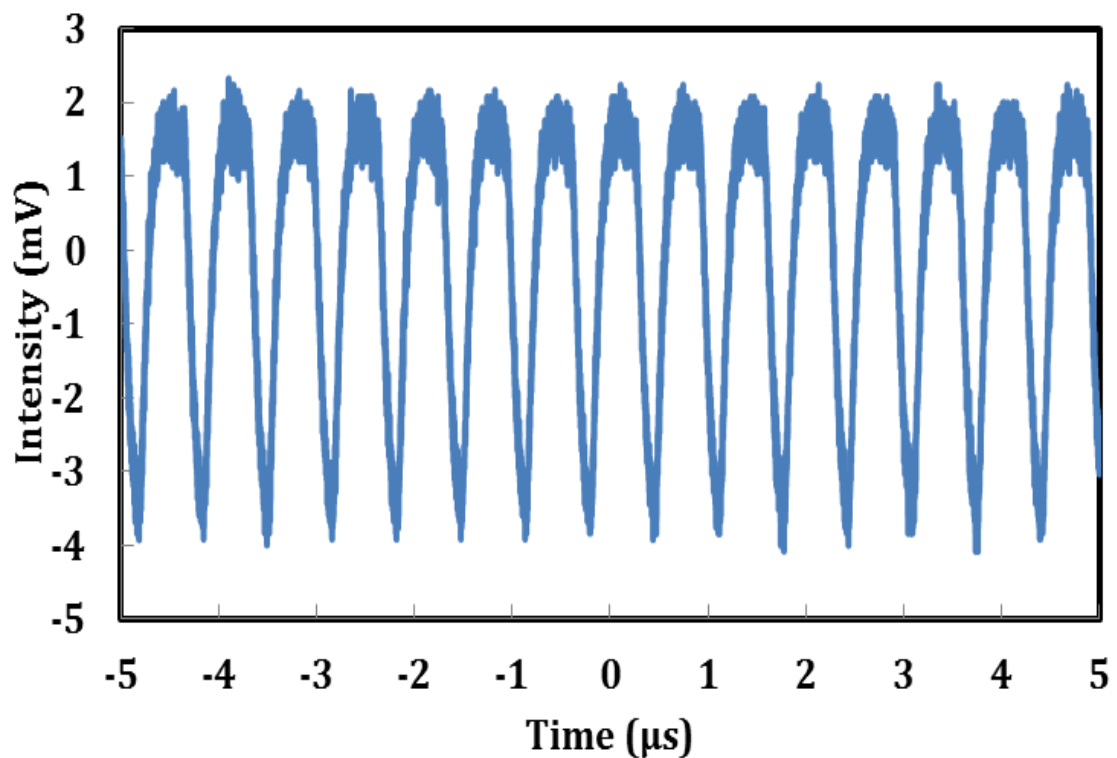


Figure 5.7: Typical DW dark pulse train at pump power of 140 mW

Figure 5.8 depicts the output spectrum of the DW dark pulse, which operates at 1580 nm region. It shows multiple peak wavelengths operation within a broad spectral region. The spectral broadening is due to the self-phase modulation (SPM) effect in the ring cavity. The laser oscillates simultaneously with multi peak wavelengths in the cavity, leading to the emergence of topological defects in temporal domain. This phenomena forms dark domain wall pulses, which have an intensity dip on a strong CW

background. The stability of DW dark pulse is then investigated by an RF spectrum analyzer. As shown in Figure 5.9, the laser operates at fundamental frequency of 1.52 MHz with SNR of about 28 dB. This indicates the stability of the laser.

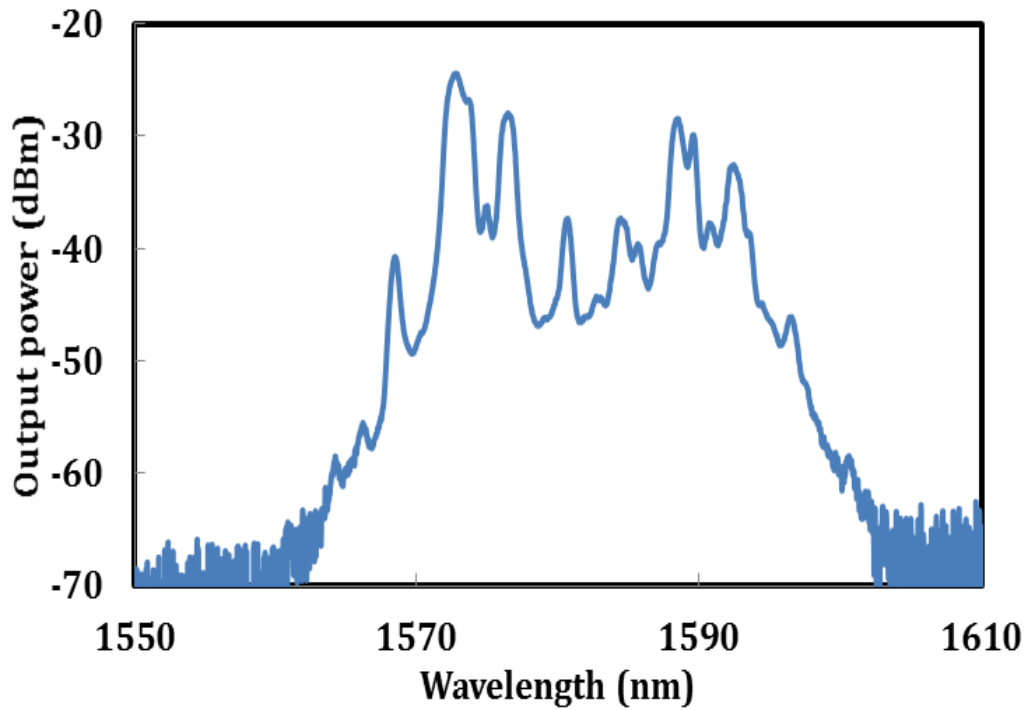


Figure 5.8: DW dark pulse spectrum of the proposed EDFL at pump power of 140 mW

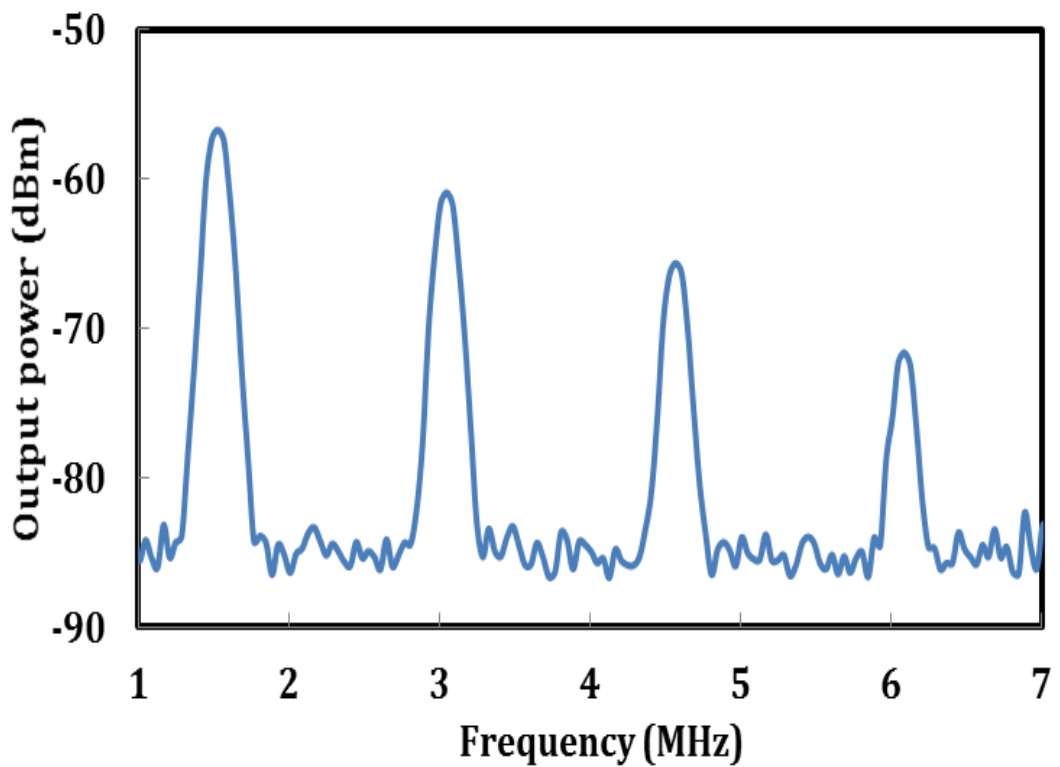


Figure 5.9: DW dark pulse RF spectrum of the proposed EDFL at pump power of 140 mW

5.3.3 CQNLSE dark pulse performance

By carefully adjusting the PC, the operating regime of the mode-locked can be switched from DW to CQNLSE as the pump power is increased above the threshold pump power of 104 mW. The threshold pump power is reasonably higher than that of the previous DW dark pulse emission. This is most probably due to the higher loss in the cavity when the position of the PC is adjusted into the new position. By varying the pump power from 104 mW to the maximum pump power of 140 mW, the CQNLSE dark soliton pulse can be observed operating at fundamental pulse repetition rate of 1.52 MHz as shown in Figure 5.10. The pulse width of CQNLSE dark pulse is about 219 ns, which is similar to DW dark pulse. The generation of CQNLSE is possible due to the non-Kerr nonlinearities, which is stronger than the Kerr nonlinearities as the laser light oscillates through the HNLF. This allows the formation of dark pulse with the assistance of higher order of nonlinearity. The output power of CQNLSE dark pulse is measured to be about 0.88 mW at the maximum pump power of 140 mW, which is comparatively lower than that of DW dark pulse. This indicates a relatively low pulse energy of 0.58 nJ at pump power of 140 mW. Figure 5.11 depicts the output spectrum of CQNLSE dark pulse, which clearly shows Kelly side bands. Unlike multiple peak wavelength operation of DW dark pulse, CQNLSE dark pulse exhibits a single peak wavelength at 1564.5 nm, which is similar to NLSE type dark pulse. This is a significant indication that differentiates between DW dark pulse and CQNLSE dark pulse. The cavity loss is slightly higher in this laser and thus the operating wavelength shifts to a shorter wavelength to acquire more gain to compensate the loss. The SNR of CQNLSE dark

pulse is obtained 35 dB, which is higher than the one of DW pulse, as shown in Figure 5.12. This shows that the generated CQNLSE pulse is more stable than the DW pulse.

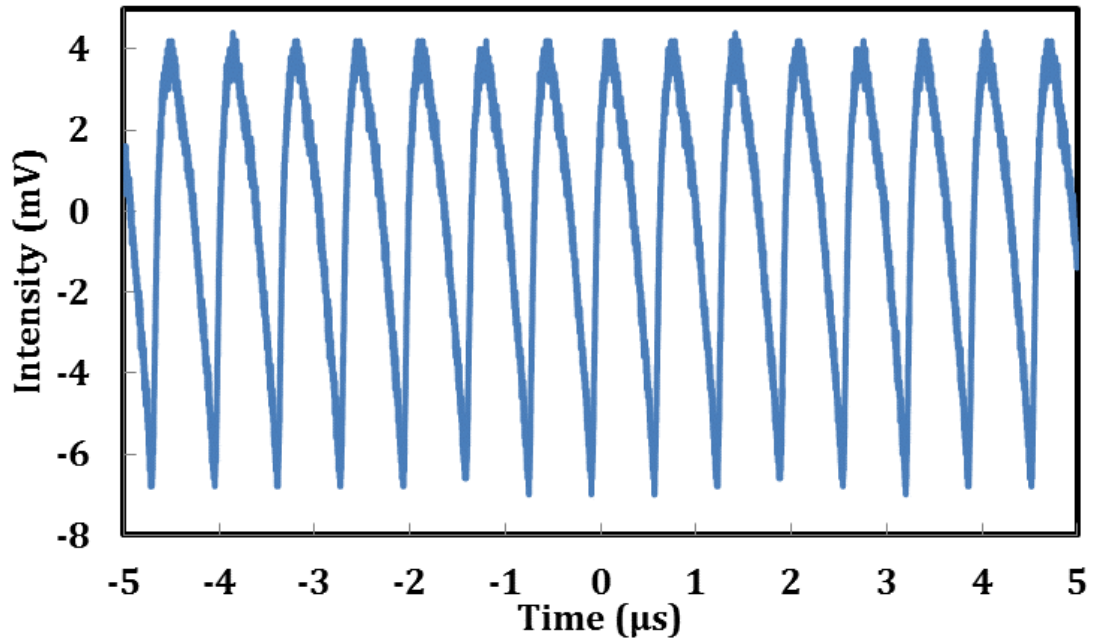


Figure 5.10: CQNLSE dark pulse train of the proposed EDFL at pump power of 140 mW

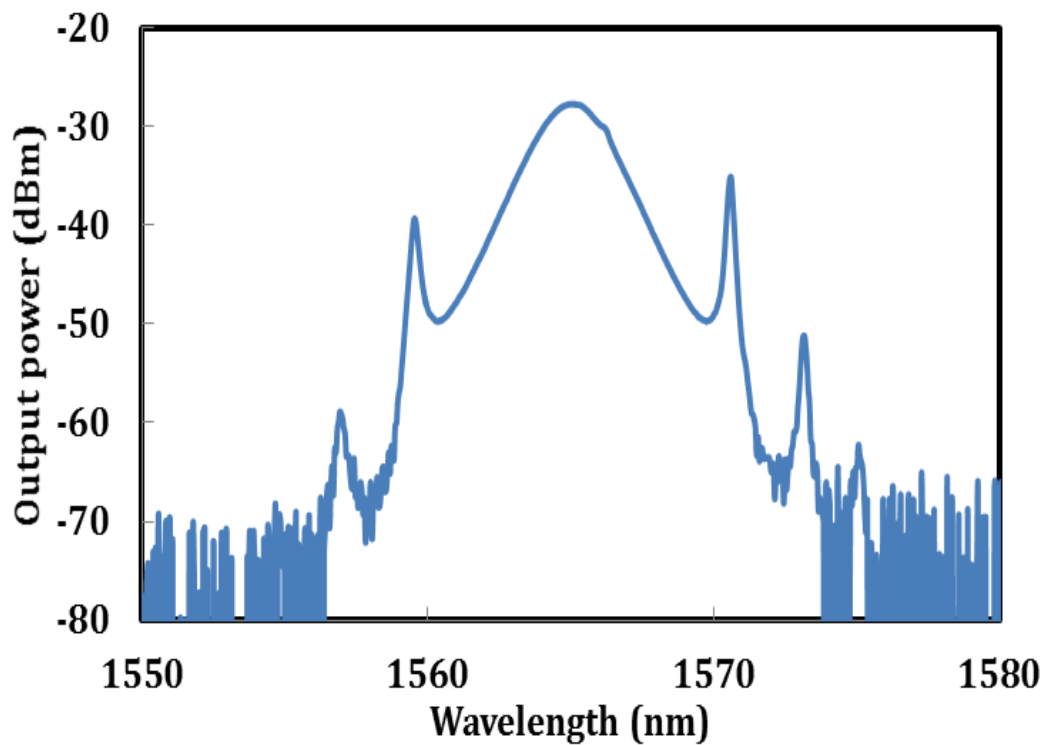


Figure 5.11: Output optical spectrum of the CQNLSE dark pulse at pump power of 140 mW

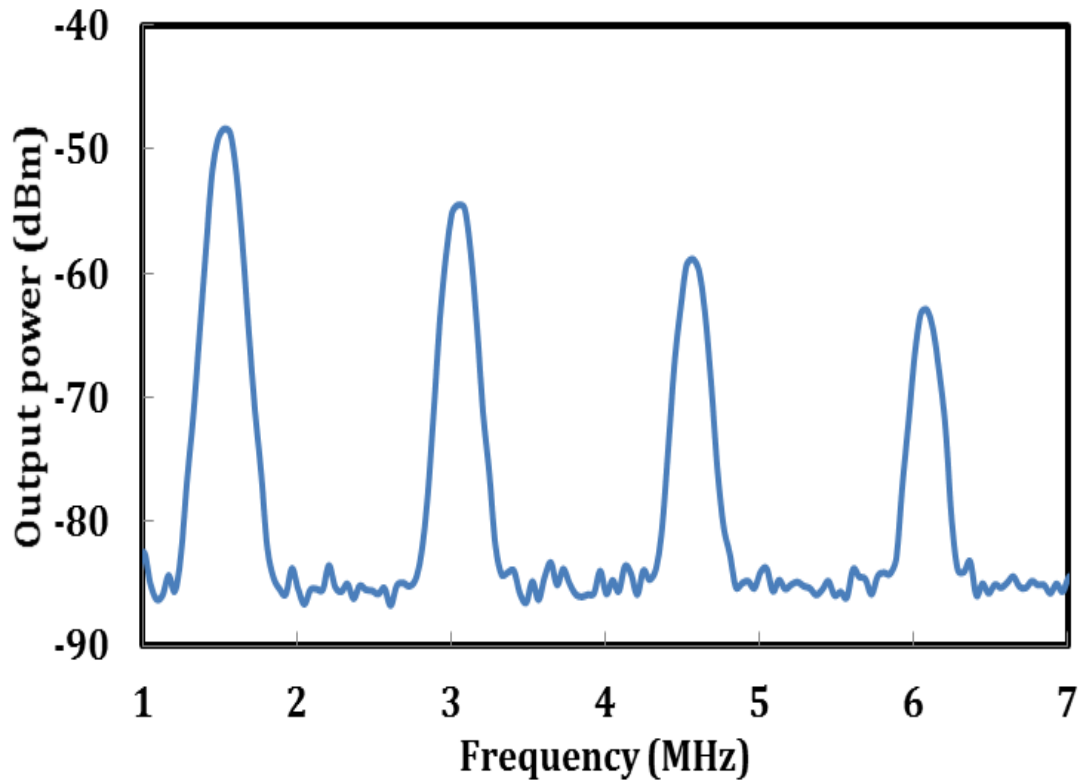


Figure 5.12: RF spectrum of the CQNLSE dark soliton pulse at pump power of 140 Mw

5.4 Multi-wavelength dark pulse EDFL in figure-of-eight cavity

Both multi-wavelength and mode-locked EDFLs have wide applications in optical communications, sensors and instrumentations. There are many different methods that have been proposed to achieve multi-wavelength lasing at room temperature such as cascaded stimulated Brillouin scattering, incorporating a semiconductor optical amplifier or raman amplifier and four-wave mixing (FWM). Recently, NPR which can induce intensity dependent loss in the laser cavity is also widely used for multi-wavelength laser generation. On the other hand, mode-locked EDFLs were demonstrated in the previous sections using NPR technique. The NPR

based lasers have shown promising results and attracted much attention for their advantages such as compactness, low cost, flexibility and simplicity of design. As discussed in chapter 4, NPR may not be able to induce both multi-wavelength and pulse generation in a single loop cavity. In this section, a mode-locked multi-wavelength EDFL is demonstrated using figure-of-eight set up by incorporating 50 m long photonic crystal fiber (PCF) and 20 km long standard SMF. The proposed EDFL setup is possible to induce both multi-wavelength and dark pulse in an EDFL based on NPR mechanism. Besides, figure-of-eight also induces higher cavity feedback, which allows the generation of higher harmonic order. Under appropriate operation conditions, the proposed fiber laser, which is configured with an all-normal dispersion and figure-of-eight cavity could produce a train of single or multiple dark pulses.

5.4.1 Configuration of the proposed multi-wavelength dark pulse EDFL

The experimental set-up of the proposed EDFL is illustrated in Figure 5.13, which the ring resonator consists of a 3.5 m long EDF as the gain medium, WDM, PDI, polarization controller (PC), 50 m long PCF, 6.9 km long dispersion compensation fiber (DCF) and 3 dB couplers. The EDF used has a doping concentration of 2000 ppm and GVD parameter of about -21.64 (ps/nm)/km. This fiber was pumped by a 1480 nm laser diode via the WDM. Other fibers in the cavity are a 6.9 km long DCF with GVD of about -4 (ps/nm)/km and a standard SMF (18 ps/nm.km), which constituted the rest of the ring. The cavity operates in large positive GVD where the net dispersion and fundamental repetition rate are estimated as 35.19 ps² and 29.0 kHz, respectively. Unidirectional operation of the ring was achieved with the use of a PDI while an in-line PC was used to fine-tune the linear birefringence of the cavity. A 2 x 2 3 dB fiber coupler was used to form a figure-of-eight structure with a piece of PCF is inserted in

the new loop. The output of the laser is collected from the cavity via a 3 dB coupler which retains 50% of the light in the ring cavity to oscillate. The OSA with a spectral resolution of 0.02 nm is used to analyze the spectrum of the proposed EDFL whereas the OSC is employed in conjunction with a 1 GHz bandwidth photodetector to capture the output pulse train of the mode-locked operation.

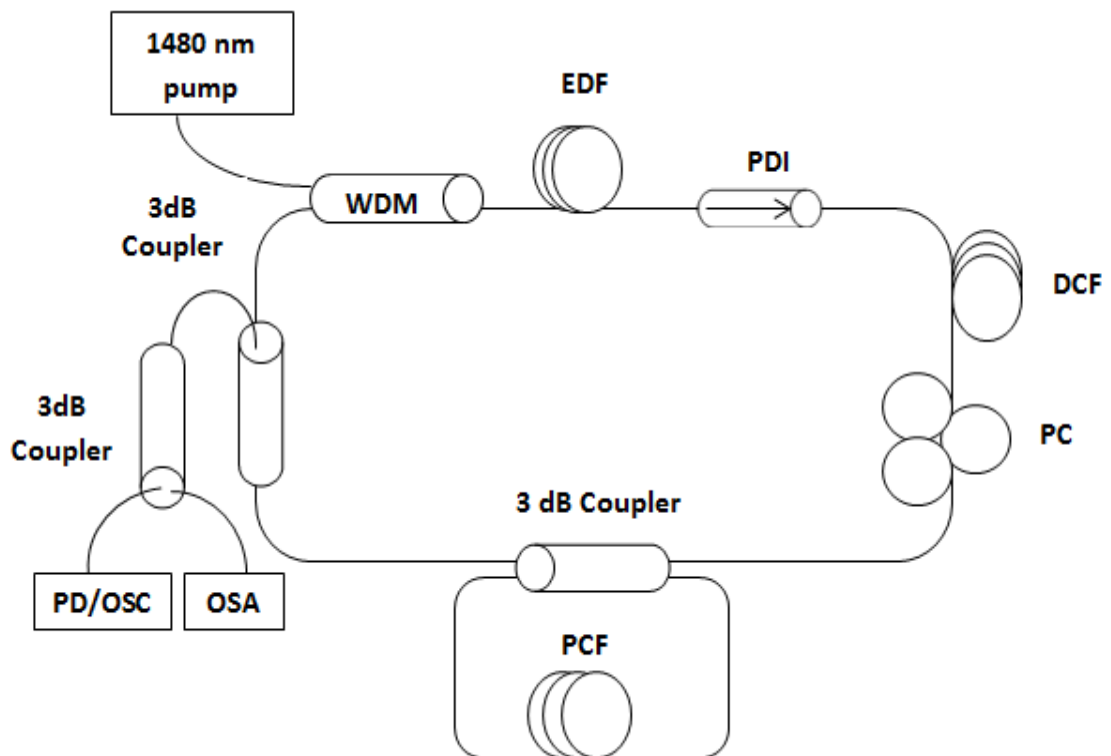


Figure 5.13: Schematic configuration of the proposed multi-wavelength mode-locked EDFL

5.4.2 Multi-wavelength dark pulse performance

We use the NPR technique for both mode locking and multi-wavelength generation in the proposed ring EDFL. Under the optimum polarization setting, a multi-wavelength laser output could be achieved in the laser as the pump power is increased above the pumping power threshold of 24 mW. Figure 5.14 shows evolution of the

output spectrum of the multi-wavelength with 1480 nm pump power variation from 24 mW to 145 mW. It is observed that the number of lines and the peak power increase with the pump power. At the maximum pump power of 145 mW, the laser produces at least 9 lines with free spectral range (FSR) of 0.47 nm, which is determined by the length and the effective group indices of the PCF. It is worth noting that there is no multi-wavelength emission when the PCF is removed from the cavity. The multi-wavelength generation is due to the intensity dependent loss induced by NPR. The role of PCF is to increase the nonlinear effect as well as to constitute an inline periodic filter with the PDI.

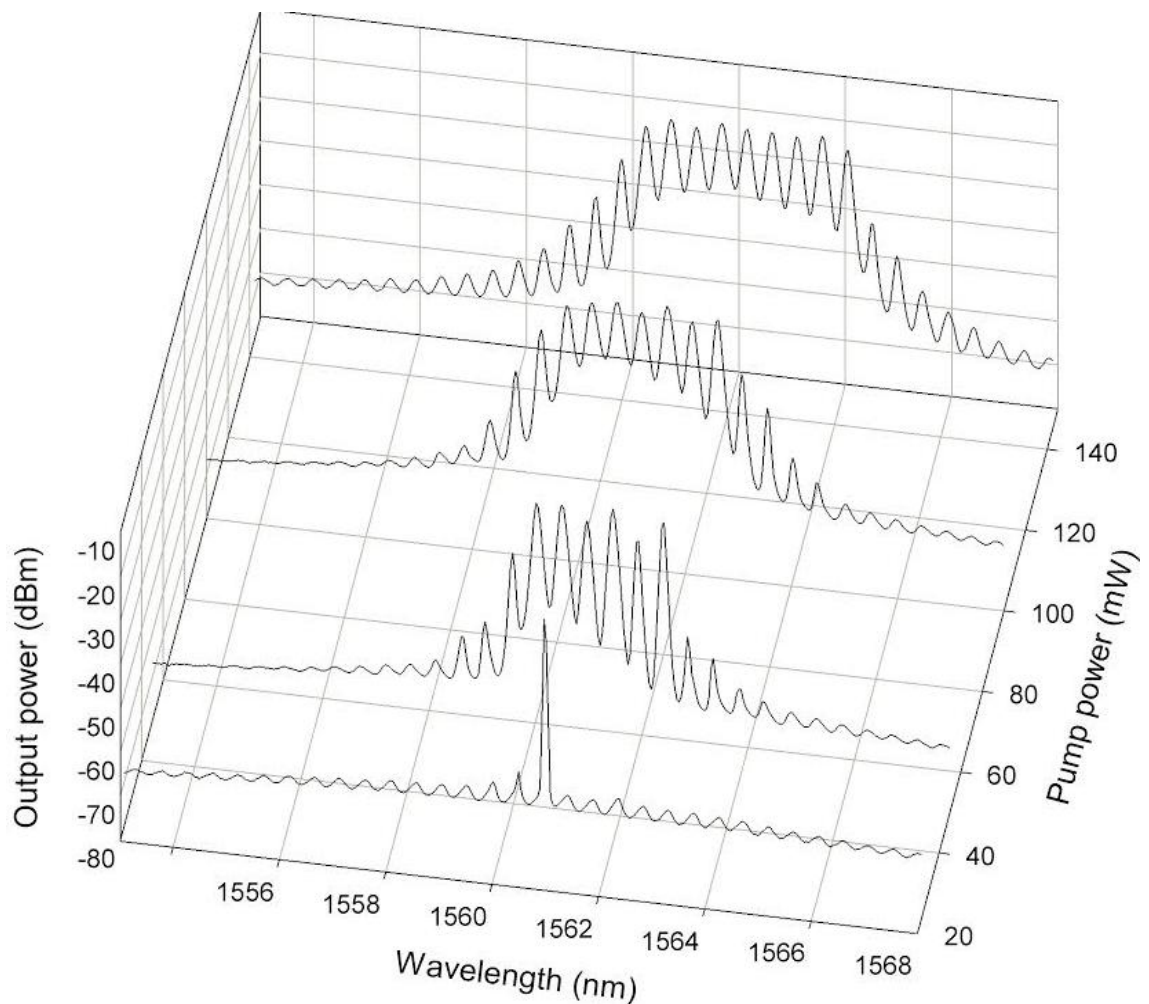
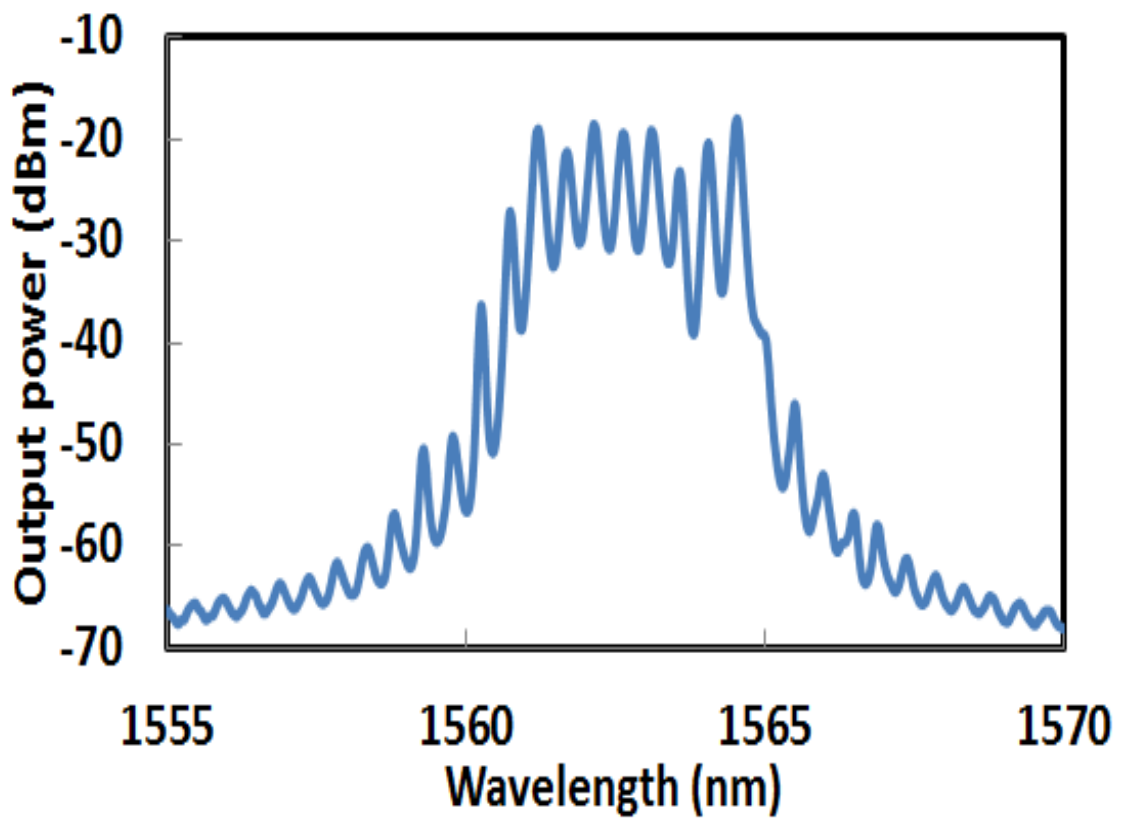


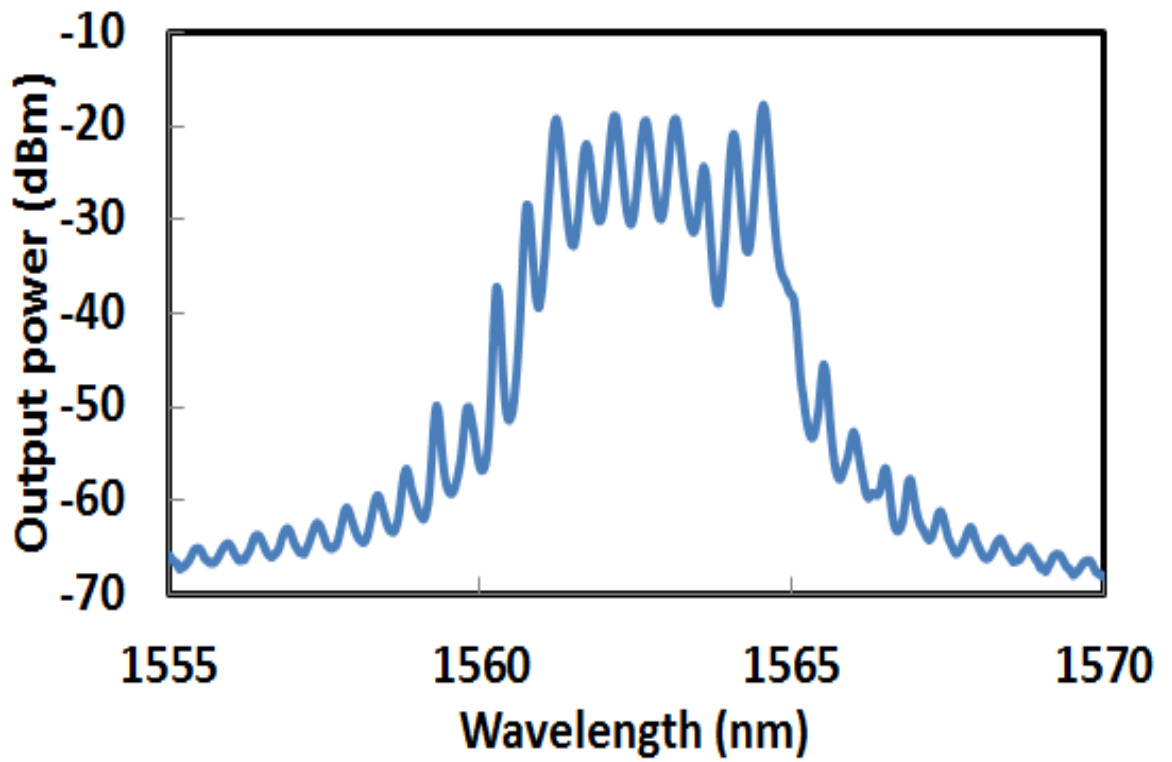
Figure 5.14: Multi-wavelength output spectrum evolution against 1480 nm pump power

As the pumping power exceeded 133 mW, self-started mode-locked pulse train is obtained. Figures 5.15 and 5.16 show the optical spectrum and the oscilloscope trace

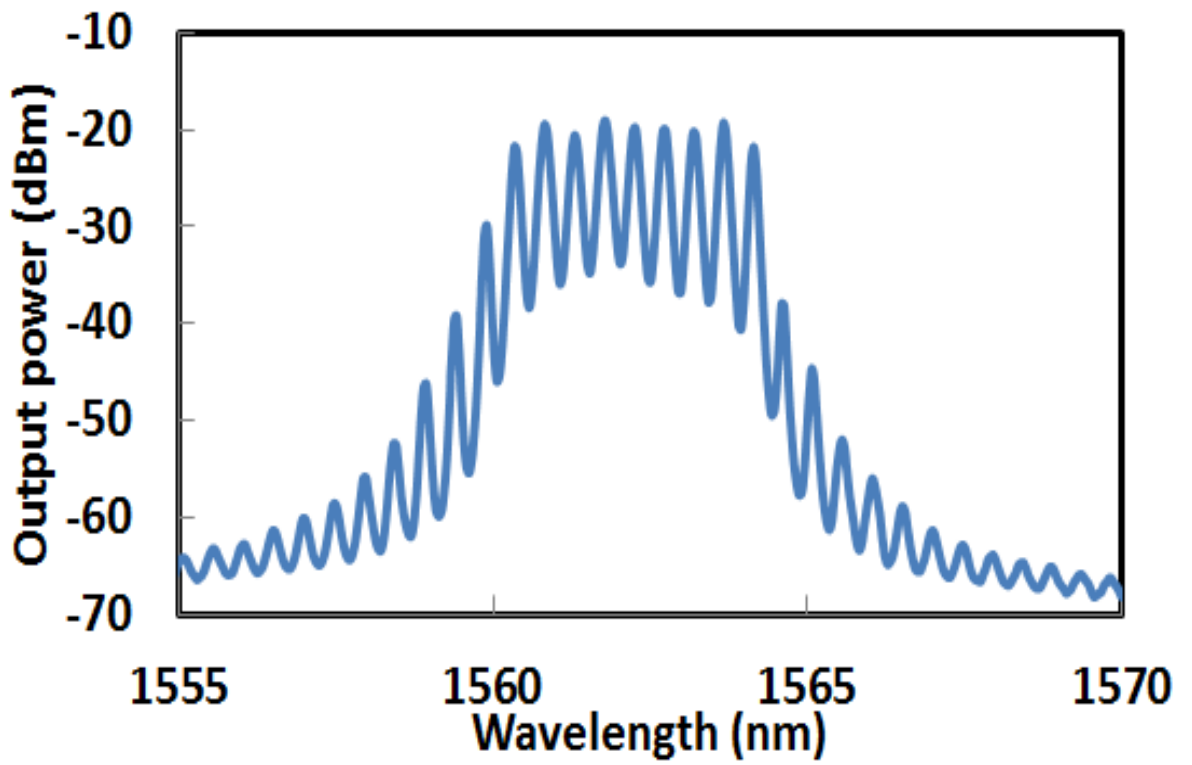
of the multi-wavelength laser respectively, at four different orientation of PC. By carefully adjusting the PC, dark pulse emission operating in fundamental repetition rate of 29 kHz could be observed as shown in Figure 5.16 (a). As seen, in the time domain, the dark pulse is represented as a narrow intensity dip in the strong CW laser emission background. The full width at the half minimum of the dark pulse is about 2.7 μ s. On the OSA trace of Figure 5.15(a), the optical spectrum of the dark pulses shows a multi-wavelength operation within a broad spectral region. The spectral broadening is due to the SPM effect in the ring cavity. When the laser oscillates simultaneously at multiple wavelengths in the cavity, the laser emission could switch between these wavelengths due to their incoherent nonlinear coupling. This phenomena forms vector dark domain wall pulses, which have an intensity dip on a strong CW background.



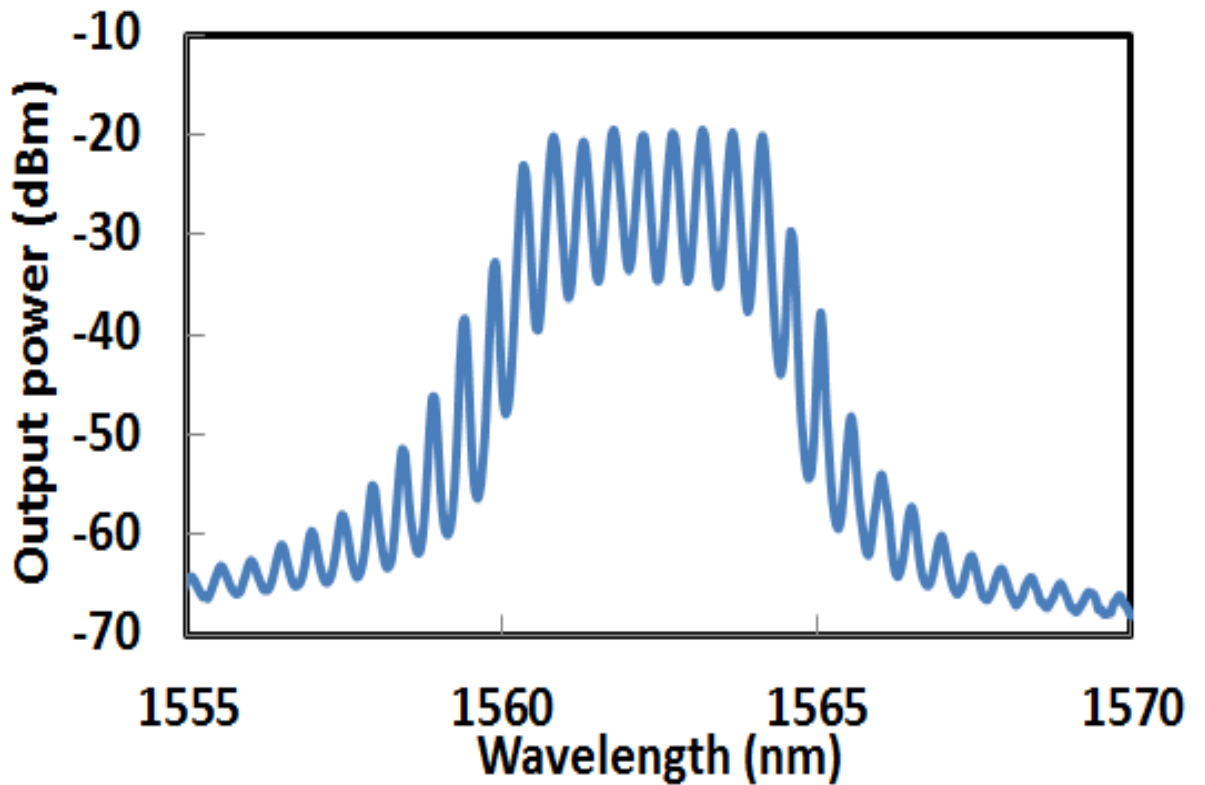
(a)



(b)

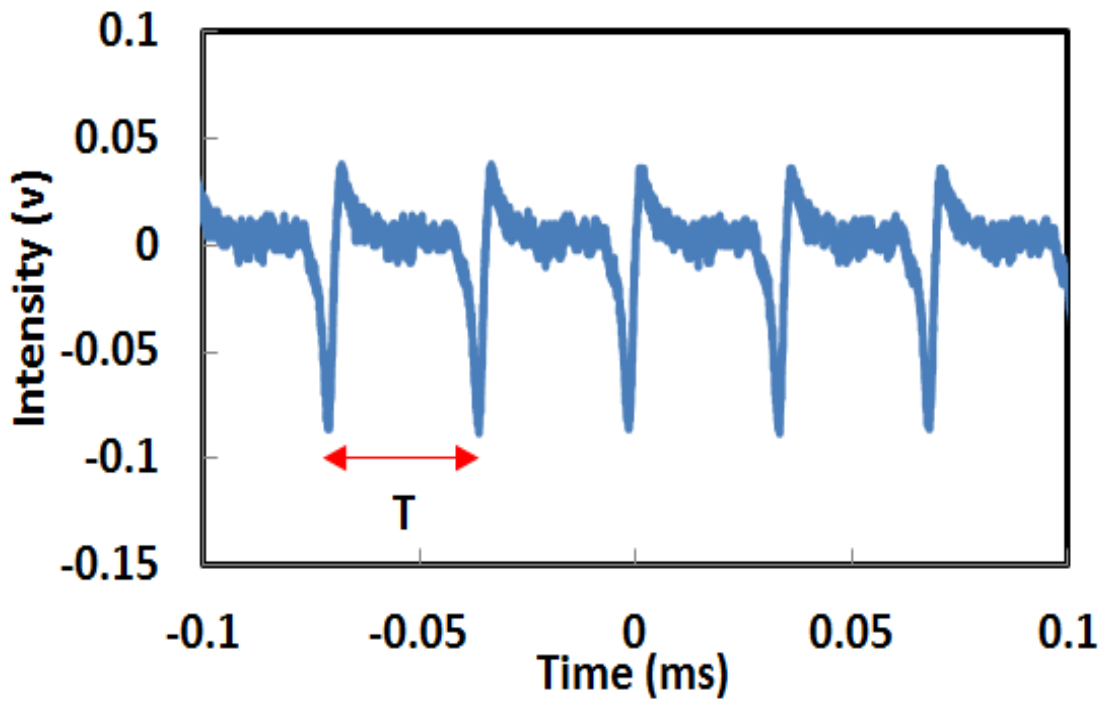


(c)

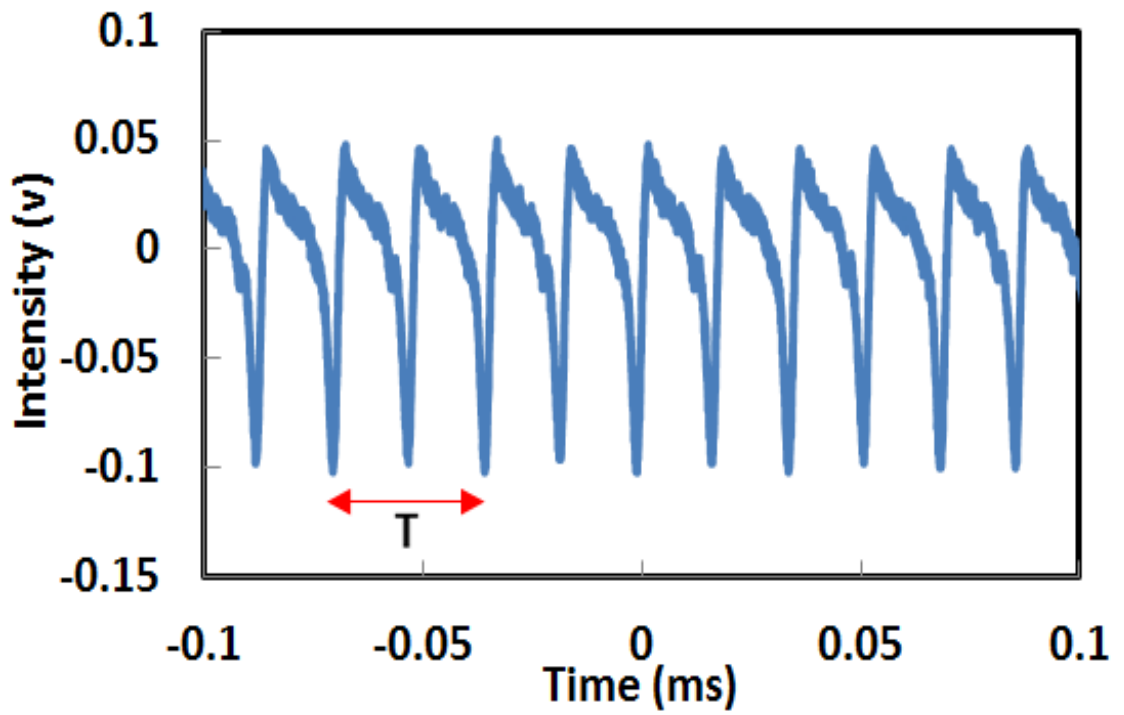


(d)

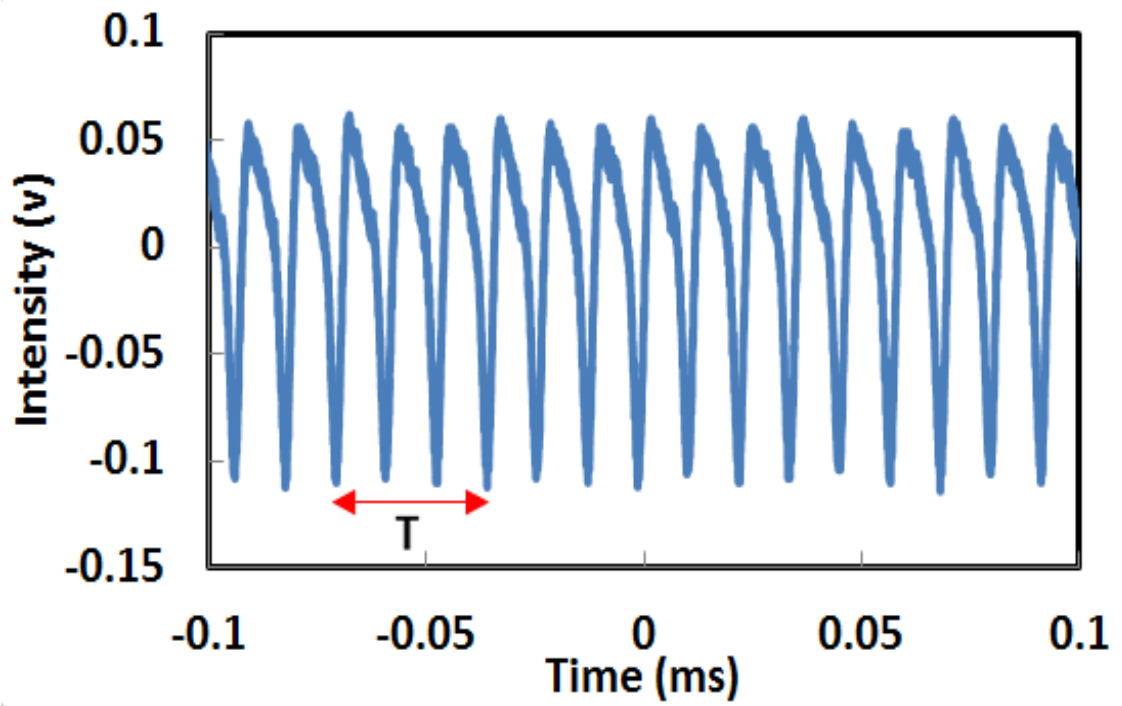
Figure 5.15: Optical spectrum of the proposed multi-wavelength dark pulse EDFL at four different orientation of PC when the pump is fixed at 146 mW (a) fundamental (b) 2nd order (c) 3rd order and (d) 4th order harmonic operation



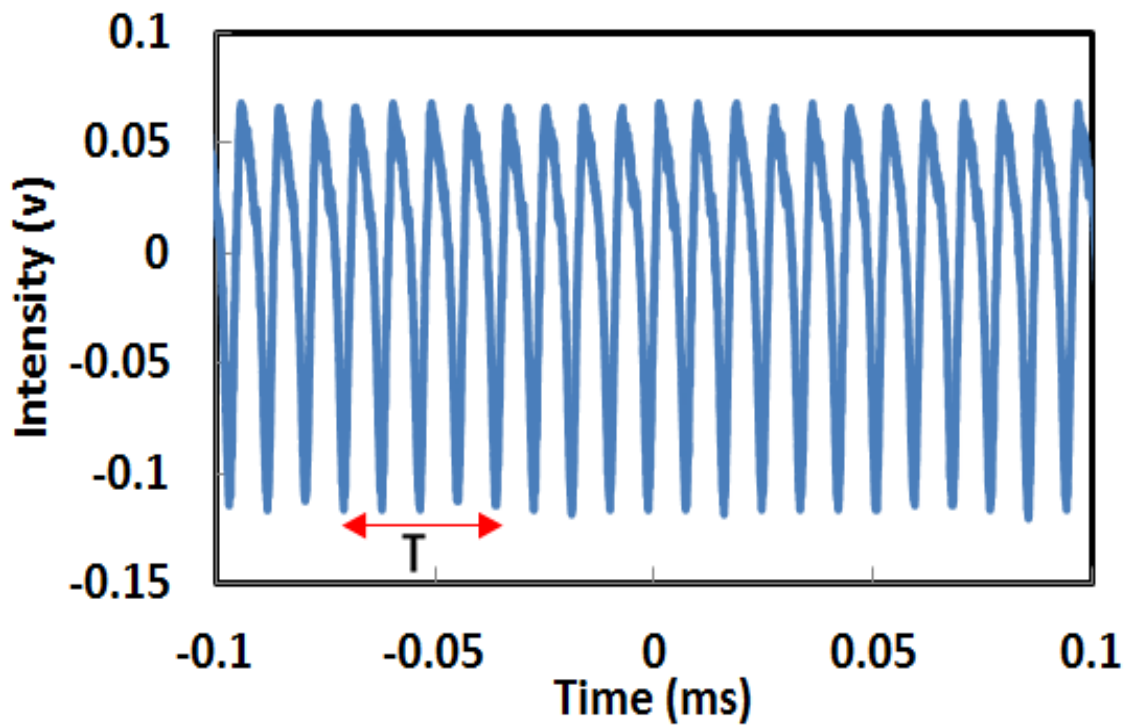
(a)



(b)



(c)



(d)

Figure 5.16: Dark pulse train of the proposed multi-wavelength dark pulse EDFL at four different orientation of PC when the pump is fixed at 146 mW (a) fundamental (b) 2nd order (c) 3rd order and (d) 4th order harmonic operation

Compared to single bright pulse emission of the laser, the single dark pulse emission state was difficult to maintain. This is most probably due to the laser noise and/or weak environmental perturbations, which allows new dark pulses to appear automatically in the cavity. This causes the laser to operate in a state of multiple dark-pulse. By carefully adjusting the PC, dark pulse train can be shifted to 2nd order, 3rd order and 4th order of dark pulses as shown in Figures 5.16 (b), (c) and (d) respectively. Assuming the different rotational angle ($\Delta\alpha$) to achieve fundamental repetition rate is 0° , dark pulse train can be shifted to 2nd order with $\Delta\alpha$ less than 15° in anti-clockwise direction. Besides, from 2nd \rightarrow 3rd \rightarrow 4th order harmonic, $\Delta\alpha$ for each order change are also less than 15° in anti-clockwise direction. It is observed that the 5th harmonic cannot be achieved in the experiment. This is most probably due to the maximum pump power limitation, which constraints the pulse from further breaking after the 4th order harmonic. Figure 5.17 compares the pulse width and pulse energy for different repetition rate of the harmonic operations when the the 1480 nm pump is fixed at 146 mW. It is found that the pulse width varies from 2.70 μs to 3.11 μs as the repetition rate changes from fundamental to 4th order harmonic of 116 kHz. Inset of Figure 5.17 shows a single dark pulse of 4th order harmonic with pulse width of 2.70 μs . The pump to signal efficiency of the cavity is measured at 0.68%. The average output power of the laser are obtained at 940 μW , 950 μW , 1000 μW and 1010 μW for fundamental, 2nd, 3rd and 4th order harmonic respectively. Since the pump power is fixed and the order of dark pulse is increased, pulse energy experienced a decreasing trend as expected. From the results of dividing output power by pulse repetition rate, the pulse energy decreases from 32.4 nJ to 8.7 nJ with the pulse breaks from fundamental to 4th order mode-locking as shown in Fig. 5.17. The results suggest that the dark pulse formation could be an intrinsic feature of the all-normal dispersion cavity. It is found that the figure-of-eight setup induced competition between two cavity modes and cavity feedback, leading to

the formation of vector dark domain wall solitons. This could have played an important role on the stability of the dark pulses in the laser.

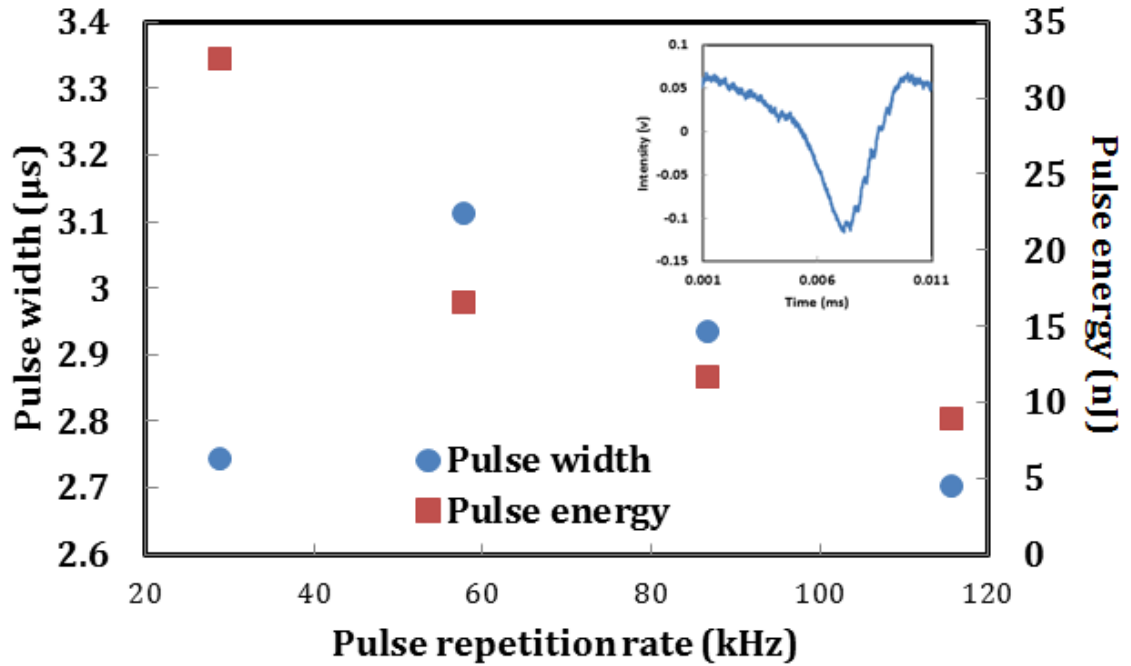


Figure 5.17: Pulse width and pulse energy at different orders of harmonic. Inset shows single dark pulse at 4th order harmonic

5.5 Generation of Q-switched Mode-locked EDFL operating in dark regime

Basically, mode-locking operation can be classified into two categories, which are continuous wave mode-locked (CWML) (French et al., 1993) and Q-switched mode-locked (QML) (Zhang et al., 2004). For CWML, the ultra-short pulses can be generated for each round trip time in the laser cavity, which typically produces megahertz pulse repetition rate. Different from CWML, QML possesses both Q-switching modulation frequency in kilohertz and frequency relates with the round trip time. Compared with CWML, QML lasers possess high peak power and high pulse energy over the CWML. These properties are attractive to achieve wavelength conversion and super continuum generation (Lin et al., 2007). In this section, we have

experimentally demonstrated the emission of Q-switched dark pulse in EDFL based on NPR technique.

5.5.1 Experimental setup

The experimental set-up of the proposed QML EDFL is illustrated in Figure 5.18, which the ring resonator consists of a 3.5 m long EDF as the gain medium, WDM, PDI, polarization controller (PC) and 95:5 output coupler. The EDF and pumping wavelength are similar with the previous work. A standard SMF with dispersion of 18 (ps/nm)/km constitutes the rest of the ring. The total cavity length is around 25 m. Unidirectional operation of the ring was achieved with the use of a PDI while an in-line PC was used to fine-tune the linear birefringence of the cavity. The output of the laser is collected from the cavity via a 95:5 coupler which retains 95% of the light in the ring cavity to oscillate. The OSA and oscilloscope are used for the spectral and temporal analysis, respectively.

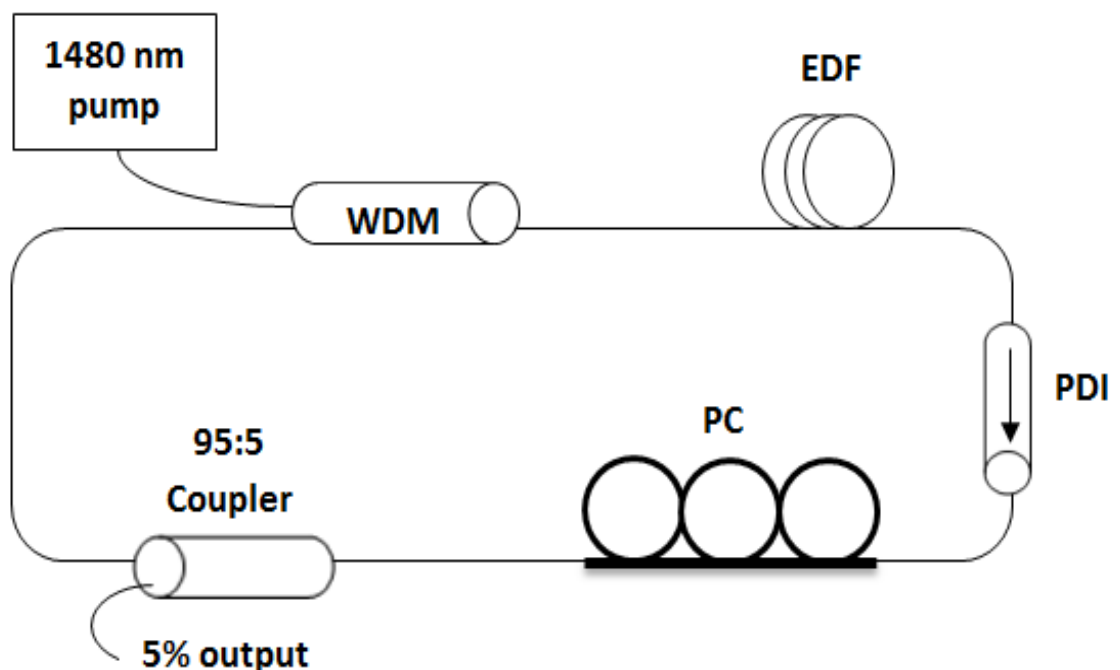


Figure 5.18: Schematic configuration of the proposed QML EDFL emitting dark pulse

5.5.2 Q-switched dark pulse performance

At the optimum polarization orientation, Q-switched dark pulse is achieved as pump power hits the pumping power threshold of 55 mW. The Q-switching pulse train can be sustained up to the pump power of 145 mW. Figure 5.19 shows a typical pulse train of the Q-switched dark pulse againsts pump power. In this experiment, we observe that the multiple dark pulses are combined to form the Q-switched envelope, which operates in dark regime as shown in Figure 5.20. Figure 5.21 shows the output spectrum of the Q-switched laser at pump power of 145 mW. As shown in the figure, the laser operates at wavelength around 1570 nm. Spectral broadening is also observed due to self-phase modulation effect in the cavity.

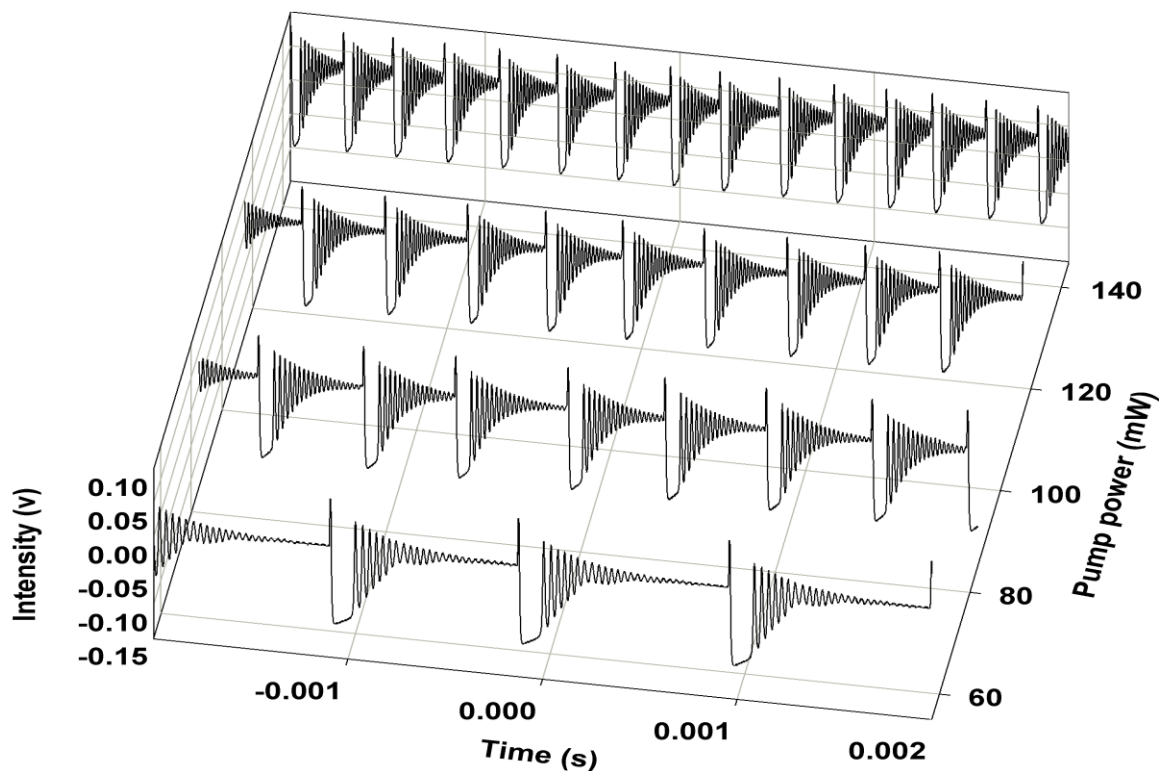


Figure 5.19: Emission of Q-switched dark pulse train againsts pump power

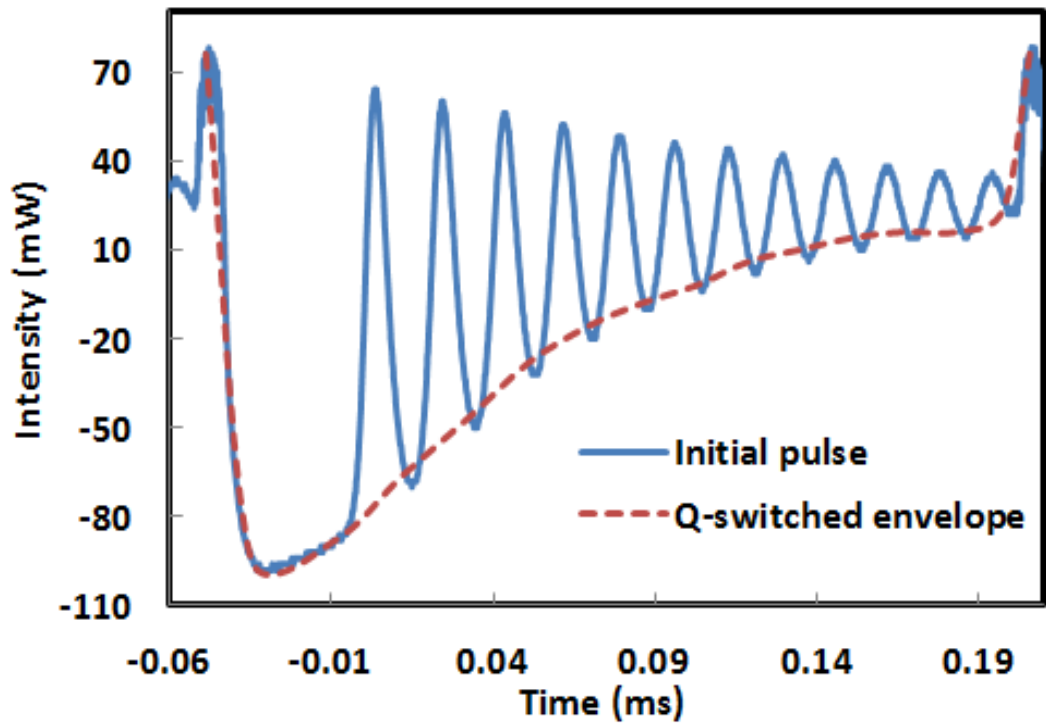


Figure 5.20: Emission of single Q-switched dark pulse at pump power of 145 mW

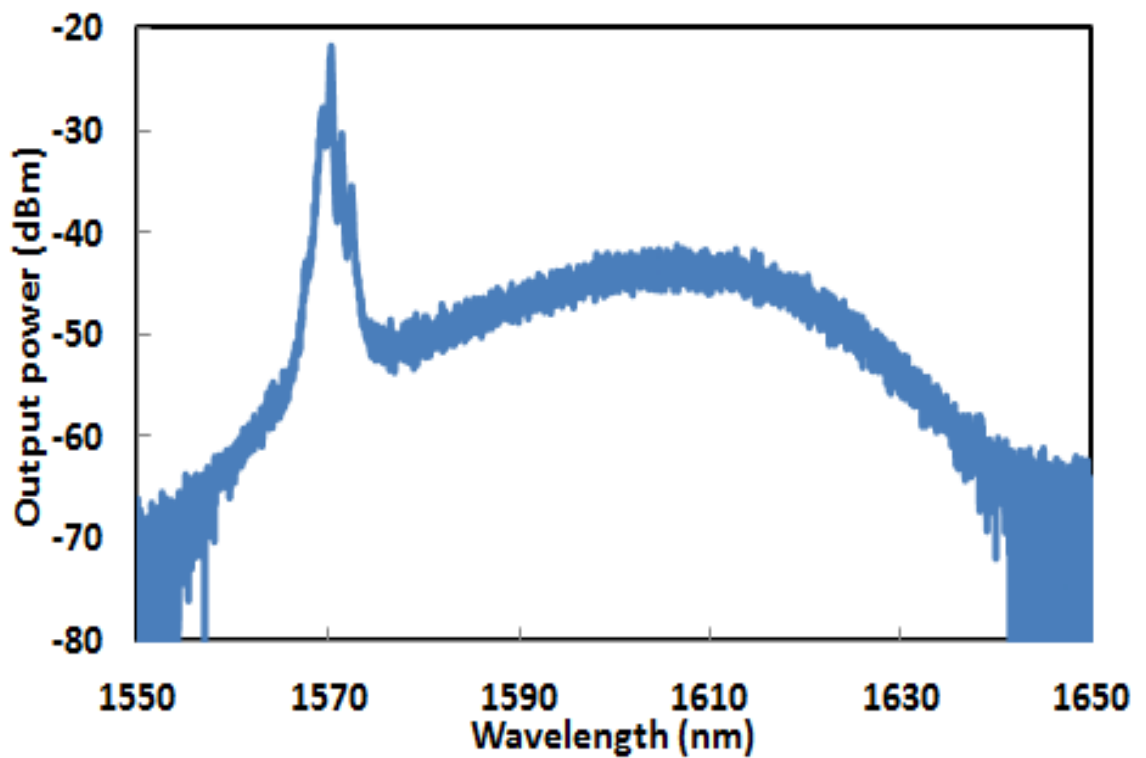


Figure 5.21: Output spectrum at pump power of 145 mW

Even though the Q-switched envelope operates in dark regime, the pulse characteristic is still in compliance with the conventional Q-switched operation. Figure 5.22 shows the repetition rate and pulse width of the Q-switched envelope of the proposed EDFL against pump power. Pulse repetition rate is observed to proportionally increase with the pump power. Pulse repetition rate increases from 0.96 kHz to 3.26 kHz by varying the pump power from 55 mW to 145 mW. The dependence of the pulse width can be seen to decrease almost linearly with the pump power. Pulse width decreases from 211 μ s to 86 μ s as pump power increases from 55 mW to 145 mW. Figure 5.23 shows the relationship of average output power and pulse energy of the Q-switched dark pulse EDFL with the pump power. As shown in the figure, average output power increases almost linearly from 0.46 mW to 1.18 mW as the pump power increases from 55 mW to 145 mW. Besides, the pulse energy fluctuates within 333 nJ to 479 nJ at the same pump power range.

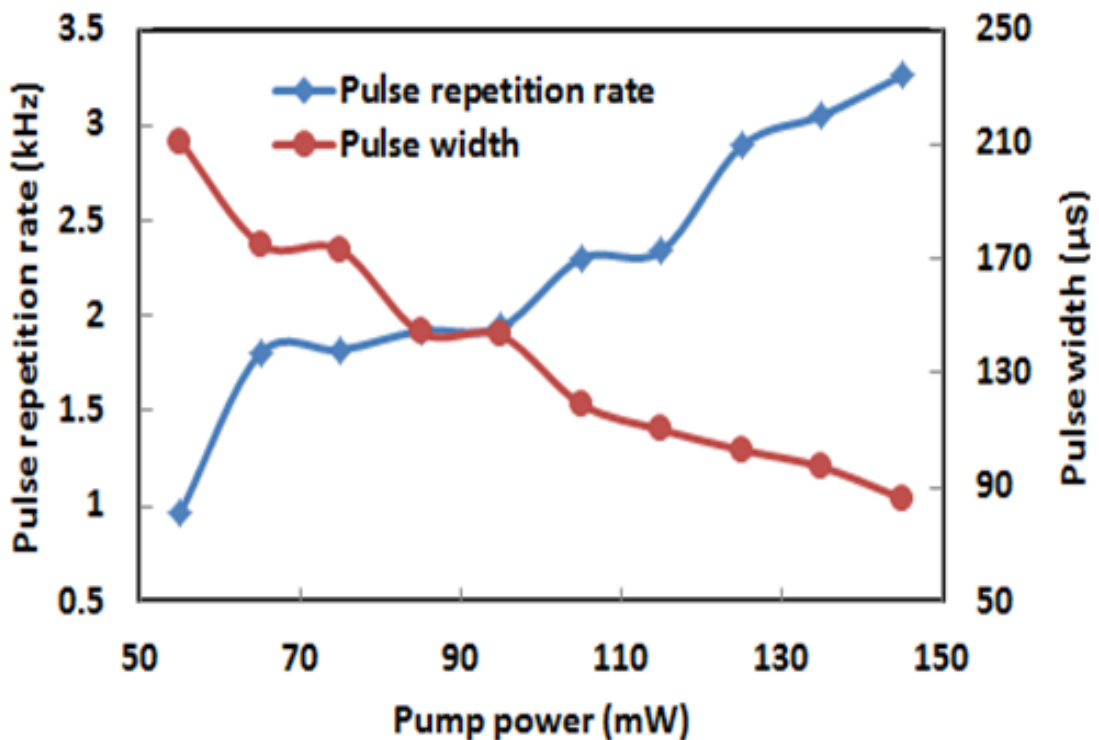


Figure 5.22: Pulse repetition rate and pulse width of the proposed Q-switched dark pulse EDFL

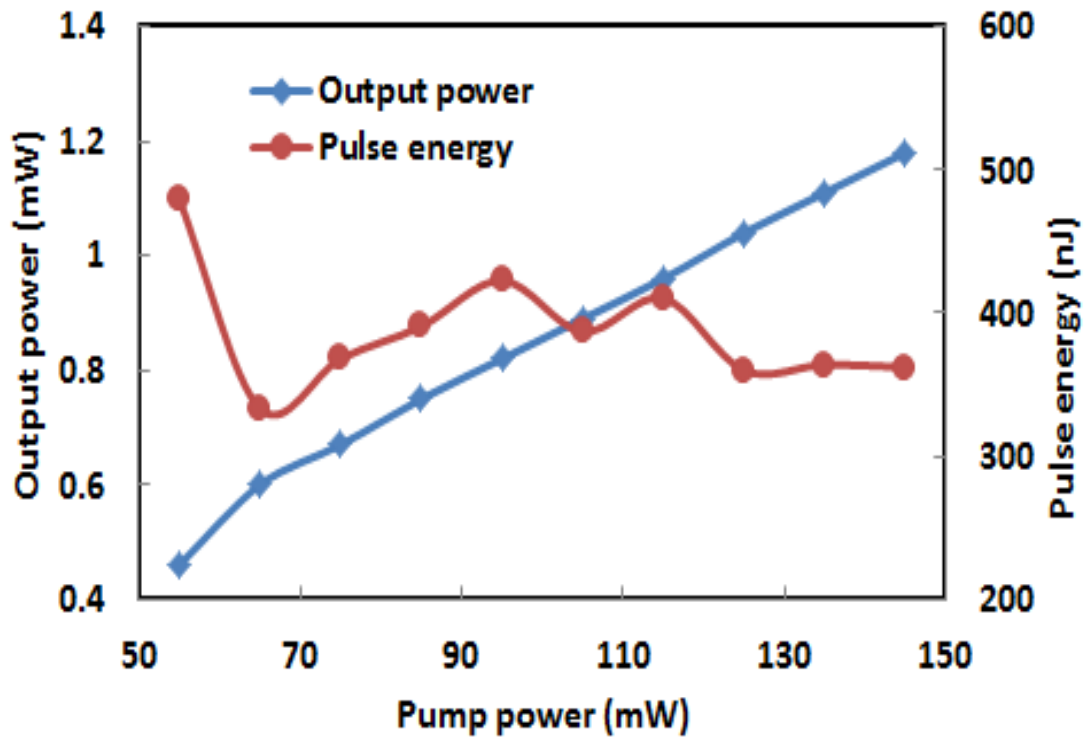


Figure 5.23: Output power and pulse energy of the proposed Q-switched dark pulse EDFL

By zooming to the dark pulses inside the Q-switched envelope, we observe that the pulse train consists of two different parts; the first dip and trailing dark pulses as shown in the inset of Figure 5.24. The first dip represents the dark square pulse, whose pulse width experiences a decreasing trend from 114 μs to 40.5 μs as pump power increases from 55 mW to 145 mW. However, the negative peak intensity is approximately constant at -96 mV throughout the tuning range of Q-switched dark pulse operation as shown in Figure 5.24. For the trailing dark pulses, the repetition rate increases from 27.62 kHz to 50 kHz as pump power increases from 55 mW to 145 mW. The dark pulse generation inside the Q-switched pulse envelope is most probably due to the Q-switching instability effect in the laser cavity. The dark pulse train in the cavity is modulated by the Q-switching operation, which is created under a certain polarization state based on NPR effect. The dark pulses are then bounded in a Q-switched envelope to form a bunch of dark pulse as shown in Figure 5.20. The Q-switched modulation

process exhibits similar characteristics as the conventional Q-switching pulse operation, which increases in pulse repetition rate and decreases in pulse width as pump power increases. Therefore, the dark pulses under the Q-switched envelope are modulated and complied to conventional Q-switching pulse operation. Commonly, the Q-switched instability or QML cannot sustain under a wide pump power tuning range. It is worthy to notice that in this experiment, the pump power tuning range of Q-switched dark pulse operation is more than 90 mW. Q-switched modulation process has intensively increase the negative peak amplitude and pulse energy for the dark pulse. These properties are attractive to achieve wavelength conversion and super continuum generation.

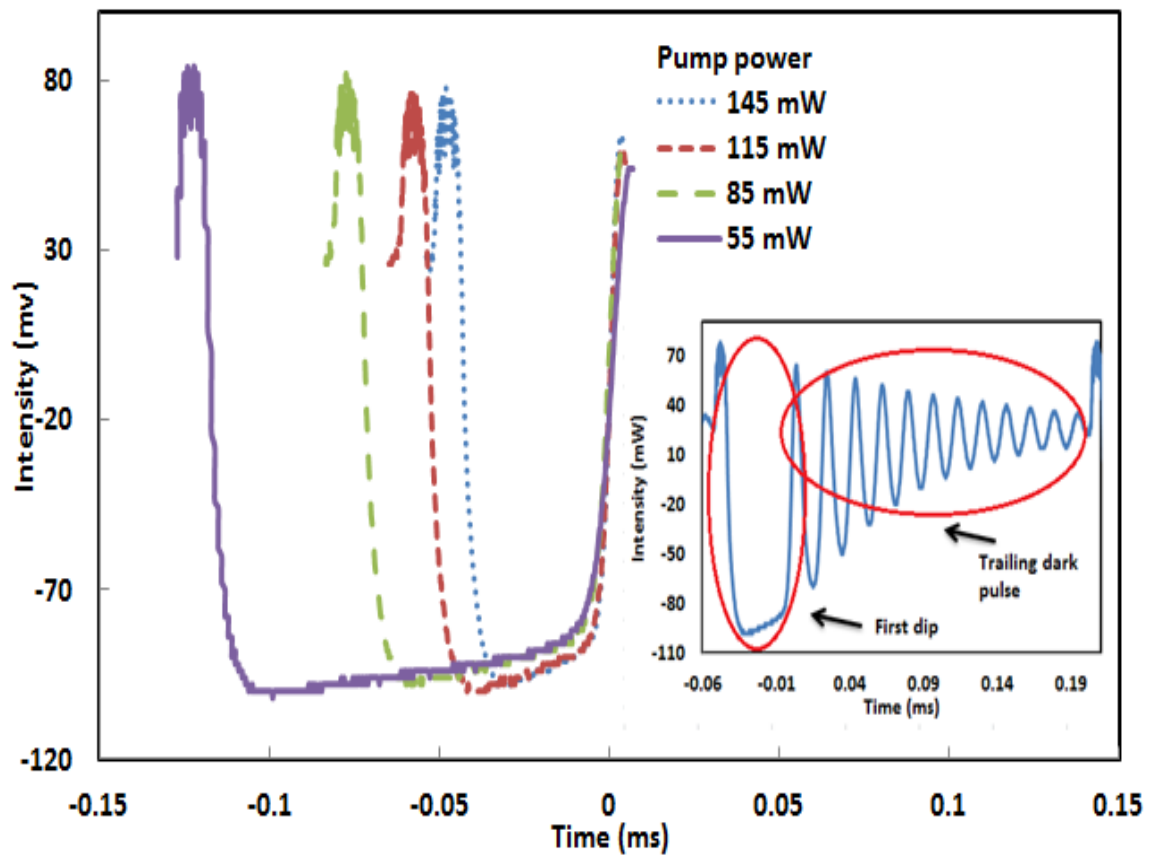


Figure 5.24: Dark square pulse at different pump power, Inset shows single Q-switched dark pulse which consists of first dip and trailing dark pulses

5.6 Summary

In this chapter, various types of dark pulse operations have been demonstrated based on NPR techniques, which included NLSE dark pulse, CQNLSE dark pulse, DW dark pulse, multi-wavelength dark pulse and Q-switched dark pulse in EDFL. It is found that the NPR based dark pulses are highly relied on the cavity dispersion and nonlinearity. For instance, NLSE dark pulse required normal dispersion cavity, DW dark pulse required dual wavelength oscillation, and CQNLSE required high nonlinearity to dominate the Kerr effect. Similar to mode-locking operation in chapter 4, dark pulse generation required a polarization tuning process to achieve a stable pulsing in dark regime. Compared to single bright pulse emission of the laser, the single dark pulse emission state was difficult to maintain. This is most probably due to the laser noise and/or weak environmental perturbations, which allows new dark pulses to appear automatically in the cavity. In section 5.2 and section 5.4, harmonic dark pulses are achieved in figure-of-eight cavity. This proved that figure-of-eight cavity can enhance the cavity feedback and to achieve higher harmonic order as we have observed in chapter 4. On the other hand, similar to multi-wavelength mode-locked that demonstrated in chapter 4, multi-wavelength dark pulse is achieved in figure-of-cavity. Dark pulse induced by NPR is formed in the main loop, whereas PCF in second loop ‘sliced’ the spectrum into multi-wavelength. Compare to pure dark pulse operation, Q-switched dark pulse considered as an unstable state, in which both Q-switched and dark pulse are co-existed in a same cavity. However, the amplitude of the dark pulse increases tremendously with the Q-switched modulation process. This unstable state carries an important advantage in certain application such as super continuum generation.

CHAPTER 6

CONCLUSION AND FUTURE OUTLOOK

In this final chapter, we will summarize and conclude what has been demonstrated and future outlook will be discussed.

6.1 Conclusion

Pulsed lasers have been of great interest as they have been widely used in various fields such as micromachining, medicine and telecommunication. For instance, ultra-short optical pulses have high potential applications optical transmission system especially for achieving a high speed and long distance network. The generation of pulsed laser can be categorized into two techniques; the active and passive techniques. Passively mode-locked fiber lasers have become established tools for generating nanosecond, picosecond and femtosecond pulses due to their compact design, alignment-free waveguide format and low cost. These advantages over their solid-state counterparts have driven further interest and more works on this field. This thesis aims to propose and demonstrate both bright pulse and dark pulse train generations in Erbium-doped fiber lasers (EDFLs) using passive techniques based on nonlinear polarization rotation (NPR) technique. In this work, various techniques such as saturable absorbers (SAs) and nonlinear polarization rotation (NPR) techniques have been explored to generate the laser pulses.

Three passive techniques for generating Q-switching pulse have also been evaluated and demonstrated; graphene film based SA, solid state thulium-doped fiber (TDF) SA and NPR in Chapter 3. It is found that the NPR based Q-switching operation

occurs at a relatively lower pump power of around 12 mW compared to other Q-switching techniques. Other techniques require higher pump power to initiate Q-switching operation mainly due to the device loss. For instance, Q-switched EDFLs, which were generated using a graphene and solid state TDF SA have a threshold pump power in a range of 20 mW and 33 mW respectively. NPR technique proved its multi-functional operation where we have successfully achieved both Q-switched and multi-wavelength operations in our proposed EDFL. Furthermore, NPR also offers advantages such as tunable saturable absorption strength and ease of implementation with only conventional optical fiber components. Besides, NPR technique exhibits a high potential to obtain different types of pulsed laser by only changing the polarization state. Therefore, NPR technique is chosen to be the most suitable method for further investigation in different type of pulsed laser.

In chapter 4, various types of mode-locking operations have been demonstrated based on NPR techniques, which included mode-locked EDFL with switchable operating states, mode-locked square pulse EDFL and multi-wavelength mode-locked EDFL. It is found that the NPR based mode-locking operations are highly relied on the polarization state. Therefore, different mode-locking operation can be generated in a same cavity with the change of polarization state. On the other hand, pump power is another key parameter to induce mode-locking operation based on NPR technique. Under a sufficiently high pump power, mode-locked laser experiences pulse breaking process to generate square pulse or higher order harmonic mode-locked. The advantages of higher order harmonic mode-locked are to achieve higher pulse repetition rate and narrower pulse width. On the other hand, the balance between the inhomogeneous loss induced by NPR and the mode competition effect can lead stable multi-wavelength oscillations. Multi-wavelength and mode-locking operation can be simultaneously achieved in a single loop cavity set-up since mode-locking and multi-wavelength

operation required different NPR mechanism to induce the phenomena. However, multi-wavelength and mode-locked are able to co-exist in figure-of-eight set-up; the main loop induces the mode-locking operation, whereas another loop induces the multi-wavelength operation to ‘slice’ the spectrum of the cavity.

All the pulse train obtained in chapter 3 and chapter 4 are operated in bright pulse regime. Besides the bright pulse regime, there is another type of operation regime, called dark pulse regime. Dark pulse regime is represented as a narrow intensity dip under a strong CW laser emission background. In chapter 5, several types of dark pulse lasers are investigated via NPR method, which included NLSE dark pulse, CQNLSE dark pulse, DW dark pulse, multi-wavelength dark pulse and Q-switched dark pulse in EDFL. It is found that the NPR based dark pulses are highly relied on the cavity dispersion and nonlinearity. For instance, NLSE dark pulse required normal dispersion cavity, DW dark pulse required dual wavelength oscillation, and CQNLSE required high nonlinearity to dominate the Kerr effect. Similar to mode-locked by NPR, dark pulse generation required a polarization tuning process to achieve a stable pulsing in dark regime. Compared to single bright pulse emission of the laser, the single dark pulse emission state was difficult to maintain. This is most probably due to the laser noise and/or weak environmental perturbations, which allows new dark pulses to appear automatically in the cavity. Besides, harmonic dark pulses are achieved in figure-of-eight cavity. This further identified that figure-of-eight cavity can enhance the cavity feedback and to achieve higher harmonic order as we have observed in bright pulse regime. Similar to multi-wavelength mode-locked that demonstrated in bright pulse regime, multi-wavelength dark pulse is achieved in figure-of-cavity. Dark pulse induced by NPR is formed in the main loop, whereas PCF in second loop ‘sliced’ the spectrum into multi-wavelength. Compare to pure dark pulse operation, Q-switched dark pulse is considered to operate in an unstable state, where both Q-switching and dark pulse are

co-existed in the same cavity. However, the amplitude of the dark pulse tremendously increases with the Q-switched modulation process. This unstable state carries an important advantage in certain applications such as super continuum generation.

In summary, various types of bright and dark pulse profiles can be manipulated based on the variable saturable absorption strengths of NPR technique. Therefore, simple, compact and multi-function pulsed laser can be realized with NPR technique. Characteristic of pulsed laser can be controlled to produce different pulse width and pulse repetition rate that suit the needs for different applications. From the experiments conducted and obtained results, it is proven that NPR is indeed a powerful tool that can be exploited for pulsed laser

6.2 Recommendations for Future Works

Much work has been carried out on the generation of pulsed laser. However, it can be further explored in the future. The performance of Q-switched pulse energy can be improved, Future study on mode-locked and dark pulse based NPR may also focus on higher pulse repetition rate and better signal to noise ratio (SNR).

Q-switched pulse energy of EDFL incorporated with SAs can further increase by optimizing the gain medium length. Besides, Q-switched EDFL based on NPR can incorporate a shorter nonlinear medium to decrease the cavity loss. Pulse width of mode-locked EDFL can further be reduced by replacing the birefringence fiber (SMF, DSF and DCF) with shorter nonlinear medium. Moreover, pulse width of NPR based EDFL can also be made narrower, near transform limit by optimizing the net dispersion in the cavity. With the advancement of ultra-fast laser system, the cavity length can be reduced to several meters to allow high pulse repetition rate in high capacity telecommunication systems and optical switching devices. Additionally, high pulse

repetition rate can also be achieved with a higher pumping power to induce higher harmonic order.

Future directions can also include comparison of pulse propagation characteristics between bright and dark pulses to produce more reliable light source in telecommunication field. With this, it is hoped that this work will contribute to the ultra-fast optics.

REFERENCES

- Adib, B., Heidari, A., & Tayyari, S. F. (2009). RETRACTED: An analytical approach to soliton of the saturable non-linear Schrödinger equation determination and consideration of stability of solitary solutions of cubic–quintic non-linear Schrödinger equation (CQNLSE). *Communications in Nonlinear Science and Numerical Simulation*, 14(5), 2034-2045.
- Agrawal, G. P. (1987). Modulation instability induced by cross-phase modulation. *Physical review letters*, 59(8), 880.
- Agrawal, G. P., Baldeck, P. L., & Alfano, R. R. (1989). Modulation instability induced by cross-phase modulation in optical fibers. *Physical Review A*, 39(7), 3406.
- Agrawal, G. P., & Olsson, N. A. (1989). Self-phase modulation and spectral broadening of optical pulses in semiconductor laser amplifiers. *Quantum Electronics, IEEE Journal of*, 25(11), 2297-2306.
- Alfano, R. R, & Ho, P. P. (1988). Self-, cross-, and induced-phase modulations of ultrashort laser pulse propagation. *IEEE Journal of Quantum Electronics*, 24(2), 351-364.
- Aubin, G., Jeanney, E., Montalant, T., Moulu, J., Pirio, F., Thomine, J. B. & Devaux, F. (1995). 20 Gbit/s soliton transmission over transoceanic distances with a 105 km amplifier span. *Electronics Letters*, 31(13), 1079-1080.
- Baek, I. H., Lee, H. W., Bae, S., Hong, B. H., Ahn, Y. H., Yeom, D. I., & Rotermund, F. (2012). Efficient mode-locking of sub-70-fs Ti: sapphire laser by graphene saturable absorber. *Applied Physics Express*, 5(3), 032701.
- Bonaccorso, F., Sun, Z., Hasan, T., & Ferrari, A. C. (2010). Graphene photonics and optoelectronics. *Nature photonics*, 4(9), 611-622.
- Bao, Q., Zhang, H., Wang, Y., Ni, Z., Yan, Y., Shen, Z. X., & Tang, D. Y. (2009). Atomic layer graphene as a saturable absorber for ultrafast pulsed lasers. *Advanced Functional Materials*, 19(19), 3077-3083.
- Blow, K. J., & Doran, N. J. (1985). Multiple dark soliton solutions of the nonlinear Schrödinger equation. *Physics Letters A*, 107(2), 55-58.
- Brackett, C. A. (1990). Dense wavelength division multiplexing networks: Principles and applications. *Selected Areas in Communications, IEEE Journal on*, 8(6), 948-964.
- Buryak, A. V., Di Trapani, P., Skryabin, D. V., & Trillo, S. (2002). Optical solitons due to quadratic nonlinearities: from basic physics to futuristic applications. *Physics Reports*, 370(2), 63-235.

- Chang, W., Ankiewicz, A., Soto-Crespo, J. M., & Akhmediev, N. (2008). Dissipative soliton resonances. *Physical Review A*, 78(2), 023830.
- Chen, H. R., Tsai, C. Y., Cheng, H. M., Lin, K. H., & Hsieh, W. F. (2014). Passive mode locking of ytterbium-and erbium-doped all-fiber lasers using graphene oxide saturable absorbers. *Optics express*, 22(11), 12880-12889.
- Chen, L., Zhang, M., Zhou, C., Cai, Y., Ren, L. & Zhang, Z. (2009). Ultra-low repetition rate linear-cavity erbium-doped fibre laser modelocked with semiconductor saturable absorber mirror. *Electronics letters*, 45(14), 731-733.
- Cordova-Plaza, A., Dignonnet, M. J., & Shaw, H. J. (1987). Miniature CW and active internally Q-switched Nd: MgO: LiNbO₃ lasers. *Quantum Electronics, IEEE Journal of*, 23(2), 262-266.
- Crosta, M., Fratalocchi, A., & Trillo, S. (2011). Bistability and instability of dark-antidark solitons in the cubic-quintic nonlinear Schrödinger equation. *Physical Review A*, 84(6), 063809.
- Degnan, J. J. (1989). Theory of the optimally coupled Q-switched laser. *Quantum Electronics, IEEE Journal of*, 25(2), 214-220.
- Deng, L., Hagley, E. W., Wen, J., Trippenbach, M., Band, Y., Julienne, P. S., & Phillips, W. D. (1999). Four-wave mixing with matter waves. *Nature*, 398(6724), 218-220.
- Doran, N. J., & Wood, D. (1988). Nonlinear-optical loop mirror. *Optics Letters*, 13(1), 56-58.
- Eichler, H. J., Liu, B., Kayser, M., & Khomenko, S. I. (1996). Er: YAG-laser at 2.94 μm Q-switched by a FTIR-shutter with silicon output coupler and polarizer. *Optical materials*, 5(4), 259-265.
- El-Sherif, A. F., & King, T. A. (2003). High-energy, high-brightness Q-switched Tm³⁺-doped fiber laser using an electro-optic modulator. *Optics communications*, 218(4), 337-344.
- Feng, M., Silverman, K. L., Mirin, R. P., & Cundiff, S. T. (2010). Dark pulse quantum dot diode laser. *Optics express*, 18(13), 13385-13395.
- Feng, X., Tam, H. Y., & Wai, P. K. A. (2006). Stable and uniform multiwavelength erbium-doped fiber laser using nonlinear polarization rotation. *Optics express*, 14(18), 8205-8210.
- Fermann, M. E., Haberl, F., Hofer, M., & Hochreiter, H. (1990). Nonlinear amplifying loop mirror. *Optics Letters*, 15(13), 752-754.
- Fok, M. P., & Shu, C. (2006). Spacing-adjustable multi-wavelength source from a stimulated Brillouin scattering assisted erbium-doped fiber laser. *Optics express*, 14(7), 2618-2624.

- Fukuda, H., Yamada, K., Shoji, T., Takahashi, M., Tsuchizawa, T., Watanabe, T., & Itabashi, S. I. (2005). Four-wave mixing in silicon wire waveguides. *Optics Express*, 13(12), 4629-4637.
- Gao, M., Zuo, J. M., Twosten, R. D., Petrov, I., Nagahara, L. A., & Zhang, R. (2003). Structure determination of individual single-wall carbon nanotubes by nanoarea electron diffraction. *Applied Physics Letters*, 82(16), 2703-2705.
- Giallorenzi, T. G., Bucaro, J. A., Dandridge, A., Sigel, G. H., Cole, J. H., Rashleigh, S. C., & Priest, R. G. (1982). Optical fiber sensor technology. *Microwave Theory and Techniques, IEEE Transactions on*, 30(4), 472-511.
- Going, R., Popa, D., Torrisi, F., Sun, Z., Hasan, T., Wang, F. & Ferrari, A. C. (2012). 500fs wideband tunable fiber laser mode-locked by nanotubes. *Physica E: Low-Dimensional Systems and Nanostructures*, 44(6), 1078-1081.
- Haelterman, M., & Emplit, P. (1993). Optical dark soliton trains generated by passive spectral filtering technique. *Electronics Letters*, 29(4), 356-357.
- Han, Y. G., Van Anh Tran, T., & Lee, S. B. (2006). Wavelength-spacing tunable multiwavelength erbium-doped fiber laser based on four-wave mixing of dispersion-shifted fiber. *Optics letters*, 31(6), 697-699.
- Harun, S. W., Parvizi, R., Shahi, S., & Ahmad, H. (2009). Multi-wavelength erbium-doped fiber laser assisted by four-wave mixing effect. *Laser Physics Letters*, 6(11), 813-815.
- Haus, H. A., Ippen, E. P. & Tamura, K. (1994). Additive-pulse modelocking in fiber lasers. *Quantum Electronics, Journal of IEEE*, 30(1), 200-208.
- Haus, H. A., Tamura, K., Nelson, L. E., & Ippen, E. P. (1995). Stretched-pulse additive pulse mode-locking in fiber ring lasers: theory and experiment. *Quantum Electronics, IEEE Journal of*, 31(3), 591-598.
- Haus, H. A. (2000). Mode-locking of lasers. *Selected Topics in Quantum Electronics, IEEE Journal of*, 6(6), 1173-1185.
- Hossain, M. A., Namihira, Y. & Razzak, S. A. (2012). Supercontinuum generation at 1.55 μm using highly nonlinear photonic crystal fiber for telecommunication and medical applications. *Optical Review*, 19(5), 315-319.
- Huang, P. L., Lin, S. C., Yeh, C. Y., Kuo, H. H., Huang, S. H., Lin, G. R., & Cheng, W. H. (2012). Stable mode-locked fiber laser based on CVD fabricated graphene saturable absorber. *Optics express*, 20(3), 2460-2465.
- Hudson, D. D., Holman, K. W., Jones, R. J., Cundiff, S. T., Ye, J., & Jones, D. J. (2005). Mode-locked fiber laser frequency-controlled with an intracavity electro-optic modulator. *Optics letters*, 30(21), 2948-2950.

- Ilday, F.Ö., Wise, F.W. & Sosnowski, T. (2002). High-energy femtosecond stretched-pulse fiber laser with a nonlinear optical loop mirror. *Optics letters*, 27(17), 1531-1533.
- Im, J. H., Choi, S. Y., Rotermund, F., & Yeom, D.I. (2010). All-fiber Er-doped dissipative soliton laser based on evanescent field interaction with carbon nanotube saturable absorber. *Optics express*, 18(21), 22141-22146.
- Ippen, E. P., & Stolen, R. H. (1972). Stimulated Brillouin scattering in optical fibers. *Applied Physics Letters*, 21(11), 539-541.
- Ippen, E. P. (1994). Principles of passive mode locking. *Applied Physics B*, 58(3), 159-170.
- Isomäki, A., & Okhotnikov, O. G. (2006). Femtosecond soliton mode-locked laser based on ytterbium-doped photonic bandgap fiber. *Optics express*, 14(20), 9238-9243.
- Jabczynski, J., Zendzian, W., & Kwiatkowski, J. (2006). Q-switched mode locking with acousto-optic modulator in a diode-pumped Nd: YVO₄ laser. *Optics express*, 14(6), 2184-2190.
- Jeon, M. Y., Lee, H. K., Kim, K. H., Lee, E. H., Oh, W. Y., Kim, B.Y., & Koh, Y. W. (1998). Harmonically mode-locked fiber laser with an acousto-optic modulator in a Sagnac loop and Faraday rotating mirror cavity. *Optics communications*, 149(4), 312-316.
- Kaiser, R., & Huttl, B. (2007). Monolithic 40-GHz mode-locked MQW DBR lasers for high-speed optical communication systems. *Selected Topics in Quantum Electronics, IEEE Journal of*, 13(1), 125-135.
- Keller, U. (2003). Recent developments in compact ultrafast lasers. *Nature*, 424(6950), 831-838.
- Kezirian, G. M. & Stonecipher, K. G. (2004). Comparison of the IntraLase femtosecond laser and mechanical keratomes for laser in situ keratomileusis. *Journal of Cataract & Refractive Surgery*, 30(4), 804-811.
- Kim, A. D., Kutz, J. N., & Muraki, D. J. (2000). Pulse-train uniformity in optical fiber lasers passively mode-locked by nonlinear polarization rotation. *Quantum Electronics, IEEE Journal of*, 36(4), 465-471.
- Kivshar, Y. S., & Luther-Davies, B. (1998). Dark optical solitons: physics and applications. *Physics Reports*, 298(2), 81-197.
- Kong, J., Cassell, A. M., & Dai, H. (1998). Chemical vapor deposition of methane for single-walled carbon nanotubes. *Chemical Physics Letters*, 292(4), 567-574.
- Laubereau, A., & Kaiser, W. (1974). Generation and applications of passively mode-locked picosecond light pulses. *Opto-electronics*, 6(1), 1-24.

- Lega, J., & Fauve, S. (1997). Traveling hole solutions to the complex Ginzburg-Landau equation as perturbations of nonlinear Schrödinger dark solitons. *Physica D: Nonlinear Phenomena*, 102(3), 234-252.
- Lehmann, K. K., & Romanini, D. (1996). The superposition principle and cavity ring-down spectroscopy. *The Journal of chemical physics*, 105(23), 10263-10277.
- Lin, J. H., Lin, K. H., Hsu, C. C., Yang, W. H., & Hsieh, W. F. (2007). Supercontinuum generation in a microstructured optical fiber by picosecond self Q-switched mode-locked Nd: GdVO₄ laser. *Laser Physics Letters*, 4(6), 413.
- Liu, X. M., Wang, T., Shu, C., Wang, L.R., Lin, A., Lu, K.Q. & Zhao, W. (2008). Passively harmonic mode-locked erbium-doped fiber soliton laser with a nonlinear polarization rotation. *Laser physics*, 18(11), 1357-1361.
- Liu, X. (2009). Dissipative soliton evolution in ultra-large normal-cavity-dispersion fiber lasers. *Optics express*, 17(12), 9549-9557.
- Luo, A.P., Luo, Z. C., Xu, W., Dvoyrin, V. V., Mashinsky, V. M. & Dianov, E. M. (2011). Tunable and switchable dual-wavelength passively mode-locked Bi-doped all-fiber ring laser based on nonlinear polarization rotation. *Laser Physics Letters*, 8(8), 601-605.
- Luo, Z., Zhou, M., Weng, J., Huang, G., Xu, H., Ye, C. & Cai, Z. (2010). Graphene-based passively Q-switched dual-wavelength erbium-doped fiber laser. *Optics letters*, 35(21), 3709-3711.
- Martinez, A., & Sun, Z. (2013). Nanotube and graphene saturable absorbers for fibre lasers. *Nature Photonics*, 7(11), 842-845.
- Matsas, V. J., Newson, T. P., Richardson, D. J. & Payne, D. N. (1992). Selfstarting passively mode-locked fibre ring soliton laser exploiting nonlinear polarisation rotation. *Electron. Lett*, 28(15), 1391-1393.
- Mendez, A. J., Gagliardi, R. M., Feng, H. X., Heritage, J. P., & Morookian, J. M. (2000). Strategies for realizing optical CDMA for dense, high-speed, long span, optical network applications. *Journal of lightwave technology*, 18(12), 1685.
- Montés-Micó, R., Rodríguez-Galietero, A. & Alió, J. L. (2007). Femtosecond laser versus mechanical keratome LASIK for myopia. *Ophthalmology*, 114(1), 62-68.
- Mori, K., Takara, H., Kawanishi, S., Saruwatari, M. & Morioka, T. (1997). Flatly broadened supercontinuum spectrum generated in a dispersion decreasing fibre with convex dispersion profile. *Electronics Letters*, 33(21), 1806-1808.
- Mulvad, H. C. H., Galili, M., Oxenløwe, L. K, Hu, H., Clausen, A. T., Jensen, J. B., Peucheret, C. & Jeppesen, P. (2010). Demonstration of 5.1 Tbit/s data capacity on a single-wavelength channel. *Optics Express*, 18(2), 1438-1443.

- Nakazawa, M. (2000). Solitons for breaking barriers to terabit/second WDM and OTDM transmission in the next millennium. *Selected Topics in Quantum Electronics, Journal of IEEE*, 6(6), 1332-1343.
- Nakazawa, M., Yamada, E., Kubota, H. & Suzuki, K. (1991). 10 Gbit/s soliton data transmission over one million kilometres. *Electronics Letters*, 27(14), 1270-1272.
- Nelson, L. E., Jones, D. J., Tamura, K., Haus, H. A., & Ippen, E. P. (1997). Ultrashort-pulse fiber ring lasers. *Applied Physics B: Lasers and Optics*, 65(2), 277-294.
- Nikumb, S., Chen, Q., Li, C., Reshef, H., Zheng, H. Y., Qiu, H. & Low, D. (2005). Precision glass machining, drilling and profile cutting by short pulse lasers. *Thin Solid Films*, 477(1), 216-221.
- Noor, Y. M., Tam, C. C., Lim, L.E. N. & Jana, S. (1994). A review of the Nd: YAG laser marking of plastic and ceramic IC packages. *Journal of materials processing technology*, 42(1), 95-133
- Pan, S. D., Cui, L., Liu, J. Q., Teng, B., Liu, J. H., & Ge, X. H. (2014). Passively Q-switched mode-locking Nd: GdVO₄ laser with a chemically reduced graphene oxide saturable absorber. *Optical Materials*, 38, 42-45.
- Pitois, S., Fatome, J., & Millot, G. (2002). Generation of a 160-GHz transform-limited pedestal-free pulse train through multiwave mixing compression of a dual-frequency beat signal. *Optics letters*, 27(19), 1729-1731.
- Plamann, K., Aptel, F., Arnold, C. L., Courjaud, A., Crotti, C., Deloison, F. & Legeais, J.- M. (2010). Ultrashort pulse laser surgery of the cornea and the sclera. *Journal of Optics*, 12(8), 084002.
- Radhakrishnan, R., & Lakshmanan, M. (1995). Bright and dark soliton solutions to coupled nonlinear Schrodinger equations. *Journal of Physics A: Mathematical and General*, 28(9), 2683.
- Rairoux, P., Schillinger, H., Niedermeier, S., Rodriguez, M., Ronneberger, F., Sauerbrey, R., ... & Ziener, C. (2000). Remote sensing of the atmosphere using ultrashort laser pulses. *Applied Physics B*, 71(4), 573-580.
- Renninger, W. H., Chong, A., & Wise, F. W. (2010). Self-similar pulse evolution in an all normal-dispersion laser. *Physical Review A*, 82(2), 021805.
- Salehi, J. A., Weiner, A. M., & Heritage, J. P. (1990). Coherent ultrashort light pulse code-division multiple access communication systems. *Lightwave Technology, Journal of*, 8(3), 478-491.
- Salhi, M., Leblond, H., & Sanchez, F. (2003). Theoretical study of the erbium-doped fiber laser passively mode-locked by nonlinear polarization rotation. *Physical Review A*, 67(1), 013802.

- Serkin, V. N., & Hasegawa, A. (2000). Novel soliton solutions of the nonlinear Schrödinger equation model. *Physical Review Letters*, 85(21), 4502.
- Serbin, J., Bauer, T., Fallnich, C., Kasenbacher, A. & Arnold, W. H. (2002). Femtosecond lasers as novel tool in dental surgery. *applied surface science*, 197, 737-740.
- Set, S. Y., Yaguchi, H., Tanaka, Y., & Jablonski, M. (2004). Laser mode locking using a saturable absorber incorporating carbon nanotubes. *Journal of Lightwave Technology*, 22(1), 51.
- Shahabuddin, N. S., Mohamad, H., Mahdi, M. A., Yusoff, Z., Ahmad, H. & Harun, S. W. (2012). Broad spectral sliced multiwavelength source with a mode locked fiber laser. *Laser Physics*, 22(1), 212-215.
- Song, C., Xu, W., Luo, Z., Luo, A. & Chen, W. (2009). Switchable and tunable dual-wavelength ultrashort pulse generation in a passively mode-locked erbium-doped fiber ring laser. *Optics Communications*, 282(22), 4408-4412.
- Sotor, J., Sobon, G., Krzempek, K. & Abramski, K. M. (2012). Fundamental and harmonic mode-locking in erbium-doped fiber laser based on graphene saturable absorber. *Optics Communications*, 285(13), 3174-3178.
- Stegeman, G. I., Hagan, D. J., & Torner, L. (1996). $\chi(2)$ cascading phenomena and their applications to all-optical signal processing, mode-locking, pulse compression and solitons. *Optical and Quantum electronics*, 28(12), 1691-1740.
- Stolen, R. H., & Lin, C. (1978). Self-phase-modulation in silica optical fibers. *Physical Review A*, 17(4), 1448.
- Sutter, D. H., Steinmeyer, G., Gallmann, L., Matuschek, N., Morier-Genoud, F., Keller, U., & Tschudi, T. (1999). Semiconductor saturable-absorber mirror assisted Kerr-lens mode-locked Ti: sapphire laser producing pulses in the two-cycle regime. *Optics Letters*, 24(9), 631-633.
- Sylvestre, T., Coen, S., Emplit, P., & Haelterman, M. (2002). Self-induced modulational instability laser revisited: normal dispersion and dark-pulse train generation. *Optics letters*, 27(7), 482-484.
- Tang, D. Y., Li, L., Song, Y. F., Zhao, L. M., Zhang, H., & Shen, D. Y. (2013). Evidence of dark solitons in all-normal-dispersion-fiber lasers. *Physical Review A*, 88(1), 013849.
- Tang, W. W., Shu, C., & Lee, K. L. (2001). Rational harmonic mode locking of an optically triggered fiber laser incorporating a nonlinear optical loop modulator. *Photonics Technology Letters, IEEE*, 13(1), 16-18.
- Triki, H., Crutcher, S., Yildirim, A., Hayat, T., Aldossary, O. M., & Biswas, A. N. J. A. N. (2012). Bright and dark solitons of the modified complex Ginzburg Landau

- equation with parabolic and dual-power law nonlinearity. *Romanian Reports in Physics*, 64(2), 357-366.
- Wu, X., Tang, D. Y., Zhang, H., & Zhao, L. M. (2009). Dissipative soliton resonance in an all-normal-dispersion erbium-doped fiber laser. *Optics express*, 17(7), 5580-5584.
- Xu, K., Wu, J., Hong, X. B. & Lin, J. T. (2008). Two different operation regimes of fiber laser based on nonlinear polarization rotation: passive mode-locking and multiwavelength emission. *Photonics Technology Letters, IEEE*, 20(12), 979-981.
- Yang, Q., & Zhang, J. F. (2005). Optical Quasi-Soliton Solutions for the Cubic-Quintic Nonlinear SCHRÖDINGER Equation with Variable Coefficients. *International Journal of Modern Physics B*, 19(31), 4629-4636.
- Yoo, W. S., Kang, K., Ueda, T., & Ishigaki, T. (2009). Design of multi-wavelength micro Raman spectroscopy system and its semiconductor stress depth profiling applications. *Applied physics express*, 2(11), 116502.
- Yu, Z., Wang, Y., Zhang, X., Dong, X., Tian, J., & Song, Y. (2014). A 66 fs highly stable single wall carbon nanotube mode locked fiber laser. *Laser Physics*, 24(1), 015105.
- Zhang, H., Tang, D. Y., Zhao, L. M., & Knize, R. J. (2010). Vector dark domain wall solitons in a fiber ring laser. *Optics express*, 18(5), 4428-4433.
- Zhang, H., Tang, D., Zhao, L., & Wu, X. (2011). Dual-wavelength domain wall solitons in a fiber ring laser. *Optics express*, 19(4), 3525-3530.
- Zhang, J., & Dai, C. (2005). Bright and dark optical solitons in the nonlinear Schrodinger equation with fourth-order dispersion and cubic-quintic nonlinearity. *Chinese Optics Letters*, 3(5), 295-298.
- Zhang, S., Wu, E., Pan, H., & Zeng, H. (2004). Q-switched mode-locking with Cr⁴⁺: YAG in a diode pumped Nd: GdVO₄ laser. *Applied Physics B*, 78(3-4), 335-338.
- Zhang, X., Zhao, S., Wang, Q., Ozygus, B., & Weber, H. (1999). Modeling of diode-pumped actively Q-switched lasers. *Quantum Electronics, IEEE Journal of*, 35(12), 1912-1918.
- Zhang, X., Zhao, S., Wang, Q., Ozygus, B., & Weber, H. (2000). Modeling of passively Q-switched lasers. *JOSA B*, 17(7), 1166-1175.
- Zhang, X., Zhao, S., Wang, Q., Zhang, Q., Sun, L., & Zhang, S. (1997). Optimization of Cr⁴⁺-doped saturable-absorber Q-switched lasers. *Quantum Electronics, IEEE Journal of*, 33(12), 2286-2294.

Zhao, W., & Bourkoff, E. (1990). Generation of dark solitons under a cw background using waveguide electro-optic modulators. *Optics letters*, 15(8), 405-407.

Zhu, J., Zhang, D., Bian, Z., Li, G., Huo, Y., Lu, Y., & Li, H. (2009). Aerosol-spraying synthesis of SiO₂/TiO₂ nanocomposites and conversion to porous TiO₂ and single-crystalline TiOF₂. *Chemical Communications*, (36), 5394-5396.

APPENDIX

A selection of published works are attached in this appendix